

**Electron Transfer in Chemically and
Genetically Modified Myoglobins**

Thesis by
Thomas Edward Zewert

In Partial Fulfillment of the Requirements
for the Degree of
Doctor of Philosophy

California Institute of Technology
Pasadena, California

1990

(Submitted January 8, 1990)

Acknowledgements

None of the work in this thesis would have been possible without a great amount of help from others. First, I thank my father for always encouraging me to ask questions and, often, helping me to find answers. I also very much appreciate the help I received from my friends and collaborators. Luckily, these two groups of people often overlapped. Raghaven Varadarajan constructed the original human myoglobin mutants and is one hell of a doubles partner. Dave Lambright very patiently instructed me in the art of SDM, and Steve Boxer provided the necessary resources. I am very grateful to Seymour Koenig and Rodney Brown for allowing me to use their NMRD apparatus and helping me to interpret the data from that instrument. I thank Luet Wong for convincing me to perform kinetics experiments on the ruthenium isonicotinamide derivatives of myoglobin and, in the process, administering a strong dose of scientific enthusiasm to a relatively anemic researcher at the time. I would also like to thank Jumi Shin for being an extraordinary friend. Writing-up was a much more positive experience than it would have been without her.

Also, the Gray group provided significant technical guidance and friendship during my stay. I especially wish to thank Walter Ellis and Cindy St. Clair for patiently teaching me electrochemistry. Further, Jeff and the two Mikes were helpful colleagues and particularly good "buds." Danny, Jenny, Tom, Jimmy, Mary, and Brad also helped me more than once, and I am in their debt. Finally, I thank Harry himself for allowing me to spend his NIH and NSF money, and as a result become a more creative and independent researcher.

Abstract

The temperature dependences of the reduction potentials (E°) of wild-type human myoglobin (Mb) and three site-directed mutants have been measured by using thin-layer spectroelectrochemistry. Residue Val68, which is in van der Waals contact with the heme in Mb, has been replaced by Glu, Asp, and Asn. At pH 7.0, reduction of the heme iron (III) in the former two proteins is accompanied by uptake of a proton by the protein. The changes in E° , and the standard entropy (ΔS°) and enthalpy (ΔH°) of reduction in the mutant proteins were determined relative to values for wild-type; the change in E° at 25°C was about -200 millivolts for the Glu and Asp mutants, and about -80 millivolts for the Asn mutant. Reduction of Fe(III) to Fe(II) in the Glu and Asp mutants is accompanied by uptake of a proton. These studies demonstrate that Mb can tolerate substitution of a buried hydrophobic group by potentially charged and polar residues, and that such amino acid replacements can lead to substantial changes in the redox thermodynamics of the protein.

Through analysis of the temperature dependence and shapes of NMR dispersion signals, it is determined that a water molecule is bound to the sixth coordination site of the ferric heme in the Val68Asp and in the Val68Asn recombinant proteins while the carboxyl group of the sidechain of Glu68 occupies this position in Val68Glu. The relative rhombic distortions in the ESR spectra of these mutant proteins combined with $H_2^{17}O$ and spin interconversion experiments performed on them confirm the conclusions of the NMRD study.

The rates of intramolecular electron transfer (ET) of $(NH_3)_5Ru$ -His48 (Val68Asp, His81Gln, Cys110Ala)Mb and $(NH_3)_5Ru$ -His48 (Val68Glu, His81Gln, Cys110Ala)Mb were measured to be $.85(3)s^{-1}$ and $.30(2)s^{-1}$, respectively. This data supports the hypothesis that entropy of

reduction and reorganization energy of ET are inversely related. The rates of forward and reverse ET for $(\text{NH}_3)_5\text{Ru-His48}$ (Val68Glu, His81Gln, Cys110Ala)ZnMb $-7.2(5)\cdot 10^4\text{s}^{-1}$ and $1.4(2)\cdot 10^5\text{s}^{-1}$, respectively- demonstrate that the placement of a highly polar residue nearby does not significantly change the reorganization energy of the photoactive Zn porphyrin.

The distal histidine imidazoles of $(\text{NH}_3)_4\text{isnRu-His48 SWMb}$ and $(\text{NH}_3)_5\text{Ru-His48 SWMb}$ were cyanated with BrCN. The intramolecular ET rates of these BrCN-modified Mb derivatives are $5.5(6)\text{s}^{-1}$ and $3.2(5)\text{s}^{-1}$, respectively. These respective rates are 20 and 10 times faster than those of their non-cyanated counterparts after the differences in ET rate from driving force are scaled according to the Marcus equation. This increase in ET rate of the cyanated Mb derivatives is attributed to lower reorganization energy since the cyanated Mb heme is pentacoordinate in both oxidation states; whereas, the native Mb heme loses a water molecule upon reduction so that it changes from six to five coordinate. The reorganization energy from Fe-OH₂ dissociation is estimated to be .2eV. This conclusion is used to reconcile data from previous experiments in our lab. ET in photoactive porphyrin-substituted myoglobins proceed faster than predicted by Marcus Theory when it is assumed that the only difference in ET parameters between photoactive porphyrins and native heme systems is driving force. However, the data can be consistently fit to Marcus Theory if one corrects for the smaller reorganization in the photoactive porphyrin systems since they do not undergo a coordination change upon ET.

Finally, the intramolecular ET rate of $(\text{NH}_3)_4\text{isnRu-His48 SWMb}$ was measured to be $3.0(4)\text{s}^{-1}$. This rate is within experimental error of that for $(\text{NH}_3)_4\text{pyrRu-His48 SWMb}$ even though the former has 80mV more driving force. One likely possibility for this observation is that the tetraamminepyridineruthenium group undergoes less reorganization upon ET

than the tetraammineisonicotinamideruthenium group. Moreover, analysis of the $(\text{NH}_3)_4\text{isnRu-His48}$ SWMb experimental system gives a likely explanation of why ET was not observed previously in $(\text{NH}_3)_4\text{isnRu-Cytochrome C}$.

Table of Contents

Acknowledgements	ii
Abstract	iii
CHAPTER 1. INTRODUCTION	1
Text	2
References	17
CHAPTER 2. THE EFFECTS OF BURIED IONIZABLE AMINO ACIDS ON THE REDUCTION POTENTIAL OF RECOMBINANT HUMAN MYOGLOBIN	20
Introduction	21
Experimental	26
Results and Discussion	37
References	53
CHAPTER 3. MAGNETIC RESONANCE STUDIES OF MYOGLOBIN SITE- DIRECTED MUTANTS	55
Introduction	56
Experimental	58
Results and Discussion	66
References	98
CHAPTER 4. KINETICS OF RUTHENIUM-MODIFIED His48 DERIVATIVES OF HUMAN MYOGLOBIN	100
Introduction	101
Experimental	108
Results and Discussion	119
References	142

CHAPTER 5. KINETICS OF BrCN-MODIFIED,	
L(NH ₃) ₄ Ru-His48 SPERM WHALE MYOGLOBIN	145
Introduction	146
Experimental	149
Results and Discussion	150
References	172
CHAPTER 6. LONG-RANGE ELECTRON TRANSFER IN	
ISN(NH ₃) ₄ Ru-His48 SPERM WHALE MYOGLOBIN	174
Introduction	175
Experimental	176
Results and Discussion	177
References	186

CHAPTER 1
INTRODUCTION

The extent to which a protein can alter the properties of a charged center through both localized and long-range interactions can be quite physically substantial and biologically significant. The main concern of this thesis is investigating how proteins affect the electron transfer characteristics of a redox active cofactor. Specifically, the metalloprotein myoglobin will be altered both chemically and genetically, and the resulting physical perturbations (i.e. changes in reduction/oxidation midpoint potential, electron transfer kinetics, and spectral properties) on the metalloporphyrin (almost always heme) will be analyzed.

A fundamental question is how a prosthetic group, like heme, can display such a wide range of functional diversity. Heme proteins make up a significant part of the enzyme sequence in oxidative phosphorylation as electron carriers and oxygen reductants.¹ A number of enzymatic transformations are also carried out by these proteins including hydrogen peroxide disproportionation (catalase),² stereospecific substrate specific peroxidation (cytochrome c peroxidase)³ and hydroxylation (cytochrome P-450),⁴ and oxygen carrying (myoglobin and hemoglobin).⁵ Although there are small differences in the covalent structure of the porphyrin ring of the heme as it occurs in these natural systems (e.g. cytochromes of the a, b, and c),⁶ the surrounding protein medium is most responsible for these different activities of the heme.⁷

Electrostatic interactions are one of the most pervasive and extensively studied types of molecular interaction in proteins. The electrostatic interplay between groups of polarity ranging from charged (ionized acids and bases) through polar (carbonyls), polarizable (thiols and aromatics) to essentially non-polar (hydrocarbons) are perhaps the major factor determining the tertiary structure⁸ and dynamics of proteins.⁹ Moreover, electrostatics have been implicated to be important in enzyme catalysis¹⁰ and enzyme/substrate¹¹ and

protein/protein recognition.¹² Many conformational changes in proteins upon oxidation/reduction¹³ or proton uptake/loss¹⁴ are assisted or caused by electrostatic linkage between the center which changes in charge and the rest of the protein. This type of mechanism is somewhat responsible for the well-documented Bohr effect in hemoglobin.¹⁴ Similarly, as will be modeled in this thesis, a negative charge taken upon reducing some protein center can cause a positive charge uptake at another location in that protein. This type of process likely occurs in the proton/electron coupling and subsequent proton pumping¹³ which drives ATP formation in aerobic respiration. To better understand electrostatic effects in proteins it is necessary to have systems in which the observed phenomena (e.g. electronic spectra and redox potential) can be isolably and quantitatively linked to the dielectric of the intervening medium and changes in charge density at specific sites in that system. These types of studies are best for laying the empirical groundwork for the theoretical modelling needed to predict and interpret the extent of electrostatic interactions in proteins.

The free energy of interaction between two charges q_1 and q_2 is defined by Coulomb's Law

$$\Delta G = 332q_1q_2/\epsilon r_{12} \text{ kcal/mole}$$

where it is assumed that the charges are embedded in a homogeneous medium of macroscopic dielectric constant ϵ and separated by a distance r_{12} in Å. Obviously, proteins are not homogeneous in structure and cannot necessarily be assumed to obey strictly classical (macroscopic) behavior in their electrostatic interactions. However, early models made the classical approximation and treated the protein medium as essentially uniform because of a lack of detailed structural information. Thus, an effective dielectric constant

$$\epsilon_{\text{eff}} = 332q_1q_2/\Delta G$$

was used to approximate how charge-charge interactions were mediated by the protein.

These models also assumed that the protein was spherical and thus predicted that all charge would be on the outside surface of proteins.¹⁵ Since there was considerable evidence by that time that charged groups existed which were somewhat buried in the protein matrix, the theory was modified to take into account stabilization of charge by partial water solvation.^{16,17} With further crystal structure data available, electrostatic models were formed in which the distance of the charged groups from solvent was not only taken into account through solvation energy of the charged group but also through the distance dependence of its medium's dielectric constant.¹⁸ Since the bulk dielectric constant of dehydrated polyamides and proteins has been shown experimentally to be approximately 3-4 and the dielectric constant of water is 80, it is very important to consider how far a charge is away from water since it will be "shielded" drastically the closer any water is to it. Recent models have used highly resolved crystal structures and molecular modelling of disordered groups to simulate electric fields at locations in the protein by considering the specific geometry of the protein. One method theoretically embeds specific dipolar and polarizable residues of the protein in a surrounding protein matrix of dielectric constant 2-4 and then surrounds the protein with the dielectric 80 water constant. The electric field at any location in this 3-dimensional array is then numerically calculated using the linearized Poisson-Boltzmann equation.¹⁹ These calculations have been shown to be more successful in predicting long-range interactions than short ones. Another geometry-specific method considers the static and induced polarity of all the atoms in the protein and close to its surface explicitly, which are then allowed to interact with each other through a medium of dielectric constant 1; thus, the residues of the protein

and surrounding atoms are responsible *a priori* for the dielectric constant inside the protein. This sophisticated approach has been used to calculate energetics of ionized groups in proteins, catalytic free energy stabilization of transition states, and redox potential differences based upon specific dielectric effects:²⁰ The results agree with experiments within reason (1-5 kcal/mol); however, the large number of parameters and complexity of calculations make it difficult to determine which parts of the model best parallel experimental reality. Thus, without further data to refine these models, they are limited to rationalizing rather than predicting electrostatic phenomena in proteins.

Some attempts have been made to determine protein effective dielectric constants. Measurements were made of charge-charge interactions in site-specific mutants of subtilisin.²¹ From the shifts in pK_a of a histidine produced as a result of substitution of charged residues for uncharged ones at distances of 10-15Å away, effective dielectric constants of 50-100 were calculated. Lower values of ϵ_{eff} (greater pK_a shifts) roughly corresponded to more protein being between the histidine and the charged mutant. Similar studies were performed when surface lysines of cytochrome c were modified with *m*-trifluoromethylphenylcarbamoyl. This reagent basically converts these residues from positively charged to neutral. By measuring the change in redox potential of the heme from unmodified to modified protein an effective dielectric constant ranging from 44-128 was obtained.²² An effective dielectric constant was also calculated for the interaction between the heme propionate and heme iron in cytochrome c_{551} .²³ By monitoring the redox potential of the heme iron as a function of pH with concomitant titration of the propionyl, an effective dielectric constant of 27 was calculated. This lower value of ϵ_{eff} for this experiment (indicating a greater comparative communication between charged groups) could be due to the direct covalent link between them (i.e. an inductive effect of

heme propionyl group). A significant problem with all of the experiments just described is that at least one of the charged groups is completely exposed to the solvent. Therefore, the measured effective dielectric constants would be expected to reflect more the dielectric constant of the solvent than that of the protein. This seems to be the case since ϵ_{eff} 's are much closer to 80 than to 3-4.

A better indicator of the actual protein dielectric would come from a measurement of the interaction of buried charges. However, this situation rarely exists in proteins. From survey of 36 globular proteins only six completely buried ion pairs were discovered.²⁴ This scarcity of buried charged would suggest that it is very energetically unfavorable to have charges in the protein interior which would in turn imply that the dielectric constants of the interior of proteins (even when the protein is in water) is considerably lower than the dielectric constant of water. This data is contrary to the previously described experiments²¹⁻²³ and free energy perturbation calculations.²⁰ Unfortunately, dielectric constants cannot be determined for the medium between existing buried charge pairs since no electrostatic perturbations, like titration, can be done on one of the charges while monitoring changes in another because they are, of course, not solvent accessible.

Some experiments have been performed, however, that shed light on the nature of the intrinsic protein dielectric. Since the ferrous heme is neutral while the ferric heme has a positive charge, a more polar (higher dielectric) environment surrounding the heme would favor the ferric form and in turn lower the $\text{Fe}^{3+/2+}$ reduction potential and *vice versa*. This dielectric effect is thought to be one of the reasons for the greater than 500mV span of reduction midpoint potentials for heme proteins.²⁵ The reduction potentials of synthetic hemes have been shown to vary as much as 300mV depending on whether they are in

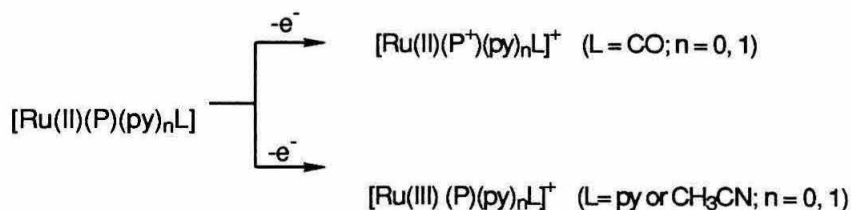
high or low dielectric solvents.²⁶ Similarly, methionine/histidine ligated hemes and peptide-linked hemes in water have E_0 's in the range of -50 – -100mV (vs. NHE) while cytochrome c which contains a methionine/histidine-ligated heme in a very nonpolar heme cavity has a reduction potential of +260mV (vs. (NHE)).²⁷ Corresponding data shows that mono-imidazole ligated hemes in 30% v/v dioxane/water ²⁸ (a very polar solvent mixture) is 250mV lower in redox potential than the mono-imidazole ligated heme in myoglobin and the hemoglobin beta chain.²⁹ The hemoglobin and myoglobin pockets are known to be nonpolar from crystal structures (most likely to deter the formation of O_2^- from heme oxidation instead of oxygen binding).³⁰

However, these comparisons of protein and model porphyrin systems must be viewed with some caveats. First, the iron-axial ligand bond distance can differ. For instance, the Fe-S distance is at least 0.1Å shorter in cytochrome c than in any of the models; some authors have suggested that this shortening gives rise to the 350-300mV potential increase, and thus is an example of a protein controlling redox potentials through geometrical restraint.³¹ A second consideration is that many other factors aside from dielectric changes and even electrostatic effects in general affect the midpoint potential of redox centers in proteins. Using the example of myoglobin in the metaquo (Fe^{3+}) state: bound to the iron is a water molecule, the oxygen of which is hydrogen bonded to a nearby histidine hydrogen³²; without this interaction the redox potential was shown to be 120mV higher.³³ Similar hydrogen bonding interactions between the protein ($NH\cdots S$) and the 4Fe-4S clusters in ferredoxin and the high potential iron-sulfur protein (HiPIP) are thought to be somewhat responsible for the 800mV difference in redox midpoint potential for the 4Fe-4S clusters, which are otherwise structurally very similar, in these proteins.³⁴ Another factor that can affect redox potentials in proteins is oxidation state-linked conformational

changes. These changes in protein structure upon reduction can be quite significant (e.g. hemoglobin)³⁰ and are well within the magnitude (5-10 kcal/mol) to stabilize preferentially one oxidation state a few hundred millivolts compared to another. A possible example of this effect is the difference in midpoint potentials between membrane bound and soluble cytochrome c. The potential for the membrane-bound form is expected to be higher because the nonpolar hydrophobic membrane has a lower dielectric constant than water. In fact, the potential for the membrane-bound form is 30mV lower³⁵; a likely explanation is that there is a conformational change in cytochrome c upon membrane binding that favors the oxidized (charged) heme.

Another factor aside from electrostatics that affects redox potentials is the nature of the ligands of the redox center. Changes in hardness/softness, stereochemistry and ligand field effects can all affect the midpoint potential in straightforward ways. One example is the difference in reduction potential between bis-histidine and histidine/methionine-ligated hemes, 150mV higher for the latter in model complexes.³⁶ This rise in E^0 is mainly due to the preferential stabilization of the Fe^{2+} through backbonding by methionine compared with the stronger Lewis acid histidine. A similar case is that of cytochrome P-450 from *P. putida* which undergoes a low to high spin change upon substrate binding and experiences an accompanying 170mV increase in redox potential. There is significant mechanistic and spectroscopic evidence that the binding occurs at the iron and is part of an enzyme activation making the potential of the heme accessible to the native reductant, putridanedoxin.³⁷ In a related situation, the nature of axial ligation in horseradish peroxidase (HRP) seems to be responsible for iron being oxidized from III to IV³⁸ in contrast to model compounds like $Fe^{3+}Cl(Tetraphenylporphyrin)$ where the porphyrin ring is oxidized instead of the iron(III) being further oxidized.³⁹ The effect of

axial ligation on the center of oxidation is well documented for Cu(I), Ni(III),⁴⁰ and Ru(II)⁴¹ porphyrin model compounds as well. An example



P = tetraphenyl, octaethyl, or etioporphyrin
 py = pyridine

demonstrates how an axial ligand can influence the relative energy positions of the metal d- π and porphyrin HOMO's. In the above case the energy of the Ru(II) d π HOMO becomes lower than the porphyrin HOMO through backbonding when CO is bound so that porphyrin is oxidized before Ru(II).

Until now I have primarily discussed enthalpic factors which affect the energetics of charged groups in proteins; however, entropic considerations are usually of similar magnitude as is well documented by reduction/oxidation thermodynamic data.⁴² An analysis of the entropy of reduction (ΔS°_{rc}) for small molecules is a good place to start since even for these single-metal, one-electron redox complexes, the factors which govern ΔS°_{rc} are somewhat complex. One of the most prominent factors of ΔS°_{rc} is the entropic component of the Born hydration energy:

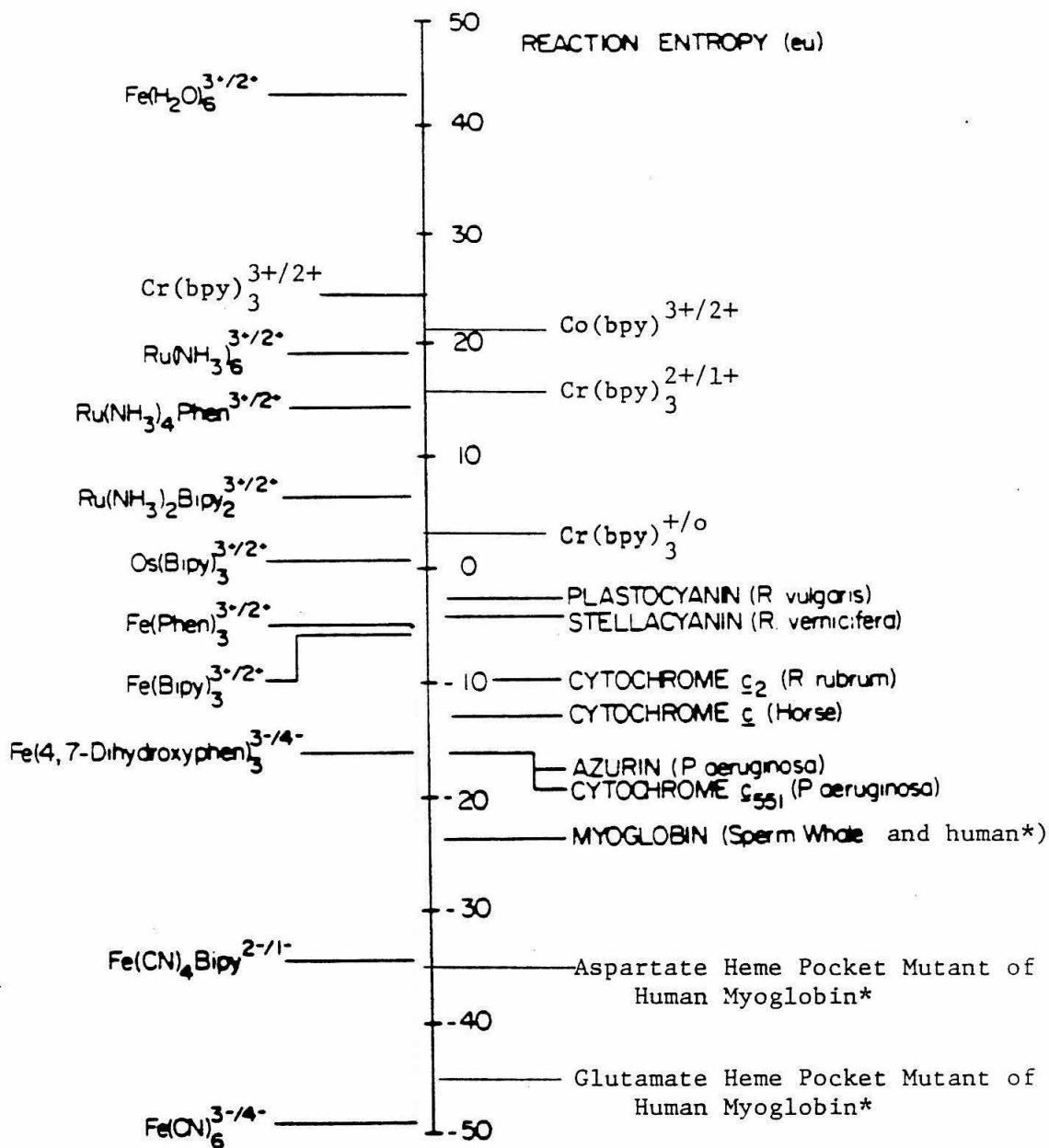
$$\Delta S^{\circ}_{rc, \text{Born}} = \frac{e^2 N}{2\epsilon T} \left[\frac{d \ln e}{dT} \right] (Z_{\text{ox}}^2 - Z_{\text{red}}^2)$$

e is the electronic charge, N is Avogadro's number, r is the radius of the ion complex, and Z is the charge of the ion. Some physical consequences of this expression are (temperature remaining constant) that the entropy change of a

solvated charge system upon reduction will be relatively small if (1) the ion has a small absolute charge value, (2) is large in size, and (3) is in a higher dielectric medium. Moreover, the ΔS°_{rc} is expected to be positive for positively charged redox couples and negative for negatively charged redox couples. The data qualitatively supports these predictions (see figure 1). The $\text{Cr}(\text{bpy})_3^{+|n/n-1|}$ data clearly confirms a charge magnitude dependence.⁴³ Similarly, as can be somewhat gleaned from figure 1, metal ions with large ligands like bipyridine or phenanthroline demonstrate the predicted size effects^{43,44}; that is, they generally have smaller ΔS°_{rc} 's than the complexes with smaller ligands. Studies have also supported the inverse dependence of magnitudes of ΔS°_{rc} on the solvent dielectric constant.⁴³ Further, experiments have shown for greater than 95% of metal redox couples tested that negatively charged redox couples have negative ΔS_{rc} 's and *vice versa*.⁴³⁻⁴⁵

The exceptions to this last correlation are positive metal couples which have large ligands and usually small magnitude of charge (e.g. ferrocene/ferricinium).⁴⁶ Small charge and large size would tend to push ΔS°_{rc} down as already discussed. At these lower $\Delta S^{\circ}_{rc, \text{Born}}$ values the effect of any non-Born entropic factors should become more obvious. One deviation from Born behavior which has been well documented is the increase in *intrinsic* solvent entropy when a charged moiety is solvated. This effect would be most pronounced for solvents with extensive hydrogen bonding networks like water which cause them to be highly ordered. An increase in charge magnitude at a solvated redox couple would break the hydrogen bonds of these solvents, decreasing the total entropy of the system (in contrast to the Born effect). An empirical relation has been constructed where this effect is ascribed to a constant term multiplied by the solvent acceptor number (AN) which is believed to be a good measure of solvent ordering.⁴³ This $\Delta S^{\circ}_{rc}(\text{AN})$ does not have as

Figure 1. Reaction entropies for some transition metal and metalloprotein redox couples. Refs. 42-52.



* vide infra

great a redox couple size or charge magnitude dependence as the Born entropic term so that when added to the Born term, an extremely good functional fit for the available ΔS°_{rc} values of a large number redox couples in different solvents can be obtained.

Other deviations from the Born equation are thought to be caused by very specific, microscopic interactions of the ligands with the solvent. One example is the increased reaction entropy for redox couples containing aquo ligands compared with those with other ligands (e.g., thiocyanate, amine, or carboxylate) in water.⁴⁴ It is thought that the aquo ligands hydrogen bond more strongly and order the solvent more strongly than the other ligands. These hydrogen bonds presumably occur at the hydrogens of the bound water with the oxygens of the solvent to relieve the electronic strain of the aquo ligand's oxygen caused by its being attached to the electropositive central cation. Accordingly, when the central cation is reduced the electronic strain on the bound oxygens is somewhat relieved so that hydrogen bonds to the aquo ligand's hydrogens are less strong (and likely). Thus, the rigidity of the solution sphere is somewhat relaxed, increasing entropy. In addition to ligand substitution studies, this phenomenon seems to be reasonably well supported by experiments in which ΔS°_{rc} was determined for aquo cations (lanthanide ions) with large first coordination spheres⁴⁴ and for redox couples in D_2O where hydrogen bonding is expected to be stronger.⁴⁶ In addition, ΔS°_{rc} will be greater if upon reduction a complex loses a solvent molecule ligand. For example, one way the entropy change for the liberation of a single H_2O molecule can be estimated is by subtracting the normalized entropy contribution of water of hydration in a solid (9.4 cal/deg•mol)⁴⁷ from the entropy of liquid H_2O (16.7 cal/deg•mol) giving 7.3 cal/deg•mol.⁴⁸ This value is very much in accord with the results of variable temperature cyclic voltammetry experiments

of $\text{Cu}^{3+/2+}$ and $\text{Ni}^{3+/2+}$ peptides in which ligand field considerations and kinetic and EPR evidence indicate that the copper (III) coordinates two water molecules upon reduction whereas the nickel (III) gives up two coordinated water molecules upon reduction. The $\Delta S^{\circ}_{\text{rc}}$ of the former couples decreased (13-15 cal/deg•mol) while that of the latter increased by an equivalent magnitude.

One final factor which has been postulated to affect $\Delta S^{\circ}_{\text{rc}}$ is the type of orbital an electron is accepted into upon reduction. If an electron is accepted into an anti-bonding orbital upon reduction, the metal-ligand bond lengths should get longer and thus to a first order approximation the ligands should have more freedom of motion and greater entropy than if the electron had gone into a non-bonding or bonding orbital and the metal-ligand bonds had not become longer. This effect seems to be evident for $\text{M}^{3+/2+}(\text{bipyridine})_3$ complexes; $\text{Cr}^{3+}(\text{bpy})_3$ and $\text{Co}^{3+}(\text{bpy})_3$ have an electron go into an anti-bonding orbital upon reduction whereas $\text{Os}^{3+}(\text{bpy})_3$ and $\text{Fe}^{3+}(\text{bpy})_3$ have an electron go into a bonding orbital and have correspondingly lower $\Delta S^{\circ}_{\text{rc}}$'s (Figure 1).

Obviously, all of the factors just mentioned which affect $\Delta S^{\circ}_{\text{rc}}$ for small molecules can be applied to proteins as well. A difference, however, is that a redox cofactor in a protein is usually surrounded somewhat by the protein matrix and therefore shielded from water. If one did not consider the surrounding protein as part of the redox complex but as peptide solvent, then one would expect a lower effective dielectric constant for the redox moiety and a stronger Born component for $\Delta S^{\circ}_{\text{rc}}$ ($1/\epsilon$ dependence). On the other hand, if the protein is considered part of the redox complex, the radius of the complex would be tremendous and would make $\Delta S^{\circ}_{\text{rc}}$ (Born) essentially go to zero through the $1/r$ dependence. The latter scenario seems to be born out by experiment. For example, reaction entropies of metalloproteins are not correlated with the

charge of the redox moiety (as the Born equation would predict) or even the overall charge of the protein.⁴⁹

One trend that is apparent in redox protein ΔS°_{rc} 's is that they are all significantly lower than would be expected for small molecule complexes of the same charge (figure 1). One explanation for this phenomenon is that the water disruption effects,⁴³ which increase entropy with increasing charge, dominate because of the suppressed Born term. This would explain why ΔS°_{rc} is negative for almost all heme proteins because the charge of the oxidized heme (+1) is neutralized upon reduction. Another effect related to charge neutralization has been proposed.⁵⁰ Basically, the authors suggest that upon reduction and thus neutralization of the redox center inside the protein, the cavity of the protein which holds the redox center becomes less polar causing the surrounding hydrophobic non-polar interior of the protein to be attracted more to the cavity. This effect would give an overall contraction of the protein causing restriction in protein motion and decreasing entropy. A corollary to this hypothesis is that ions or water molecules inside or partially buried by the protein before reduction could become trapped or at least have their motional freedom restricted when the protein contracts upon reduction. Entropy would again be decreased by this process as was thought to be the case for several blue copper proteins.⁵¹

A related proposal is that the loss of entropy due to protein tightening upon reduction is diminished the more the redox center is exposed to water.⁵² The more positive ΔS°_{rc} 's for cytochrome c' proteins, whose heme sites are more exposed, compared with the ΔS°_{rc} 's of cytochrome c are used as evidence to support this theory. Data from cytochrome c₂ is also in accord. However, cytochrome c₅₅₁ has a highly exposed heme group (much more so than cytochrome c) yet shows a more negative entropy of reduction than

cytochrome c.⁵¹ Moreover, Stellwagen compiled crystal structure data on six heme proteins and published an empirical relationship between E_o' and heme solvent exposure⁵³:

$$E_o' = -15(\% \text{ exposure}) + 345\text{mV(NHE)}$$

From this equation the redox midpoint potential (E_o') is expected to decrease as heme solvent exposure increases. Since E_o' would increase if ΔS^o_{rc} increased, this equation and the theory that ΔS^o_{rc} increases with solvent exposure are at odds.

Clearly, the factors which affect the redox thermodynamics of proteins need to be studied in more detail. It seems as though evolution has fine-tuned the interplay of these factors for the function of electron transfer proteins. One patent example is the observed entropy-enthalpy compensation effect in cytochrome c⁵⁴ and cytochrome P-450.⁵⁵ In these cases, the proteins from different organisms (or compartments of an organism) achieve the appropriate E_o' from physiological function with different enthalpic and entropic contributions. How the energetics of a protein are controlled for a specific physiological process in general is a question which deserves to be addressed more thoroughly.

In Chapter 2 of this thesis the effect of the protein environment on the redox thermodynamic properties of heme will be determined through electrochemical, spectroscopic, rheological properties of site-directed mutants of recombinant human myoglobin. In Chapter 3 the electron and nuclear magnetic properties of the heme of the site-directed mutants will be analyzed to distinguish between chemical and electrostatic interactions which affect the heme. In Chapter 4 further mutations will be constructed to facilitate ruthenium reagent modification of the previously constructed mutants of human myoglobin. The effects of placing charged groups in the heme pocket on kinetics will then

be studied. In Chapter 5 the kinetics of electron transfer of myoglobin in which the heme pocket has now been chemically altered to effect very specific changes in the axial ligation of the heme will be analyzed.

References

1. Okunuki, K., Kamen, M. D., Sekuzu, I., eds. *Structure and Function of Cytochromes* University Park Press, Baltimore (1968).
2. Schonbaum, G. R. and Chance, B. *The Enzymes* 13, 363 (1976).
3. Williams, P. G. and Stewart, P. R. *Arch. Microbiol.* 107, 63 (1976).
4. Hayashi, O. *Molecular Mechanisms of Oxygen Activation* Academic Press, New York (1974).
5. Perutz, M. F. *et al.* *Nature* 185, 416 (1960).
6. Ambler, R. P. *The Evolution of Metalloenzymes, Metalloproteins, and Related Materials* G. J. Leigh, Ed., Symposium Press, London (1977).
7. *Advances in Inorganic Biochemistry* vol. 7, G. L. Eichorn and L. G. Marzilli, Eds., Elsevier, New York, p. 1 (1988).
8. Fersht, A. *Enzyme Structure and Mechanism* 2nd ed., W. H. Freeman and Co., New York (1985).
9. Karplus, M. *Biomolecular Stereodynamics* vol. 1, R. H. Sarma, ed., Adenine Press, Guilderland, NY, p. 211 (1981).
10. Warshel, A. *Proc. Natl. Acad. Sci. USA* 75, 5250 (1978).
11. Warshel, A. and Russel, S. T. *Q. Rev. Biophys.* 17, 283 (1985).
12. Salemme, F. R. *Ann. Rev. Biochem.* 299 (1977).
13. Hatefi, Y. *Ann. Rev. Biochem.* 1015, (1985).
14. Perutz, M. F. *Ann. Rev. Biochem.* 48, 327 (1979).
15. Tanford, C. and Kirkwood, J. G. *J. Am. Chem. Soc.* 79, 5333 (1957).
16. Shine, S. J.; Hanania, G. I. H.; Gurd, F. R. N. *Biochemistry* 13, 2967 (1974).
17. Matthew, J. B. and Richards, F. M. *Biochemistry* 21, 4989 (1982).
18. Gilson, A. J. *et al.* *J. Mol. Biol.* 183, 503 (1985).
19. Gilson, M. K. and Henry, B. *Biopolymers* 25, 2097 (1986).
20. Churg, A. K. and Warshel, A. *Biochemistry* 25, 1675 (1986).
21. Russell, A. J. and Fersht, A. R. *Nature* 328, 496 (1987).

22. Rees, D. C. *J. Mol. Biol.* 141, 323 (1980).
23. Rogers, N. K., Moore, G. R., Sternberg, M. J. E. *J. Mol. Biol.* 182, 613 (1985).
24. Rashin, A. and Henry, B. *J. Mol. Biol.* 173, 515 (1984).
25. Henderson, R. W. and Morton, T. C. *CRC Handbook of Biochemistry* Chemical Rubber Co., Cleveland, J41 (1973).
26. Kassren, R. J. *Proc. Natl. Acad. Sci. USA* 69, 2263 (1972).
27. Harbury, H. A. *et al. Proc. Natl. Acad. Sci. USA* 54, 1658 (1965).
28. Warne, P. K. and Hager, L. P. *Biochemistry* 9, 1606 (1970).
29. Hanania, G. I. H. *Ph. D. Thesis* Cambridge, England (1953).
30. Reed, C. A. and Chung, S. K. *Proc. Natl. Acad. Sci. USA* 74, 1780 (1977).
31. Moore, G. R. and Williams, R. J. P. *FEBS Lett.* 79(2), 229 (1977).
32. Phillips, S. E. V. and Schoenborn, B. P. *Nature* 292, 81 (1981).
33. Tsukahara, K. *Chem. Lett.* 1291 (1987).
34. Carter, C. W. *Iron Sulfur Proteins* Academic Press, New York, NY, vol. 3, p.157 (1977).
35. Huang, Y. Y. and Kimura, T. *Biochemistry* 23, 2231 (1984).
36. Mashiko, T. *et al. J. Am. Chem. Soc.* 101, 3653 (1979).
37. Sligar, S. G. and Gunsalus, J. C. *Proc. Natl. Acad. Sci. USA* 73, 1078 (1976).
38. Schulz, C. E. *et al. FEBS Lett.* 103, 102 (1979).
39. Gans, P. *et al. Nouv. J. Chimie* 5, 203 (1981).
40. Cocolios, P. and Kadish, K. M. *Isr. J. Chem.* 25, 138 (1985).
41. Brown, G. M. *et al. J. Am. Chem. Soc.* 95, 5939 (1973).
42. Ellis, W. *Ph. D. Thesis* California Institute of Technology, Pasadena, CA, (1984).
43. Hupp, J. T. and Weaver, M. J. *Inorg. Chem.* 23, 3639 (1984).

44. Yee, E. L. *et al.* *J. Am. Chem. Soc.* 101, 1131 (1979).
45. Yee, E. L. and Weaver M. J. *Inorg. Chem.* 19, 1077 (1980).
46. Weaver, M. J. and Nettles, S. M. *Inorg. Chem.* 19, 1641 (1980).
47. Latimer, W. M. *Oxidation Potentials* 2nd ed., Hall, Englewood Cliffs, NJ, p.364, (1952).
48. *NBS Tech. Note.* No. 270-3 (1952).
49. Youngblood, M. P. and Margerum, D. W. *Inorg. Chem.* 19, 3068 (1980).
50. Taniguchi, V. T. *et al.* *Pure and Appl. Chem.* 52, 2275 (1980).
51. Scott, N. S., Anson, F. C., Gray, H. B. *J. Am. Chem. Soc.* 101, 455 (1979).
52. Taniguchi, V. T. *et al.* *Adv. Chem. Ser.* 201, 51 (1982).
53. Stellwagen, E. *Nature* 275, 73 (1978).
54. Huang, Y. Y. and Kimura, T. *Biochemistry* 23, 2231 (1984).
55. Huang, Y. Y. *et al.* *Biochemistry* 25, 1390 (1986).

CHAPTER 2

THE EFFECTS OF BURIED IONIZABLE AMINO ACIDS ON THE REDUCTION POTENTIAL OF RECOMBINANT HUMAN MYOGLOBIN

Introduction

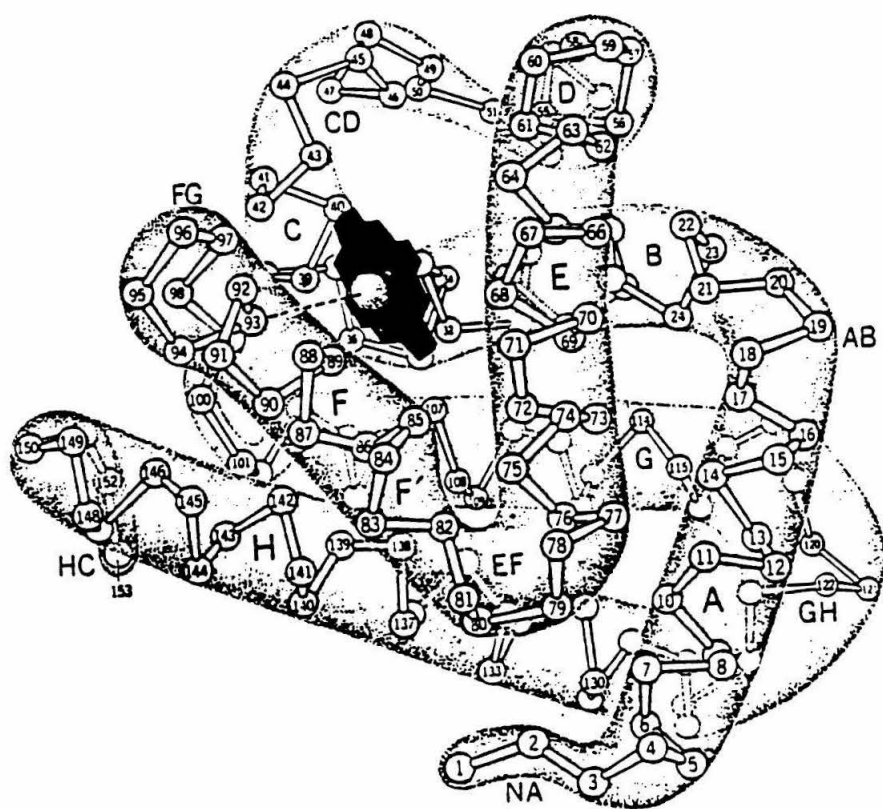
Here are reported measurements of the temperature dependences of the reduction potentials of wild-type and four single-site mutants of human myoglobin. Specifically, mutations in which Val68 has been changed to the potentially charged residues Glu and Asp, and to Asn, which is uncharged and polar, have been investigated in order to evaluate the influences of the local electrostatic field on the redox properties of this protein.

These studies were motivated by extensive theoretical^{1,2} and experimental^{3,4} investigations of the degree to which a protein can influence the redox potential of a prosthetic group or stabilize separated charges following electron transfer. Important factors that affect the reduction potential of a protein include (1) the nature of ligands at the redox center,³ (2) conformational changes associated with reduction, and (3) electrostatic interactions of the redox center with charged groups both on the surface⁵ and in the interior of the protein.⁶ The latter interactions are affected by water molecules and ions both in solution and bound at specific sites on the protein, and dipolar and polarizable groups that are present within the protein.⁷ In a recent report, the magnitude of electrostatic interactions between pairs of charged residues was estimated in mutants of subtilisin.^{8,9} These studies focused on interactions between residues that are accessible to aqueous solvent. However, little is known about the magnitudes of electrostatic interactions between charged groups that are buried within the protein. Since surface charges are well solvated by water, their interactions with the redox center are expected to be smaller than those of buried charges.

In order to assess the magnitude of various contributions to E^0 , studies have typically been made of structurally similar proteins and most extensively for the cytochromes.⁴ Such analyses are complicated in that the proteins

studied differ at several positions in their primary amino acid sequence. With the advent of site-specific mutagenesis, the effects of individual amino acid changes on redox thermodynamics can be systematically studied. We have chosen myoglobin because it has been extensively characterized and because of the recent availability of a cDNA clone for human Mb and an efficient method for overproduction in *E. coli*.¹⁰ An x-ray structure of recombinant human Mb is now available which shows that residues in the heme pocket are the same as those found in sperm whale Mb (figure 1). Also, the positions of residues inside and outside the pocket are virtually superimposable. Moreover, the optical, ligand binding, nuclear magnetic resonance (NMR), and redox (*vide infra*) properties of the two proteins are very similar.¹⁰ Residue Val68 (also denoted ValE11) is situated below heme ring I¹¹ on the distal side of the heme pocket and within van der Waals contact of the heme (Figure 2). Val68 is completely inaccessible to external solvent in sperm whale metaquo Mb.^{11,12} (Metaquo refers to the heme iron in the ferric state with water as the only exogenous ligand.) Val68 is readily detected in the NMR spectra of carboxy Mb's¹³ and appears in wild-type human carboxy Mb at essentially the same chemical shift as in the sperm whale derivative.¹⁴ In the naturally occurring, single-site hemoglobin (Hb) mutants, Hb Milwaukee and Hb Bristol, Val68 in the β chains is replaced by Glu and Asp, respectively. The Glu in Hb Milwaukee has been shown by x-ray crystallography¹⁵ to be weakly coordinated to the heme iron (III), replacing a water molecule that normally occupies this site in wild-type metaquo Hb's and Mb's.¹⁶ Hb Bristol is much less stable and has not been well characterized.¹⁷ However, examination of computer graphics models shows that the shortening of the side chain by one methylene group that occurs by replacing Glu by Asp makes it impossible for the Asp carboxyl group to coordinate to iron without substantial protein conformational changes. That Hb

Figure 1. Structure of deoxy sperm whale as determined from X-ray crystal diffraction data. Capital letters denote standard helix nomenclature. The heme iron is coordinated to residue 93, the axial histidine.



can tolerate such drastic changes at this residue position prompted us to replace Val68 with Glu and Asp in human Mb. These mutants are named V68E and V68D, respectively. To determine whether the Asp is protonated when buried in the protein, we replaced Val68 by Asn to give the mutant V68N'.¹⁸

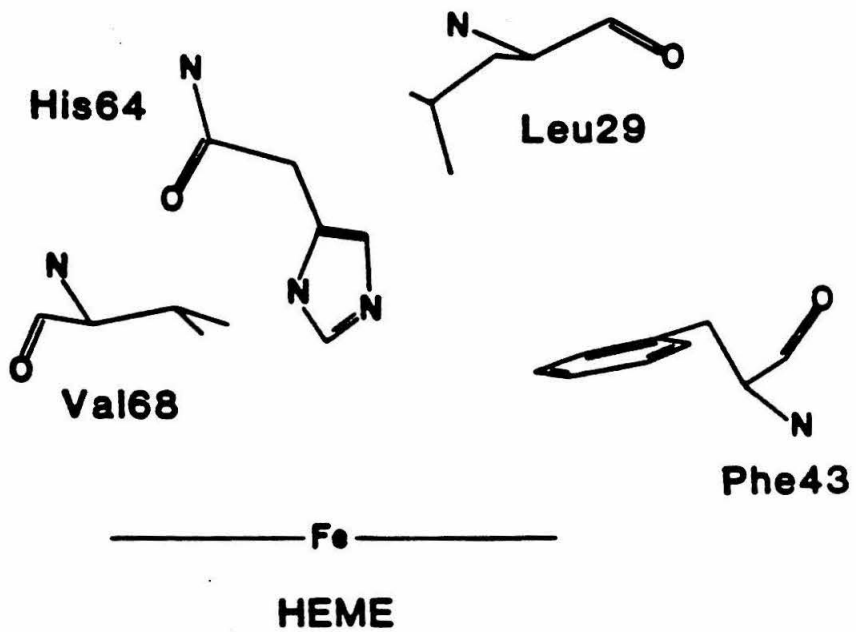
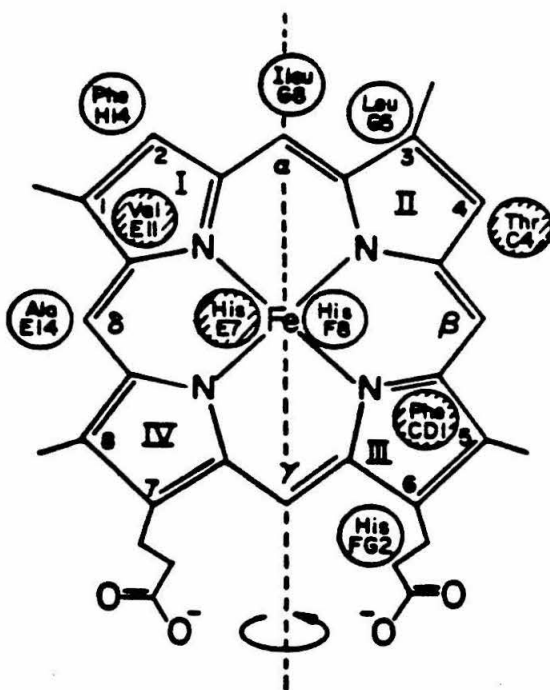
<u>Myoglobin</u>	<u>Mutation(s)</u>
WTMB	—
C110A	Cys110ÆAla
V68D	Val68ÆAsp
V68E	Val68ÆGlu
V68N	Val68ÆAsn
V68D'	Val68ÆAsp, Cys110ÆAla
V68E'	Val68ÆGlu, Cys110ÆAla
V68N'	Val68ÆAsn, Cys110ÆAla

Experimental

All of the mutations were constructed by using the Kunkel method.¹⁹ In each case the entire protein coding region was sequenced to ensure that no additional mutations had occurred. Expression and purification were essentially as described previously.¹⁰ The standard free energy, and the entropy and enthalpy changes at pH 7.0 associated with reduction of the ferriheme were determined by using isothermal variable temperature spectroelectrochemistry (figure 6 and Table 1).^{20,21}

The advantages of spectroelectrochemistry (namely, greater tractability compared with coulometry and accuracy compared with indirect calculations) have been well documented.²² Reduction potential measurements were made with an optically transparent thin-layer cell (OTTLE) with an electrode configuration and accompanying equipment previously described²³ with the following modifications. The optical path length was approximately 0.24mm with two teflon tape spacers (Dilectrix Corp.) between the gold minigrad working electrode (Interconics, 100 lines/inch, 60% transmittance). An 18-gauge copper wire was connected to the working electrode with Tra-Duct 2902 conducting epoxy (Tra-Con) and not solder. Further, the tapers (standard 7/25) in the lucite block of the OTTLE which lead into the thin-layer cavity were bored down so that the ground glass auxiliary electrode holder and the reference electrode were within 0.5mm of touching the filling port which leads into the thin-layer cavity. This modification made sample loading more difficult, but a sample volume of 250 μ l (compared with 700 μ l before) could now be used. This modification was especially useful because of the scarcity of mutant proteins prior to the final optimization of the purification procedure (Chapter. 5 in this thesis).

Figure 2. Positions of amino acids in the heme pocket of sperm whale myoglobin.²⁶ Shaded residues are on the distal side of the heme group.



The sample was loaded into the OTTLE/electrode assembly in an inert atmosphere box (He-63-P, Vacuum Atmosphere Co.). The filled apparatus was then placed in a gas-tight, stainless steel shroud to maintain anaerobicity once the OTTLE was transferred out of the inert atmosphere box. The most difficult part of the loading procedure is the avoidance or extraction of trapped air from the OTTLE. These bubbles will cause anomalous absorbance readings when they are in the spectrophotometer path length and will cut the electrical circuit if they rise into the filling ports; further, when they cut the circuit a potential buildup often occurs which will cauterize the protein sample. The method to avoid bubbles is to slowly fill the cell through a filling port by pipette while tilting the cell towards that port. Once the thin layer and filling ports are full, the greased auxiliary electrode and holders should be added first since the holder has a flat-bottom frit and is more likely to trap bubbles than the reference electrode holder. Trapped air was also avoided by coating the inside of the quartz windows with silane.

The protein solutions were dialyzed into pH 7.0 $\mu=0.1$ M sodium phosphate buffer after storage as ammonium sulfate precipitates (70%). The solution was purified through a G-25 Sephadex column prior to use. It was found that electrolysis occurred more quickly and the sample remained intact longer, the purer the sample was. Concentrations of myoglobins (0.3-1.2mM) were determined by monitoring at the Soret and alpha bands for each mutant using a Shimadzu UV-260 spectrophotometer. A smaller-molecule, electrochemically reversible redox couple (mediator) was added to the protein solution to facilitate electron transfer between the metalloprotein and the working electrode.²² Analytical grade $[\text{Ru}(\text{NH}_3)_6\text{Cl}_3]$ ($E^0=65\text{mV}$) was obtained from Strem, twice recrystallized and added for this purpose. Ruthenium hexammine is known not to interfere with the monitored absorption regions of

myoglobin or to bind to myoglobin.²⁰ A 1,1'-dimethyl-4,4'-dipyridiniumdichloride modified, gold minigrid was also considered instead of a soluble mediator, but this approach would probably not have given reversible enough electrolysis for spectroelectrochemistry.²⁴ The protein/mediator solutions were repeatedly degassed (2 seconds at 10^{-2} Torr) and stirred under purified argon (3-4 minutes) for a total of 30 minutes. The auxiliary electrode buffer (pH 7.0, $\mu=0.1M$, NaPi) and saturated KCl for the salt bridge were degassed using the freeze/pump/thaw technique for five cycles on a high vacuum line (10^{-5} Torr). Anaerobicity was maintained mainly to avoid oxygen binding to the Fe(II) heme and hydrogen peroxide formation upon electrolysis which would react with the protein (e.g., oxidation of cysteine to cysteic acid).²⁵ Further, the platinum working electrode was cleaned in concentrated nitric acid for 30 seconds before each use.

The protein was cycled between fully oxidized and reduced states for the midpoint potential determination at each temperature with greater than 98% reversibility in A_{555} for each cycle. The difference in E° depending on the direction of electrolysis was less than 1mV. Equilibrium of the heme electrolysis was apparent at each applied potential from stabilization of A_{555} and current cessation (less than 0.02mA). Minimum potential and absorbance changes observable were $\pm 0.1mV$ and ± 0.0001 absorbance units, respectively. Six or seven points were used in each Nernst plot. Least squares analyses of the Nernst plot gave the midpoint potentials (Figures 3 and 4). The following equation was used to determine the ratios of oxidized to reduced protein at each applied potential.

$$\frac{A_{555}(\text{red}) - A_{555}(\text{ox})}{A_{555} - A_{555}(\text{ox})} = \frac{[ox]}{[red]}$$

All Nernst plot slopes were within 3mV or RT/nF (60mV), and all correlation coefficients were greater than 0.995.

The OTTLE/electrode assembly was allowed to equilibrate for 6 hours after each temperature change (intervals of approximately 5°C). The reference electrode sometimes differed in temperature from the rest of the cell. However, these deviations from isothermality were never greater than 2°C so that the error arising from a thermal junction potential between the sample and the reference electrode was insignificant.²⁶ The deviations from isothermality were also corrected for using standard procedures.²⁷ Midpoint potential values were calculated at each temperature and plotted (Figure 6, Table 1). The time taken to reach electrolysis equilibrium was dependent upon the applied potential since this dictated the amount of mediator available for ET with the protein. Generally, electrolysis times were between 5 and 15 minutes for WTMB, V68N', and C110A and between 45 minutes and 2 hrs for V68E and V68D. The longer times for the last two were probably caused by the significant difference between E° for the mediator and these proteins (200mV).

Figure 3. Spectral changes occurring upon reduction of human metaquo myoglobin at pH 7, 25°C.

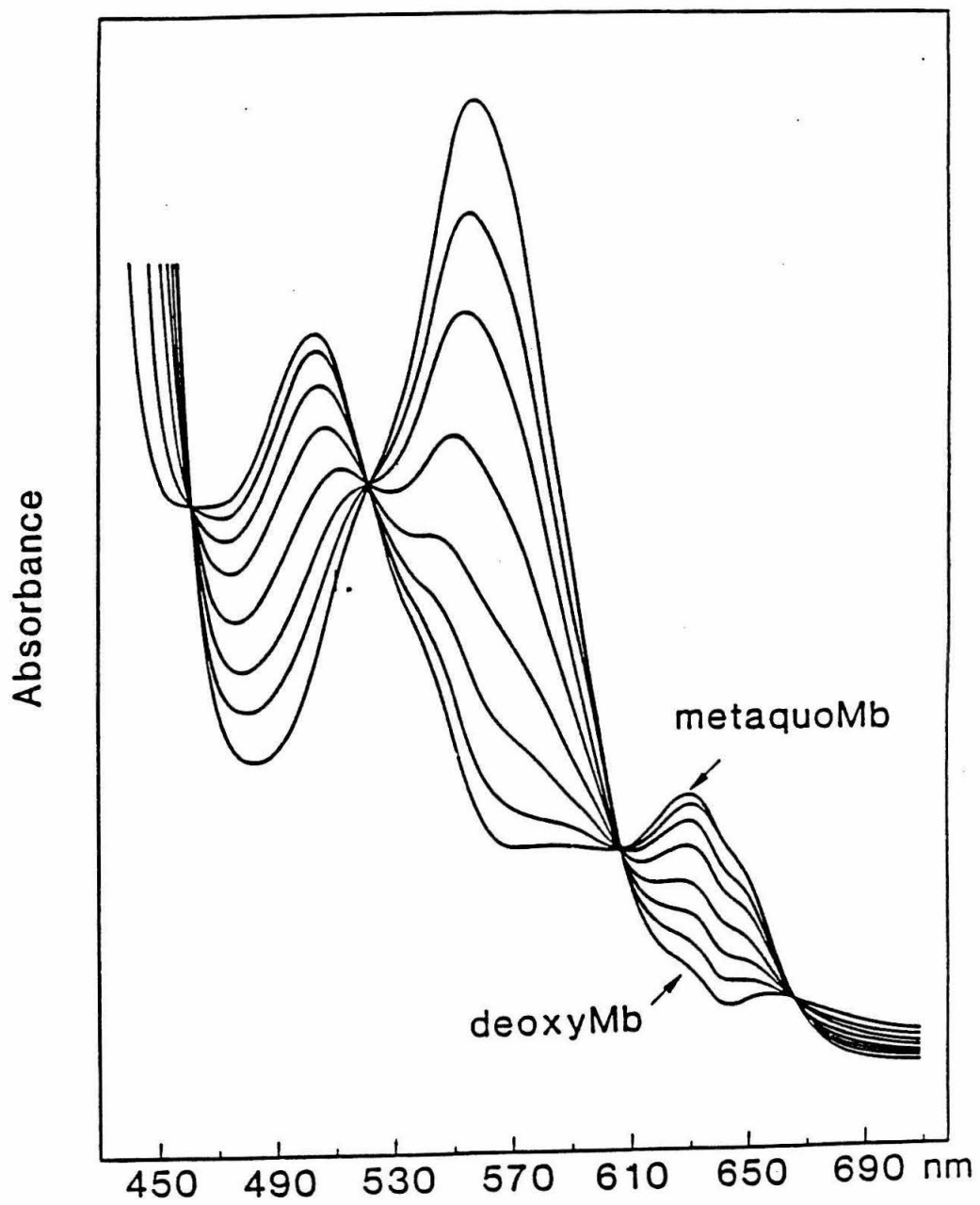
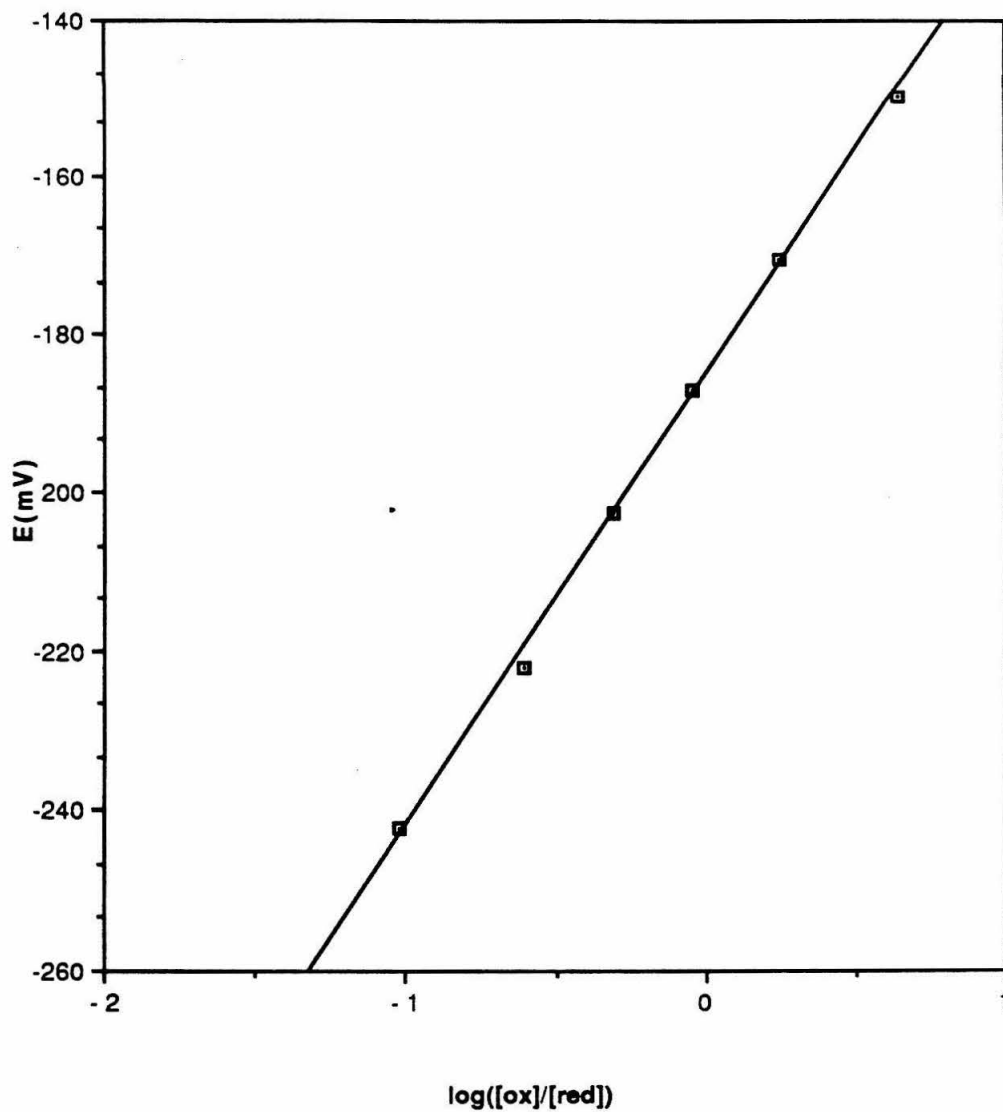


Figure 4. Nernst plot of the data in Figure 3. A least squares fit to the data yields $E^{\circ'}=59.3\text{mV}$ vs. NHE after conversion from reference to SCE. $r^2=0.998$, $RT/nF=57.6\text{mV}$.



Replacement of Val68 by the potentially charged residues Glu and Asp decreases E° by about 200mV, whereas replacement by the polar but uncharged residue Asn lowers E° by 82.7mV. These are substantial effects. Also, a subtle interplay occurs between the entropic and enthalpic contributions to changes in E° .

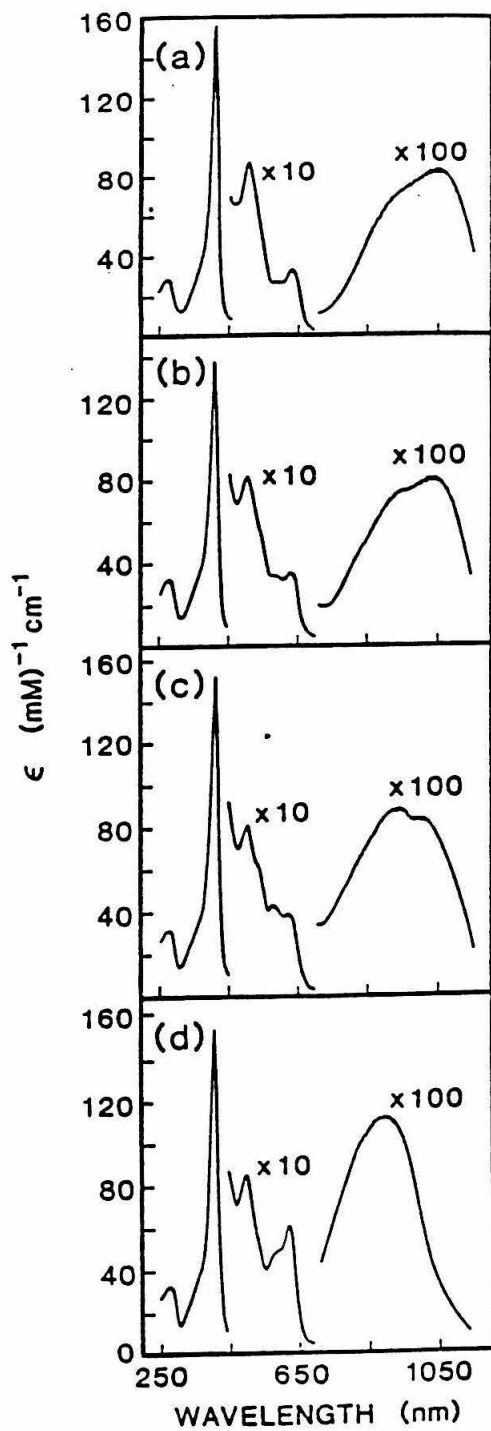
The non-denaturing anaerobic polyacrylamide gels (PAGE) contained 5% acrylamide, 0.125% bisacrylamide, 0.005% ammonium persulfate, 60mM MOPS, pH 7.7. The buffer was freeze/pump/thawed through five cycles (1×10^{-4} Torr) prior to transfer to an inert atmosphere box where the gel was mixed and then run at 150V for 1.5 hrs in a mini-gel apparatus (Hoefer). Care was taken to pour the gel quickly after the components had been mixed since polyacrylamide formation occurs much more rapidly in anaerobic conditions and can occur without initiator. Protein samples were dialyzed overnight in argon saturated buffer; moreover, sodium dithionite was added to reduce them before loading ($10 \mu\text{g}/\text{lane}$).

Analytical isoelectric focusing gels were obtained from Pharmacia. Protein isoelectric points were assigned relative to IEF standards (Pharmacia) and migration distances. Gels were run on an LKB multiphor power supply (model 2117) for 30 minutes.

Results and Discussion

The mutants have been characterized extensively.¹⁴ The following are salient features that are relevant for the interpretation of the results in Table 1. Two-dimensional NMR spectroscopy of the CO derivatives of C110A and other mutant proteins demonstrates that there are no major conformational differences between any of these proteins. NMR and CD also confirmed that the heme orientation is the same in WT Mb and all the mutant myoglobins.³² The observed orientation is shown in figure 2; another orientation which has been observed in monomeric hemoglobins is a 180° rotation about the pseudo-C₂ symmetry axis of the heme.³³ Electronic absorption spectra are virtually identical (shifts in peak maxima relative to wild type of 2nm or less) for wild-type and mutant proteins for several different ligated forms, as well as for the reduced deoxy form. A significant exception is the metaquo form of the protein (Figure 5). The absorption bands at 635 and 1025 nm in the wild-type protein (assigned as ligand-to-metal charge-transfer bands³⁴) are shifted to 622 and 950 nm in V68D and to 620 and 900 nm in V68E, whereas V68N' has an absorption spectrum similar to the wild type. Since the interactions of a protonated Asp group with the heme should be similar to those of an Asn, this observation is consistent with the suggestion that the carboxylate side chain at residue 68 in metaquo-V68D is ionized even when buried in the protein. The observed spectral shifts in metaquo-V68E and metaquo-V68D could be due to either global conformational changes in these proteins, localized changes in bonding at the heme iron, or purely electrostatic effects of introducing a negative charge near the heme iron. The absence of differences in other regions of the electronic absorption spectrum, as well as the resistance of both wild-type and mutant metaquo forms of the protein to tryptic digestion, and the superimposability of the CD spectra for all of the mutants and native metaquo

Figure 5. Absorption of metaquo derivatives of (a) WT**Mb**, (b) V68**N'**, (c) V68**D**, and (d) V68**E** in 10mM sodium phosphate pH 6.0 at 28°C.



forms make it unlikely that there are large conformational changes occurring in any of the mutant proteins. By analogy with Hb Milwaukee, in which the Glu replaces the water molecule that is coordinated to the heme iron (III) in the wild-type protein,¹⁵ it is likely that this occurs in metaquo-V68E. Since Asp cannot coordinate to the heme without a substantial change in protein conformation, these results imply that the observed spectral shifts in metaquo-V68D are due to electrostatic interactions. As expected, ligand-to-metal charge-transfer transitions are highly sensitive to electrostatic effects, whereas the heme-centered $\pi\pi^*$ transitions are little affected.

A similar effect could be responsible for the red shift of the spectrum of retinal in rhodopsin and bacteriorhodopsin compared to retinal in organic solvents. Calculations²⁸ and studies of retinal Schiff base analogs²⁹ support this idea that electrostatic interactions between charged groups in the protein and the chromophore are the cause. Several aspartate residues thought to be responsible for the shift have been substituted with asparagine by site-directed mutagenesis. However, these changes did not perturb the spectrum of the bacteriorhodopsin-bound retinal. More recent studies have demonstrated small but significant changes in the absorption spectrum of rhodopsin when certain glutamates were replaced by glutamines.³⁰ Conclusive evidence await refined crystal structure data. A parallel example is the photosynthetic reaction center where it is thought the protein interactions might cause fluorescence spectral shifts in chlorophyll and bacteriochlorophyll.³¹

Isoelectric focusing gels indicate that the metaquo forms of V68E and V68D mutants have an isoelectric point (pI) that is about 0.5 pH units lower than the metaquo forms of either wild-type or V68N' and that is similar to the pI of reduced (ferrous) Mb, confirming that Glu and Asp are ionized in the metaquo forms of V68E and V68D, respectively (Figure 7 and Table 2). Since the

Figure 6. Redox potential at pH 7.0 (E°) versus temperature for Mb, C110A, V68N', V68D, and V68E. The entropy change occurring upon reduction in the protein containing half cell, $\Delta S^{\circ}_{rc} = F(\partial E^{\circ}/\partial T)_P$, is obtained from the slope of these plots. All fits had correlation coefficients greater than 0.99.

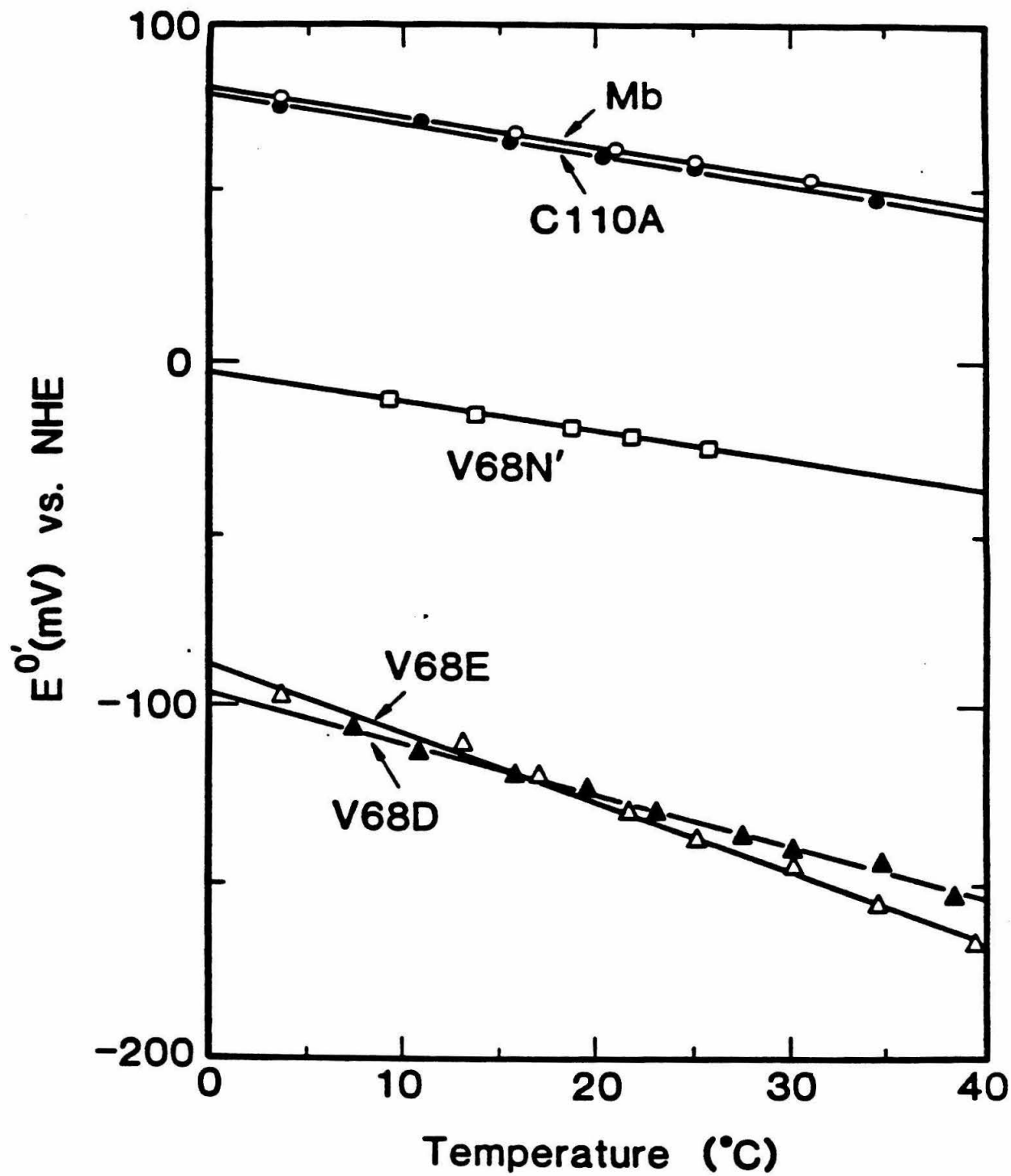


Table 1. Thermodynamic parameters for the reduction of sperm whale myoglobin (20), and for wild-type human myoglobin and four of its site-specific mutants.^a $\Delta S^{\circ'}$, the total entropy change for the whole-cell reaction (referenced to the standard hydrogen electrode) is given by $\Delta S^{\circ'} = \Delta S^{\circ'}_{rc} - 15.6$ eu (25). $\Delta H^{\circ'} = -FE^{\circ'} + 298\Delta S^{\circ'}$ where F is Faraday's constant. Values of $\Delta H^{\circ'}$ and $\Delta S^{\circ'}_{rc}$ for Mb are -12.2 kcal/mole and -20.9 eu, respectively.

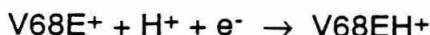
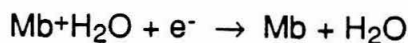
Myoglobin	$E^{\circ'}$ (25°C) (mV)	$\Delta\Delta G^{\circ'}$ (25°C) (kcal/mole)	$\Delta\Delta H^{\circ'}$ (kcal/mole)	$298\Delta\Delta S^{\circ'}$ (kcal/mole)	$\Delta\Delta S^{\circ'}_{rc}$ (eu)
Sperm whale	58.8	-0.0	-0.80	-0.80	-2.7
Human	58.9				
C110A	57.0	0.05	-0.04	-0.09	-0.3
V68E	-136.8	4.52	-2.63	-7.15	-24.0
V68D	-132.1	4.41	0.69	-3.72	-12.5
V68N'	-23.8	1.91	2.51	0.60	2.0

^aThe experimental errors in $E^{\circ'}$ and $\Delta S^{\circ'}_{rc}$ are ± 3 mV and ± 1.5 eu, respectively, and were estimated as described in [20].

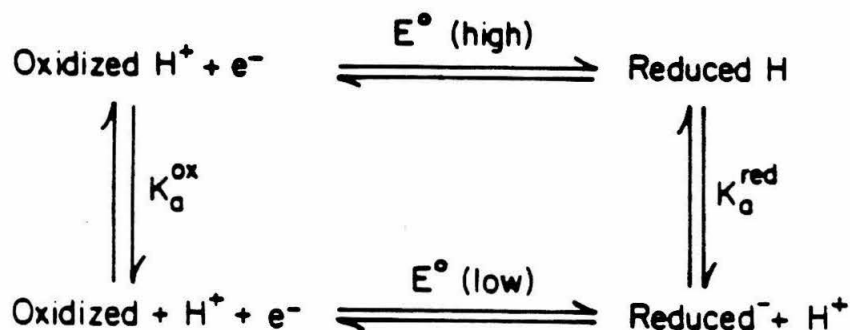
reduced derivatives of V68D and V68E are rapidly oxidized by atmospheric oxygen back to the ferric form, it was not possible to measure the isoelectric point of the reduced forms of these proteins. Mb reconstituted with Zn protoporphyrin IX (ZnPPIX-Mb) has been used as a model for the reduced deoxy state. Wild type and all of the mutant proteins reconstituted with ZnPPIX were found to have approximately the same isoelectric point as oxy-Mb, metaquo-V68D and metaquo-V68E. (The pI's of the cyanide derivatives were determined to be roughly the same.) This suggests that either the carboxylate at residue 68 or a nearby residue (for example the distal HisE7, Figure 2), is protonated in ZnPPIX-V68E and ZnPPIX-V68D and the corresponding heme cyano derivatives.

Wild type and mutant proteins were also run on non-denaturing polyacrylamide gels (from cathode to anode). The mobilities of CO-WTMb Fe (II), V68D' Fe(III), and V68E' Fe(III) were approximately equal but were all greater than metaquo WTMb and V68N' Fe(III). This result is again consistent with the other data that the carboxylate sidechains are ionized in V68D' Fe(III) and V68E' Fe(III). An anaerobic gel was poured and run in an anaerobic box to determine the mobilities of the reduced forms of the mutant proteins. The mobilities of V68D' and V68E' were unchanged upon reduction compared to their respective Fe(III) forms further suggesting that reduction of the heme iron in these mutants is accompanied by uptake of a proton by the protein. Further studies have shown that there is proton uptake upon the binding of cyanide, an anionic ligand, to the Fe(III) heme.³²

Also, the reduction potential should increase by approximately 59mV per unit decrease in pH at 25°C assuming that the pH range measured is between the pK_a's of the carboxylate groups for the reduced and oxidized heme. The half-cell reactions occurring in Mb, V68D, and V68E are



where e^- is an electronic charge. The half-cell reactions in C110A and V68N' are identical with the one shown for Mb. If we neglect changes in protein structure and charge distribution that occur upon decreasing the pH from 7.0 to 6.0, then for the half-cell reactions shown above for V68D and V68E, $E^{\circ'} = E^{\circ}(6.0) - 2.303RT/F$. Differentiating with respect to temperature, we obtain $\Delta S^{\circ'}_{rc} = \Delta S^{\circ}_{rc}(6.0) - 2.303R$, where R is the gas constant and F is the Faraday constant. The following is a schematic of the thermodynamic cycle for coupled electron- and proton-transfer reactions:



$E^{\circ}(6.0)$ was measured at 25°C for V68D, V68E, and V68N'. The $E^{\circ}(6.0)$ values for V68D and V68E are greater than $E^{\circ'}$ by 64.5 and 53.2mV, respectively, whereas $E^{\circ}(6.0)$ for V68N' is essentially the same as $E^{\circ'}$, confirming that reduction in the former two proteins is accompanied by proton uptake.

We now consider the origins of the changes in redox thermodynamics summarized in Table 1. Since the redox properties of a protein are determined by many different factors (see Chapter 1), we restrict our discussion to the observed differences in redox thermodynamics between wild-type and mutant proteins rather than on the absolute values of $\Delta G^{\circ'}$, $\Delta H^{\circ'}$, and $\Delta S^{\circ'}_{rc}$ for each

Figure 7. Isoelectric focusing gel: lane 1, metaquo C110A; lane 2, metaquo V68N'; lane 3, metaquo V68E'; lane 4, metaquo V68D'; lane 5, ZnPChla C110A; lane 6, ZnPchla V68E'; lane 7, ZPPIX C110A; lane 8, ZnPPIX V68E'. The fainter bands of lower pI in each lane are most likely deamidated protein.

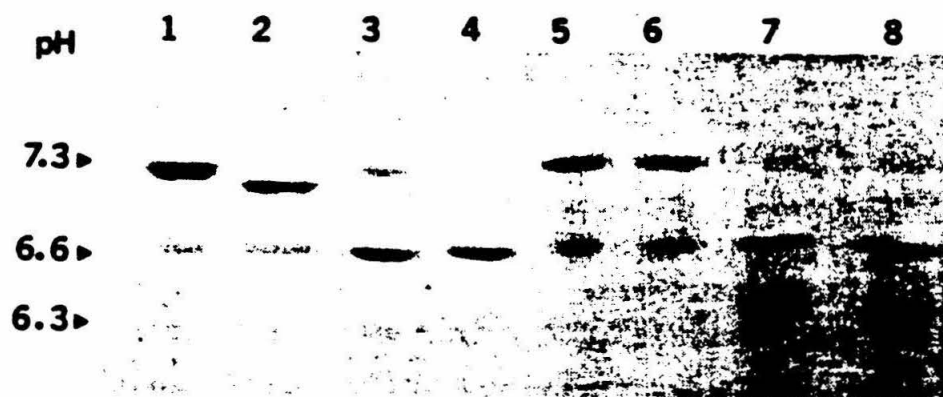
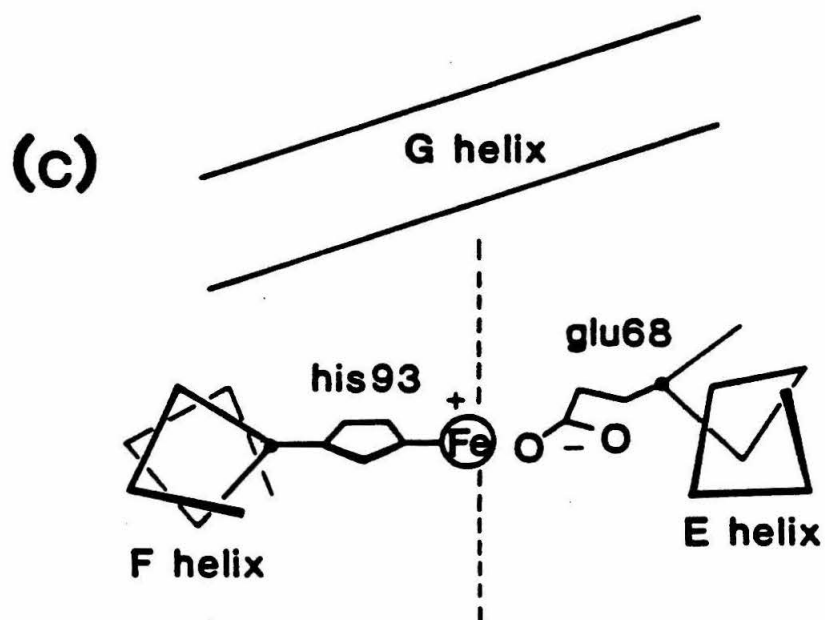
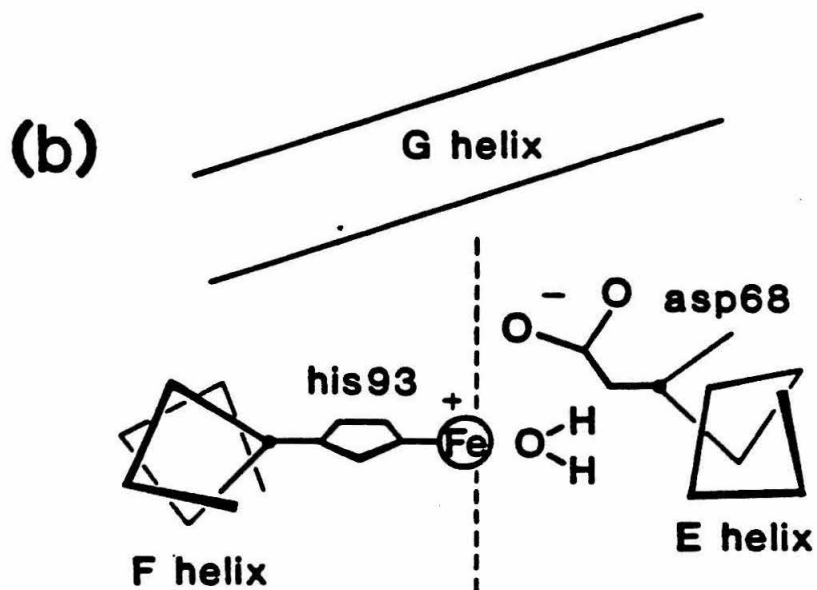
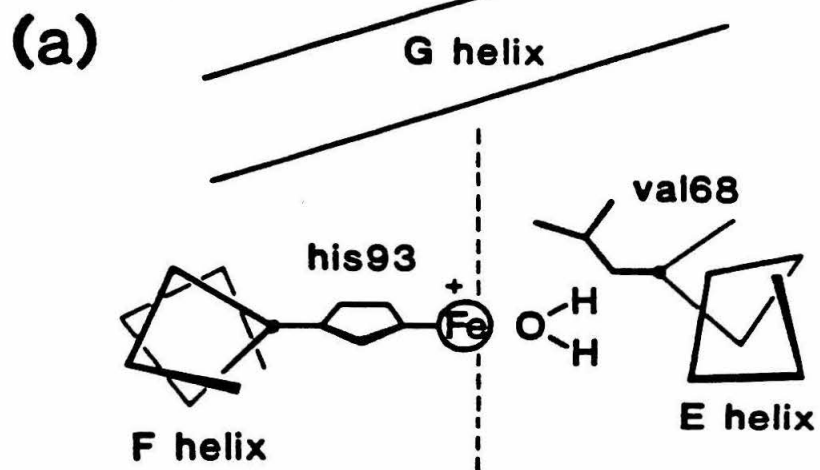


Table 2. Isoelectric points of derivatives of wild type and mutant myoglobins. The estimated error is ± 0.03 based on 2-3 separate determinations of each isoelectric point.

Derivative	WTMb	C110A	V68D'	V68E'	V68N'
metaquo	7.20	7.27	6.64	6.63	7.14
ZnPPIX	-	6.76	6.76	6.76	6.76
ZnPChla	-	7.31	7.31	7.31	7.31
CO	6.62	6.65	-	-	-

Figure 8. Schematic representation of the proposed coordination of the heme iron in the metaquo derivatives of (a) Mb, (b) V68D, (c) V68E.



protein. In the metaquo forms of V68E and V68D, the negative charges on Glu and Asp are stabilized by a favorable coulombic interaction with the heme iron, which has an effective charge of +1. The magnitude of this iron-carboxylate interaction is large because of the close proximity of the charges and because they are surrounded by a nonpolar medium. Upon reduction of the iron, this interaction is lost. The relatively nonpolar protein interior does not appear to be able to solvate an isolated buried negative charge. Hence, reduction is accompanied by uptake of a proton.

The ΔS°_{rc} value is significantly more negative for both V68E and V68D than for Mb and V68N'. As with the redox potential, this large decrease is a consequence of the pH of measurement and the choice of standard state. If all of the observed pH dependence of the redox potential in V68E and V68D were due to changes in ΔS°_{rc} , then $\Delta\Delta S^{\circ}_{rc}$ [$\Delta S^{\circ}_{rc}(\text{mutant}) - \Delta S^{\circ}_{rc}(\text{Mb})$] would increase by about 4.6 eu per unit decrease in pH.²⁴ The release of a bound water molecule from the heme iron that occurs upon reduction of metaquo-Mb should be an entropically favorable process. Since the Glu is coordinated to the oxidized heme iron in metaquo-V68E, this process cannot occur. This is likely to be the reason that ΔS°_{rc} is more negative for V68E than for V68D. Assuming that the entropy of the water molecule bound to the heme iron is small, the increase in entropy upon transferring this molecule to bulk water is the partial molar entropy of water, equal to 16.72 eu at 25°C. If one subtracted the entropy of water of hydration in solid state (9.4 eu) then one would get 7.3 eu for the entropy of release. Note that the difference between the ΔS°_{rc} values for V68D and V68E is 11.5 eu which is between the two semiempirically derived values above. It seems reasonable to assume that H₂O specifically bound to a heme site would have less entropy than randomly bound water in a hydrated solid and therefore one would expect greater than 7.3 eu for the release of water.

Enthalpy changes upon reduction can be due to either variations in the strengths of specific metal-to-ligand or hydrogen bonds within the protein or to charge rearrangements involving solvent molecules and ions in solution. $\Delta\Delta H^{\circ}$ [ΔH° (mutant) — ΔH° (Mb)] for V68E and V68D are -2.63 and +0.69 kcal/mole, respectively. This difference could be due to the differences in bonding at the redox center in the oxidized states of the two proteins. For V68N', the +2.51 kcal/mole increase in ΔH° is the main contributor to ΔE° . This increase in ΔH° is in part due to a favorable hydrogen-bonding interaction involving the Asn, the bound water molecule, and possibly the distal His, which would stabilize the oxidized (metaquo) state of the protein. Such an interaction can be inferred from the observation that the pK_a of the bound water molecule changes from 8.8 in the wild-type protein to 8.1 in the Asn mutant. This corresponds to a free energy change of about 1 kcal/mole at 25°C.

Replacement of Val68 by charged and polar residues leads to large changes in the reduction potential of the heme iron. In the metaquo derivatives of V68D and V68E, the negative charge at residue 68 is stabilized by the positively charged heme iron. Upon reduction, the relatively nonpolar protein interior cannot stabilize an isolated buried negative charge and proton uptake by the protein occurs. Hence the observed changes in redox thermodynamics in these two proteins are strongly pH dependent. These measurements should stimulate theoretical calculations that attempt to reproduce the observed changes in redox thermodynamics.

References

1. Kassner, R. J. *J. Am. Chem. Soc.* 95, 2674 (1973).
2. Churg, A. K. and Warshel, A. *Biochemistry* 25, 1675 (1986).
3. Harbury, H. A., *et al.* *Proc. Natl. Acad. Sci. U.S.A.* 54, 1658 (1965).
4. Pettigrew, G. W.; Bartsch, R. G.; Meyer, T. E.; Kamen, M. D. *Biochim. Biophys. Acta* 503, 509 (1978).
5. Rees, D. C. *J. Mol. Biol.* 141, 323 (1980).
6. Moore, G. R.; Leitch, F. A.; Pettigrew, G. W.; Rogers, N. K.; Williams, G. *Frontiers in Bioinorganic Chemistry* Xavier, A. V., ed.; VCH Publishers, Weinheim, Federal Republic of Germany, 1986, p. 494.
7. Moore, G. R.; Pettigrew, G. W.; Rogers, N. K. *Proc. Natl. Acad. Sci. U.S.A.* 83, 4998 (1986).
8. Sternberg, M. J. E.; Hayes, F. R. F.; Russell, A. J.; Thomas, P. G.; Fersht, A. R. *Nature* 330, 86 (1987).
9. Gilson, M. K. and Honig, B. H. *ibid.* p.84.
10. Varadarajan, R.; Szabo, A.; Boxer, S. G. *Proc. Natl. Acad. Sci. U.S.A.* 82, 5681 (1985).
11. Takano, T. *J. Mol. Biol.* 110, 537 (1977).
12. Lee, B. and Richards, F. M. *ibid.* 55, 379 (1971).
13. Mabbutt, B. C. and Wright P. E. *Biochim. Biophys. Acta* 832, 175 (1985).
14. Varadarajan, R.; Lambright, D. G.; Boxer, S. G. *Biochemistry* 28, 3771 (1989).
15. Perutz, M. R.; Pulsinelli, P. D.; Ranney, H. M. *Nature New Biol.* 237, 259 (1972).
16. Antonini, E.; Brunori, M. *Hemoglobin and Myoglobin and their Reactions with Ligands* (North-Holland, Amsterdam, 1971).
17. Steadman, J. H.; Yates, A.; Huehns, E. R. *J. Haemat.* 18, 435 (1970).
18. Human Mb contains a single buried Cys at position 110 that sometimes complicates purification of the overproduced apoproteins. Thus, we have replaced this by Ala (which occurs at this position in several other Mb's) to give the mutant C110A. This change has no effect on the electronic

absorption, NMR, and redox (*vide infra*) properties. The double mutant that contains Ala at position 110 and Asn at position 68 is named V68N'.

19. Kunkel, T. A. *Proc. Natl. Acad. U.S.A.* 82, 488 (1985).
20. Ellis Jr., W. R. *Thesis* California Institute of Technology, Pasadena (1986).
21. E° is the potential of the myoglobin-containing half cell (relative to the standard hydrogen electrode), measured at pH 7.0 and ionic strength 0.1M, at which the concentrations of the reduced and oxidized proteins are equal. When measured at pH 6.0, this potential is denoted by $E^{\circ}(6.0)$.
22. Anderson, C. W., Halsall, H. B.; Heineman, W. R. *Analytical Biochem.* 93, 366 (1979).
23. Taniguchi, V. T., *et al.* *Adv. Chem. Ser.* No. 201, 51 (1982).
24. Stargardt, J. R., Hawkridge, F. M., Landrum, H. L. *Analytical Chem.* 50, 930 (1978).
25. Ellis, W. R. and Gray, H. B. *Adv. in Bioinorg. Chem.* in press.
26. Yee, E. L., *et al.* *J. Am. Chem. Soc.* 101, 1131 (1979).
27. Ellis, W. R., *et al.* *Biochemistry* 25, 161 (1986).
28. Honig, B., *et al.* *Biochemistry* 15, 4596 (1976).
29. Arnablodi, M., *et al.* *J. Am. Chem. Soc.* 101, 7082 (1979).
30. Zhukovsky, E. A. and Oprian, D. O. *Science* 246, 928 (1989).
31. Eccles, J. and Honig, B. *Proc. Natl. Acad. Sci. U.S.A.* 80, 4959 (1983).
32. Varadarajan, R., *et al.* *Biochemistry* 28, 3771 (1989).
33. Cooke, R. M. and Wright, P. E. *Biochim. Biophys. Acta* 832, 365 (1985).

CHAPTER 3

MAGNETIC RESONANCE STUDIES OF MYOGLOBIN SITE-DIRECTED MUTANTS

Introduction

Nuclear Magnetic Resonance Dispersion (NMRD) measurements were performed to elucidate some of the questions posed in the last chapter. Namely, we wanted to determine the specific molecular events which are responsible for the enthalpic and entropic contributions of the redox potential. We believed that this technique would help us discern whether the heme pocket became more solvent accessible in any of the mutants and in which proteins the sixth coordination site of Fe(III) heme was occupied--and by what. With respect to the latter question, we have some evidence that the water molecule which occupies the sixth ligand position in metaquo, native myoglobin is present in V68N and V68D, but that it is replaced by carboxylate from the mutant glutamate residue in V68E. The greatest support for this conjecture comes from the shifted charge-transfer bands in these proteins and their Mn(III) porphyrin substituted derivatives (Chapter 2). Determination of the sixth heme ligand and the solvent accessibility of the heme pocket will also greatly aid the interpretation of the intramolecular electron transfer experiments which will be performed on the ruthenium-modified derivatives of these proteins.

In NMRD the spin-lattice relaxation time (T_1^{-1}) of the bulk water protons is measured as a function of magnetic field strength in the presence of a solute which facilitates relaxation. Metalloproteins relax water protons by a variety of mechanisms. From the NMRD profile one can deduce the dominant mechanism(s) of relaxation and thus determine how water molecules interact with the protein, in particular, the metal center. Davidson and associates were the first to carry out experiments of this sort on hemoglobin and myoglobin.¹ Similar work has been done on a variety of native state proteins including iron conalbumin,² concanavalin A³ and ferredoxin,⁴ and paramagnetic metal-substituted metalloproteins like copper(II) alkaline phosphatase.⁵ Qualitative

and quantitative information regarding the position of the metal ions with respect to the protein surface, the oxidation state of the ions, and the geometry of the metalloprotein complex have been determined in these experiments. With the aid of electron spin resonance (ESR) measurements of the paramagnetic species responsible for the protein relaxation rate enhancement, one can further narrow and quantify interpretations of the environment surrounding the metal center.

Experimental

Materials and Methods

Samples for nuclear magnetic resonance dispersion were chromatographed on a size exclusion (Sephadex, G-25) column prior to use. They were then concentrated to between 2 and 4mM using ultrafiltration (Centricon, YM10). All samples were in $\mu=0.1\text{M}$, $\text{pH}=7.0$ sodium phosphate buffer (reagent grade, Baker). A three-fold excess of NaCN (reagent grade, Baker) was added to make metcyanomyoglobin from native myoglobin. Due to scarcity of sample, the volume of $100\mu\text{l}$ was placed inside a 4mM diameter tube which was then placed inside the 10mM tube normally used for these experiments. A copper coil was subsequently wound around the smaller tube. It was found that the data was reproducible with a standard deviation of $\pm 2\%$ using this modification. The relaxation rate was determined directly by observing the exponential change in the magnetization of solvent water protons in response to changes in the applied magnetic field. The measurements were performed using a variable field (with a magnetic field range corresponding a proton Larmor frequency of 0.01 to 50.0MHz) electromagnet in the laboratory of Dr. Seymour Koenig, IBM T. J. Watson Research Center. Data was required through the field cycling method under control of the IBM Device Decoupler.⁶

ESR spectra were typically recorded on 0.2ml samples containing the protein at a concentration of 1mM in a 4mm diameter quartz tube. All oxygen was removed from the sample by cycling it on a vacuum ($\sim 10^{-3}$ Torr) / argon dual-manifold line. All samples were lyophilized and then rehydrated in $\mu=0.01\text{M}$ sodium phosphate buffer, $\text{pH} 7.0$. For the H_2^{17}O studies 37.5% atom-pure, normalized H_2^{17}O was obtained from MSD Isotopes.

The ESR spectra were recorded on a Varian E-line Century Series X-band spectrometer (Noyes Laboratory, Caltech) equipped with an Oxford

Instruments cryostat (model No. C1167A). Liquid helium was pumped through the system as a heat exchanger. At temperatures above 50°K electric heating of the sample was required. Temperatures were monitored with a thermocouple placed inside the cryostat and double-checked with a thermocouple placed inside a dummy ESR tube so that temperature measurement error and variation was typically less than 0.05°K. Further, at each temperature a power dependence study was performed so that the maximum power which did not saturate the signal could be chosen.

Basic Equations

The theory related to NMRD has been developed extensively, so I will only give a summary of the features used in interpreting our results. First, it should be noted that non-dipole relaxation processes (e.g. contact and Curie) can be neglected because of the small (<60 Kdalton) metalloproteins and magnetic fields used in these experiments.⁷ The T_1^{-1} dipole-only approximation can then be separated into three terms⁸

$$T_1^{-1} = T_{1B}^{-1} + T_{1D}^{-1} + T_{1P}^{-1}$$

where T_{1B}^{-1} is the background relaxation rate of the aqueous system which includes enhancement from the buffer and dissolved oxygen ($\sim 0.1 \text{ mM}^{-1} \text{ s}^{-1}$) in the buffer. T_{1B}^{-1} has a slight temperature dependence and is corrected for by running a sample dispersion on the buffer only and using it as a background. T_{1D}^{-1} is the diamagnetic contribution to relaxation from the protein. The derivation of T_{1D}^{-1} from first principles has proved to be a very difficult problem. At first it was thought that the T_{1D}^{-1} was caused solely by a long-range hydrodynamic interaction of the slowly moving solute molecules with the rapidly moving solvent molecules.⁹ From this physical interpretation one would expect T_{1D}^{-1} to be strictly field independent. However, later work has shown that up to

half of the diamagnetic relaxation can arise from a cross-relaxation between protein and solvent protons.¹⁰ Since a paramagnetic center in the protein would alter the protein proton relaxation rates through contact and dipole interactions, there is no assurance that the two contributions T_{1D}^{-1} and T_{1P}^{-1} can be entirely separated.¹¹ With the present theory we have no way of quantitating this potential correction. Instead we know that for a similar system, hemoglobin, all of the $S=0$ and $S=1/2$ heme derivatives tested (oxy carbomonoxy, deoxy, azidemet and cyanomet) have essentially the same relaxation profile. Using their relaxation profiles (at appropriate temperature, concentration, and pH) for hemoglobin as the diamagnetic correction allowed the paramagnetic $s=5/2$ data for this protein to be fit well with existing dipole relaxation theory;¹¹ therefore, we used the same procedure for myoglobin with cyanometmyoglobin specifically as the diamagnetic control. The diamagnetic correction seemed to be linear within the concentration ranges we used (figure 1).

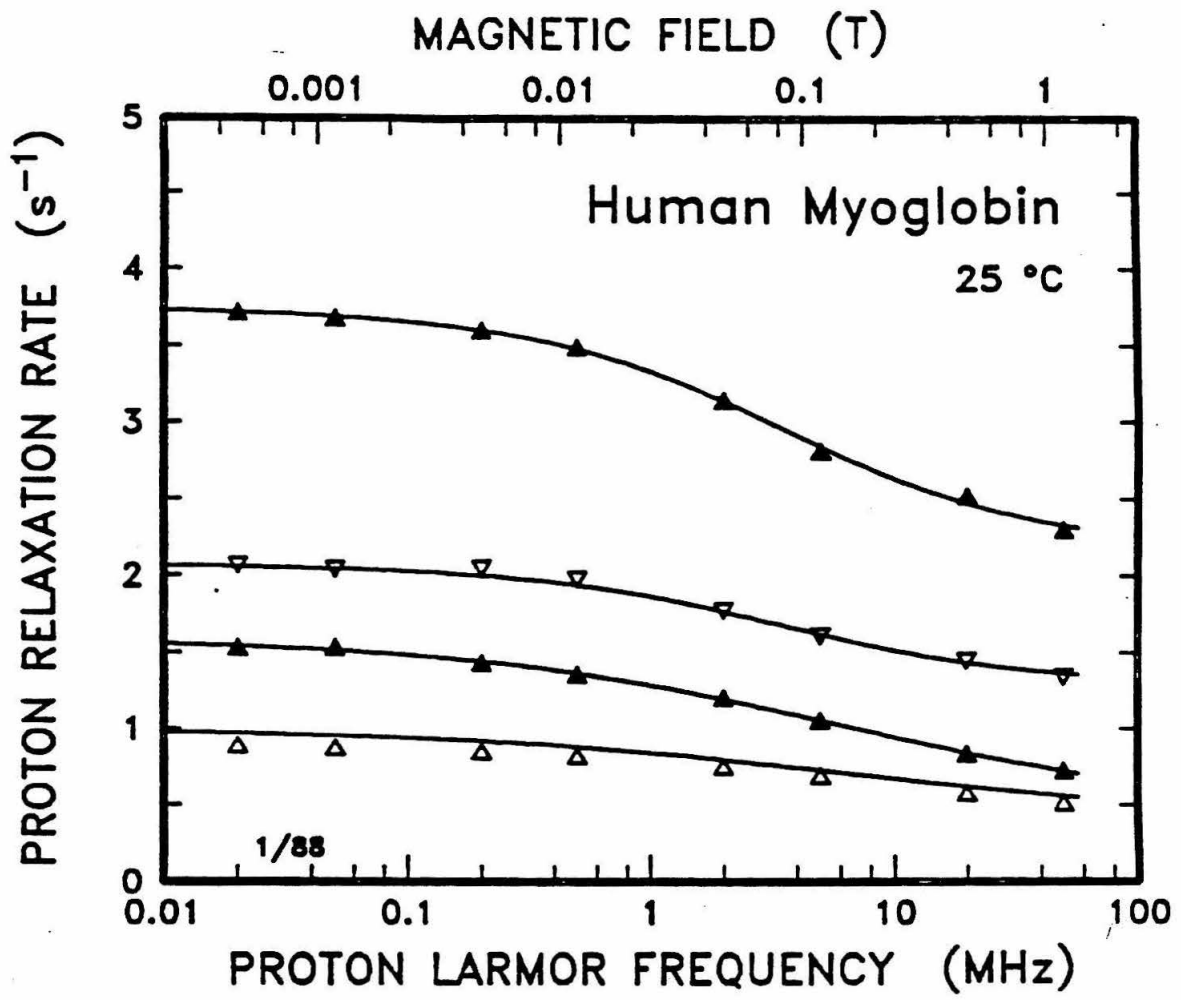
T_{1P}^{-1} , the term from which we derive our experimental conclusions, can be theoretically split into two additive parts: an inner sphere and an outer sphere component. The inner sphere contribution is given by¹²

$$1/T_{1in} = 1/\tau_R + 1/\tau_M + 1/\tau_S$$

τ_R is the rotational correlation time of the protein which for most proteins, including this case, contributes negligibly to $1/\tau_C$ because it is too slow. τ_M , the exchange time of the bound water or proton, and τ_S , the electronic relaxation time of the paramagnet are, thus, the two main competing factors in determining the inner sphere relaxation rate.

The outer-sphere contribution to T_{1P}^{-1} is considerably more complex. The following relations have been derived for an Fe(III) ion $S=5/2$.¹³

Figure 1. NMRD Concentration dependences of metaquomyoglobin (dark triangles) and cyanometmyoglobin (open triangles). The lower curves are at 2.1 mM; the higher curves are at 4.2 mM.



$$1/T_{1\text{out}}(\tau_S/\tau_S \rightarrow \infty) = f_D(8.72 \times 10^{15} \tau_D/d^3) [0.7F(\Omega_S) + 0.3F(\Omega_I)]$$

$$\text{where } \Omega_{S,I} \equiv (6\omega_{S,I}\tau_D)^{1/2}$$

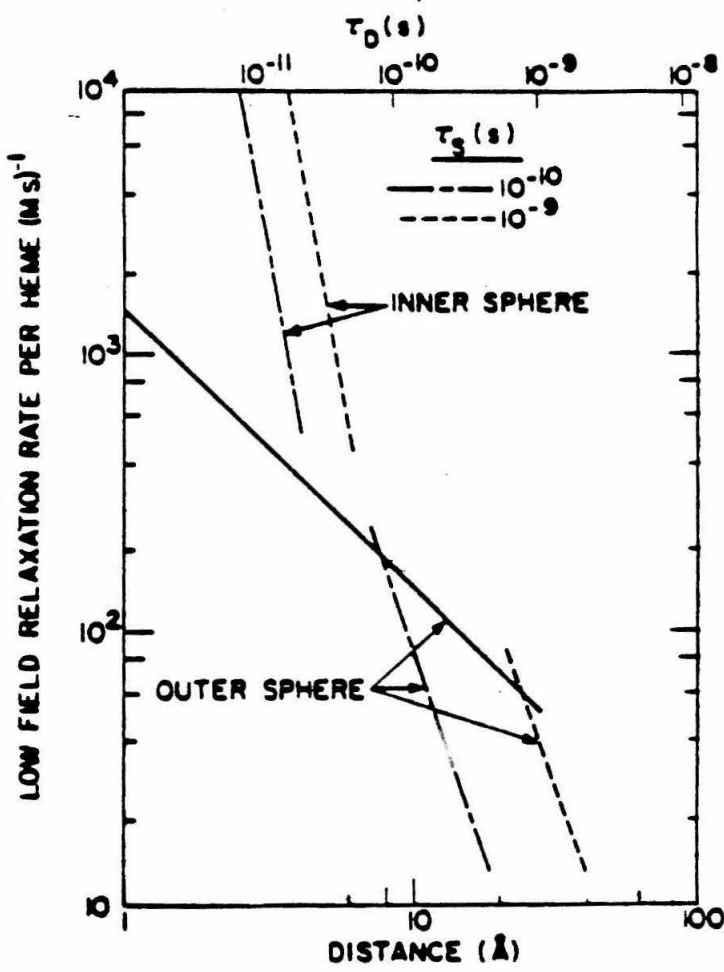
and

$$1/T_{1\text{out}}(\tau_S/\tau_S \rightarrow 0) = f_S(7.27 \times 10^{15} \tau_D/d^3) [0.7J(\omega_S\tau_S) + 0.3J(\omega_I\tau_S)]$$

Here, d is the distance of closest approach of the solvent to the Fe(III) in angstroms, $\tau_D = d^2/3D$ where D is the diffusion constant of the solvent. F is a complicated Lorentzian-like function which decreases to half its low field value of unity at $\Omega=1.3$. f_S and f_D are geometrical factors that are equal to unity if the ion is a center of a sphere, but in our calculations we assume the values 1/8 and 1/6, respectively, because the buried ion is approximated in our model as lying a distance d beneath a semi-infinite plane.¹¹

It is possible then to separate the observed paramagnetic part of the relaxivity into an inner sphere and an outer sphere part (figure 2) since our model predicts that in the high-field limit the outer sphere relaxation rate decreases to 0.3 its low-field value while any exchange-limited inner sphere contribution is independent of magnetic field strength.¹¹ This model does not take into account ligand field effects which introduce asymmetry into the paramagnetic site. It is predicted that the greater the ligand field distortion, corresponding to lower symmetry, the less likely it is that a diffusion proton will see an average of the magnetic field of the ion, so that some parts of the theory could break down. Certainly, the geometric factors would be different in this case and it would be more likely that τ_S would show a magnetic field dependence.¹⁴

Figure 2. This figure represents graphical solutions to the predicted solvent relaxation of a protein with a high spin heme buried at a solvent inaccessible distance (abscissa) in the protein matrix. Calculations using two t_S times are shown for both inner (assuming one water molecule in rapid exchange) and outer sphere relaxation processes. These results are computed in the limit of no applied magnetic field and are scaled by the geometric factors mentioned in the text. From Ref.11.



Results and Discussion

Figure 3 shows how we obtained the paramagnetic contribution to longitudinal relaxation of the V68E protein (glutamate mutant) by subtracting the normalized CN-met (cyanometmyoglobin) NMRD values from the dispersion curve of the glutamate mutant. In Figure 4 the results of the above procedure are displayed on the native (normal) form, aspartate mutant (V68D), and asparagine mutant (V68N) at 25°C as well. Figure 5 shows similar results for 5°C; note the change in vertical scale between the two figures.

In Figure 6 we have a least squares fit to the paramagnetic part of relaxivity of the glutamate mutant. This fit is not perfect; in fact, the data can be fit approximately as well with a number of curves. However, all of these curves have something in common. First, the dominant term is t_S , any significant t_D or t_M contribution worsens the fit. The t_S is in the range of $3\text{-}5 \times 10^{-10}$ which is what is observed for other Fe(III), $S=5/2$ proteins like methemoglobin^{11,15} and transferrin.¹⁶ Approximating the position of the inflection point of the dispersion curve, we estimate the distance of closest approach to be 4.5 ± 0.5 angstroms. This value would be reduced by a factor of $(105/38)^{1/6}$ if one made a first order correction for ligand field effects.¹⁷ Thus, one would obtain $3.7 \pm 0.4 \text{ \AA}$ for the distance of closest approach. (We have evidence for significant ligand field distortions from the ESR spectrum of the glutamate mutant in Figure 10.) This value is very close to that estimated for the distance of closest proton approach for fluoromethemoglobin ($3.4 \pm 0.3 \text{ \AA}$). In fluoromethemoglobin it is believed that this proton is part of a water molecule which is hydrogen bonded to the fluoride ion. The fluoride ion is, in turn, covalently bound to the iron(III) heme.¹¹ Crystal structure data in addition to the assumption of a linear $\text{H} \cdots \text{F}$ hydrogen bond predict that the proton would be 3.4 \AA away from the Fe(III).¹⁸ A similar scenario

Figure 3. NMRD profile of Val68Glu human myoglobin mutant. The paramagnetic component of proton relaxation ($T_{1\rho}^{-1}$) is obtained by subtracting the diamagnetic and buffer components (represented by the "CN-Met" curve) from the overall dispersion of the Val68Glu mutant represented by "glutamate."

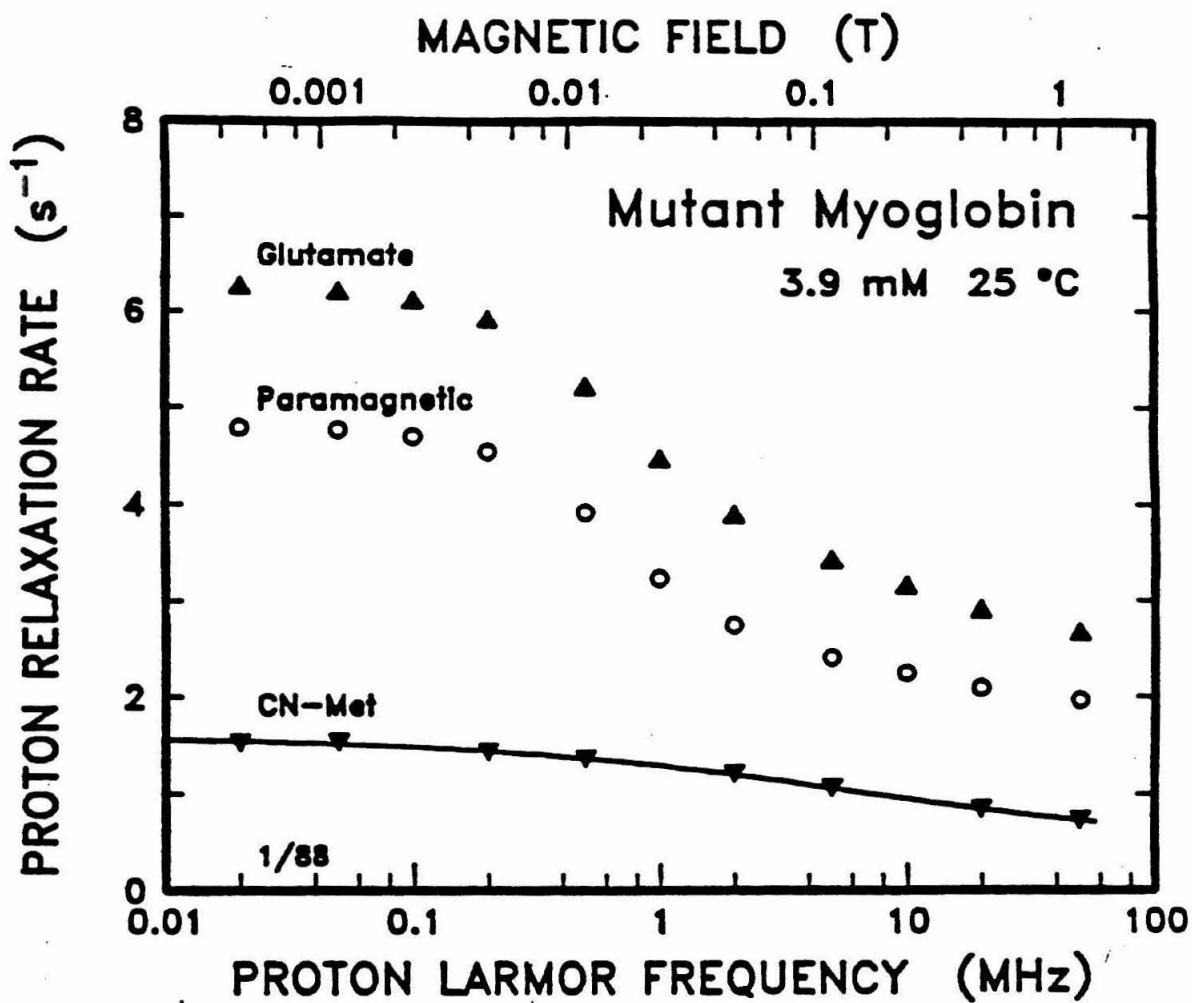


Figure 4. The paramagnetic contributions to the proton relaxation rate from the Val68Asp, Val68Asn, Val68Glu, and native myoglobins represented by "Aspartate," "Asparagine," "Glutamate," and "Native," respectively, as a function of magnetic field [$T_{1P}^{-1}(W_H)$].

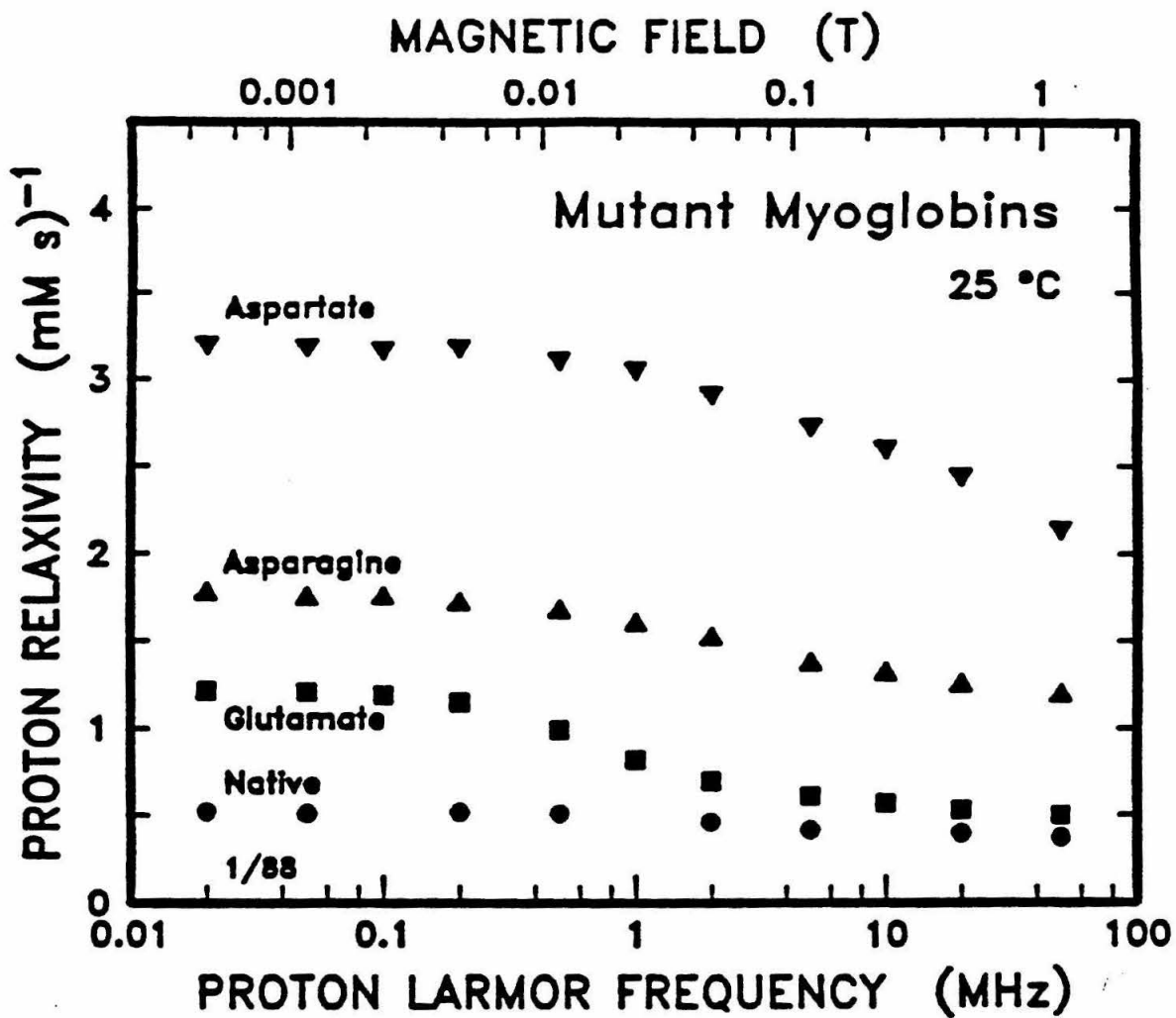


Figure 5. $T_{1\rho}^{-1}(W_H)$ at 5°C of the Val68Asp, Val68Glu, Val68Asn, and native myoglobins. Note that at low field, the Val68Glu mutant's relaxivity is now greater than that of Val68Asn.

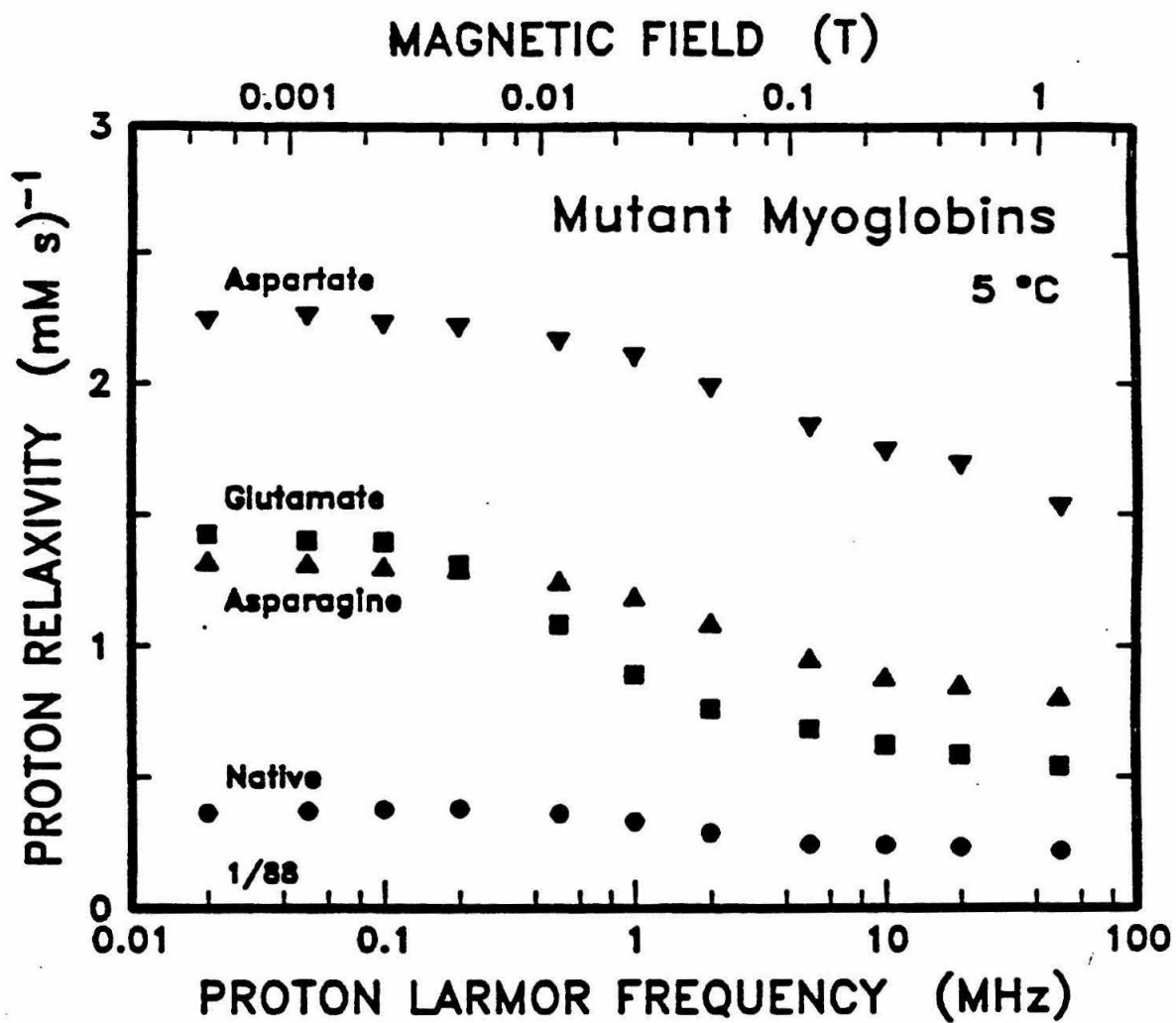
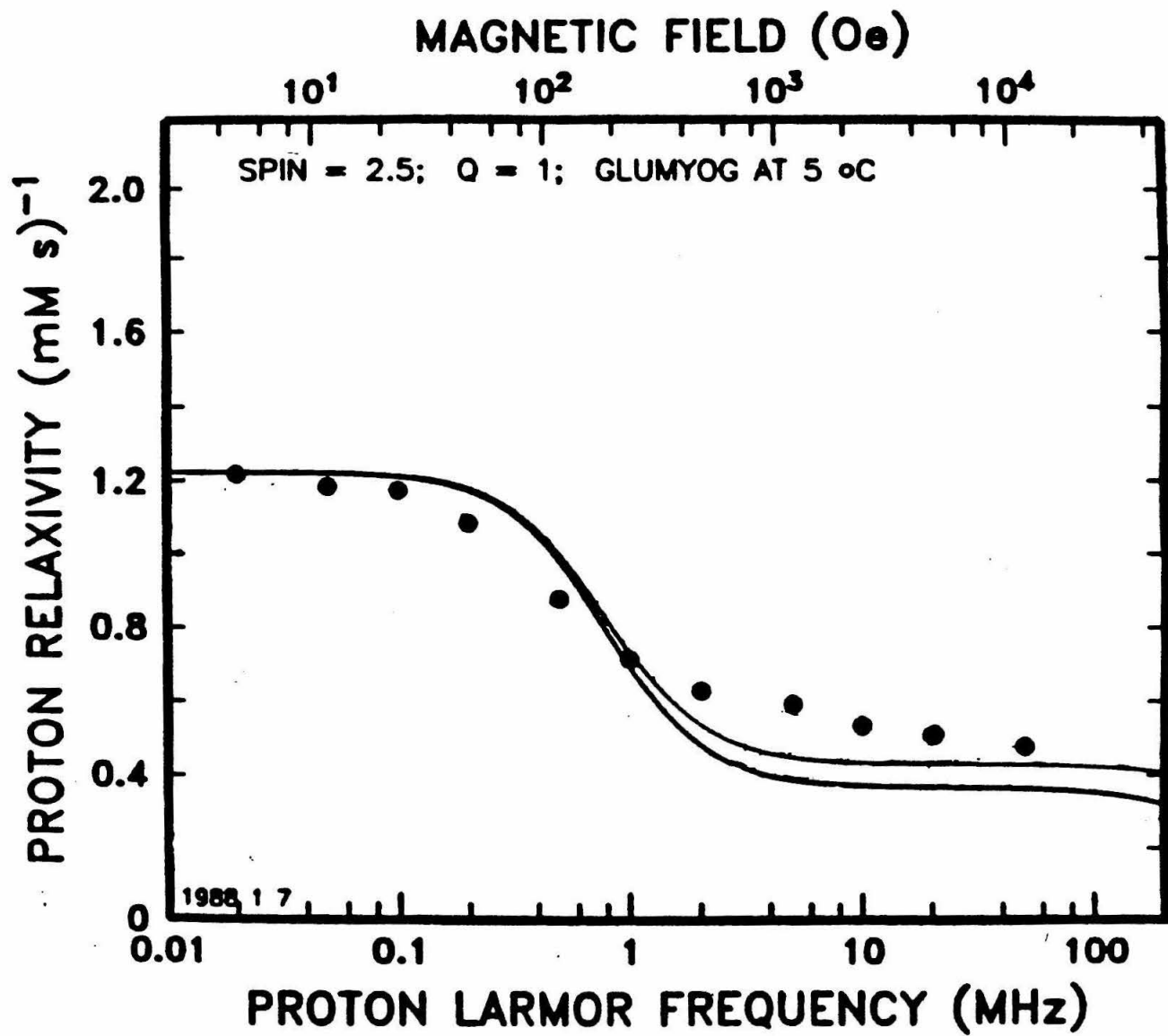


Figure 6. Fit of $T_{IP}^{-1}(W_H)$ of Val68Glu myoglobin. The upper curve gives $T_1^{-1}(W_H)$, the bottom gives $T_2^{-1}(W_H)$. For this fit, $t_S=3.1 \times 10^{-10}s$, $t_M=1 \times 10^{-7}s$, $t_R=5 \times 10^{-8}s$, and d (distance of closest approach) $=5.0 \text{ \AA}$.



could be occurring with the glutamate mutant if an oxygen from the mutant carboxyl group were bonded to the Fe(III) heme. A water molecule hydrogen bonded to that oxygen or the other (free) oxygen on the carboxyl group could account for the dominant term in the dispersion. A further similarity between the glutamate mutant and the fluoromethmyoglobin signals is the temperature dependence of their amplitudes. The high field values for both signals drop by about 30% when the temperature is increased from 5°C to 25°C (Figures 4 and 5).¹⁵ This data also confirms the assignment of t_S as the dominant, paramagnetic relaxation enhancement term because the electronic correlation time is the only correlation time in the outer sphere and inner sphere relaxation theory which can possibly decrease with increasing temperature, as such it is the only term which can account for the observed thermal deactivation of the glutamate mutant and fluoromethemoglobin relaxivities.^{8,11} It should be noted, however, that with all these similarities the iron(III) normalized fluoromethemoglobin signal is a factor of three larger than the glutamate mutant signal at low field. One possible explanation for this discrepancy could be that hemoglobin is inherently more solvent accessible than myoglobin and thus would allow water to exchange more rapidly in the heme pocket. The observation that native methemoglobin has three times greater relaxivity [normalized for iron(III)] at high and low magnetic fields compared to metmyoglobin would support this assertion.^{11,19} In general, a trend of higher relaxivities with greater solvent accessibilities has been supported by NMRD data of heme systems - with heme itself giving the highest relaxivity.¹⁹ Another explanation for the greater magnitude of fluoromethemoglobin relaxivity compared to that of the glutamate mutant could simply be that the F•••H hydrogen bond of the former is more labile than the O•••H hydrogen bond of the latter.

The NMRD profiles of the aspartate and asparagine mutants could not be fit explicitly to theory because, for the most part, they showed very little sign of a flattening out or dispersion in the curve at higher fields. The asparagine mutant comes the closest to dispersing. It has a NMRD profile shape very similar to the native myoglobin although its magnitude is more than three times greater. The native myoglobin in analogy with hemoglobin was calculated as having roughly two-thirds of its relaxivity due to inner sphere effects.¹¹ The greater magnitude of the relaxivity of the asparagine mutant could be caused by the amide in the asparagine side-chain hydrogen bonding to a coordinated water on the Fe(III) heme. This hydrogen bond could then make an Fe(III) coordinated water more labile than in the native protein. Electrochemistry suggests some hydrogen bonding interaction between the asparagine amide and an Fe(III) coordinated water (Chapter 2).

The aspartate mutant profile is similar to the asparagine mutant profile in the shallowness of the change in relaxivity from low to high fields. Both mutants have a low-to-high field ratio of 1.5 ± 0.1 while the glutamate mutant disperses much more extensively with a ratio of 2.4 ± 0.1 (figure 4). The shallowness of the aspartate and asparagine mutant profiles, most likely, indicates that the inner sphere contributions of effects in these metalloproteins significantly contribute to their paramagnetic relaxation enhancement. A similar dispersion profile has been noted for the Fe(III), $S=5/2$ metalloprotein transferrin and has been attributed to a number of inner sphere water binding sites.¹⁶

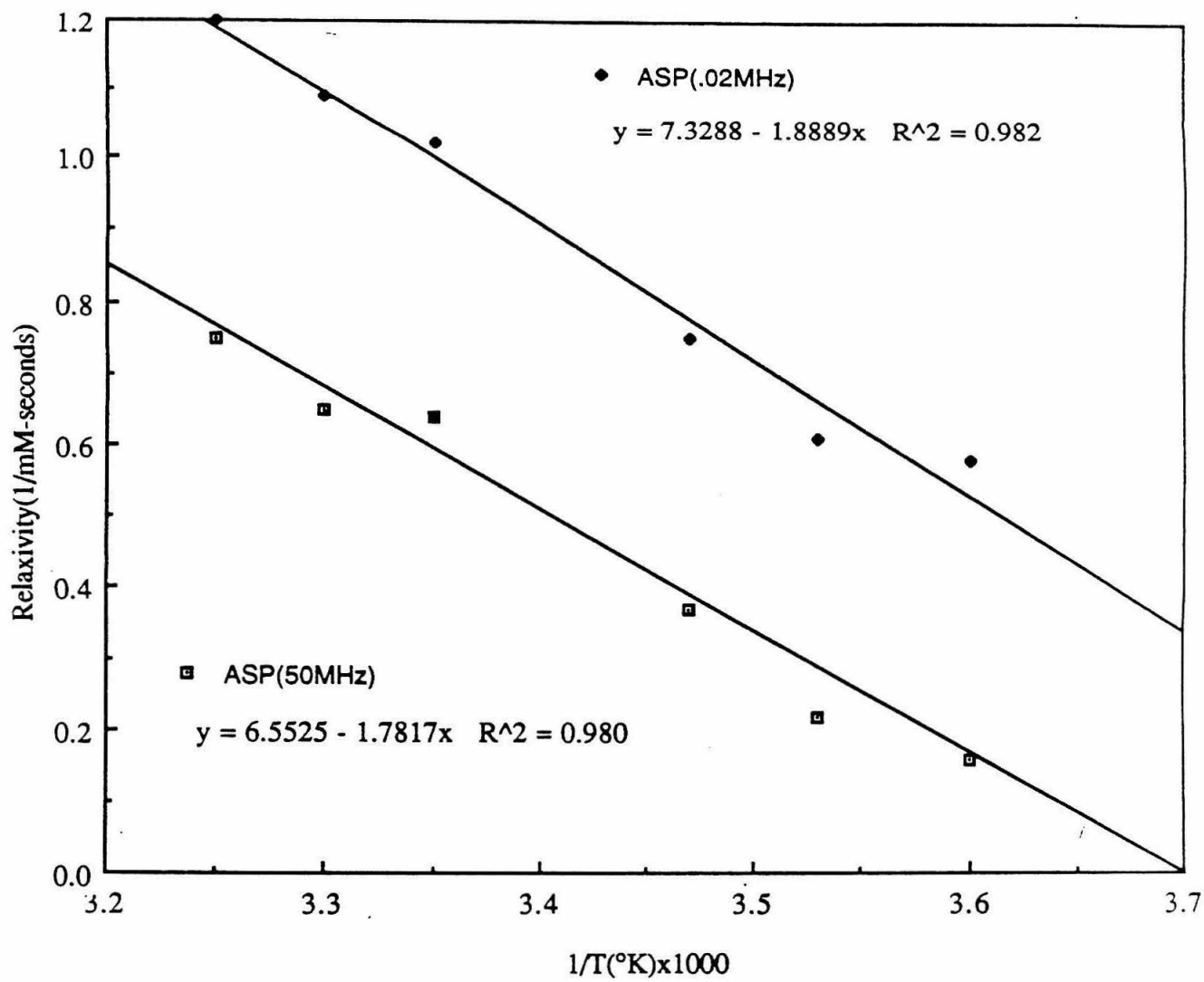
One would expect that exchange-limited inner sphere processes would be thermally activated.¹² This, indeed, is the case for the wild type protein and the asparagine and aspartate mutants. Upon raising the temperature from 5°C to 35°C the high-field relaxivity for all of these proteins is increased by $40 \pm 5\%$. As mentioned earlier, the glutamate mutant shows an inverse temperature

dependence, its high-field relaxivity actually decreases upon heating from 5 to 35°C. At the very least these observations strongly supports the thesis that the coordination environment of Fe(III) in the glutamate mutant is fundamentally different from the one of native protein and aspartate and asparagine mutants.

Activation energies for water molecules exchanging from a heme Fe(III) have been calculated from NMRD measurements of a native and inositol hexaphosphate-treated hemoglobin.¹⁵ If we assume that the exchange of water bound to the iron with solvent water is dominating the $T_{1\rho}^{-1}$ in the proteins which have thermally activated relaxivities, we can also calculate an activation energy from an Arrhenius plot (Figure 7). The obvious caveat in interpreting this variable temperature data is that the exchanging water (or even proton) may not be bound to the iron directly, but near enough to experience significant dipolar relaxation (within 5Å). Nonetheless, we calculated 4.2 ± 0.8 and 6.4 ± 2.0 kcal/mole as the activation energies (E_{act}) for the relaxivity enhancement of the aspartate mutant myoglobin and the native human myoglobin, respectively. The latter number is within experimental error of the calculated values for hemoglobin and inositol hexaphosphate-treated hemoglobin. The native myoglobin value is a very approximate number; however, as one can see the Arrhenius plot is not very well fit to a straight line. The aspartate mutant data is much better; an interesting property of it is the close correspondence of E_{act} calculated for low and high-field data (Figure 7). This result would imply either a very small temperature dependence of the outer sphere component or simply a very small outer sphere component.

Most important for further analysis of NMRD data are ESR measurement. There is evidence for significant ligand field distortion of the paramagnetic center in the glutamate and aspartate mutants (e.g., shifted charge transfer bands) even beyond the strong axial ligand field inherent in hemes. As

Figure 7. Arrhenius plots of the paramagnetic relaxivity of the aspartate mutant myoglobin at low field [ASP(0.02MHz)] and high field [(ASP(50MHz)]. R^2 is the correlation coefficient of each fit. An activation energy of 4.2 ± 0.8 kcal/mole was calculated from these and other fits at fields between 0.02 and 50MHz.



mentioned before ligand field splittings are neglected by the theory used to interpret these data.^{11,14} Paramagnetic anisotropy could give rise to a magnetic field dependence of the electronic relaxation time which could explain the incompleteness of NMR dispersion in these proteins at higher fields.

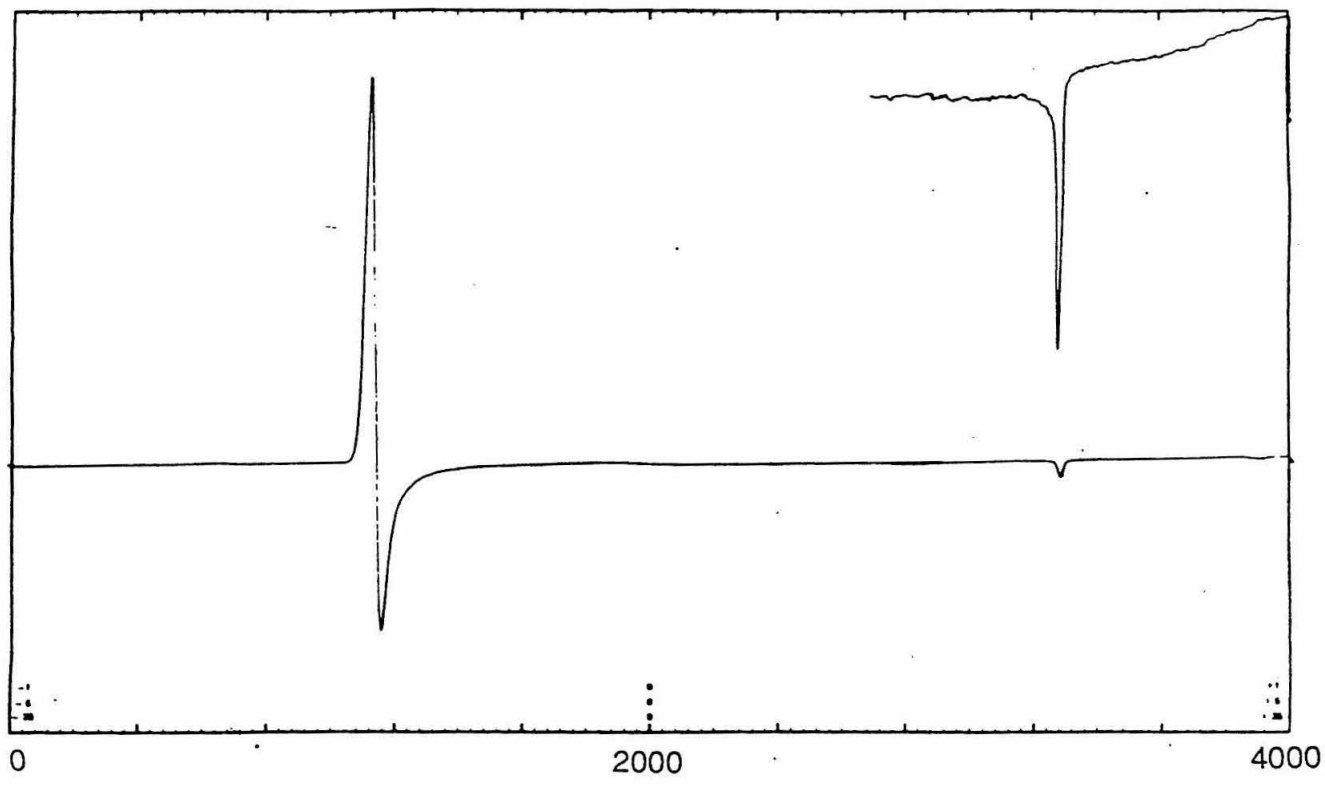
The spin Hamiltonian describing ESR spectra of iron sites of less than cubic symmetry can be characterized by two zero-field splitting parameters D and E. An axial distortion from cubic symmetry is represented by the D term while a planar or rhombic distortion is expressed in the E term. The spin Hamiltonian can then be represented as a sum of these two terms and the Zeeman energy.²⁰

$$H = \beta B \cdot g \cdot S + D[S_z^2 - 1/3S(S+1)] + E(S_x^2 - S_y^2)$$

The relative magnitudes of these terms will determine the fields at which EPR transitions are observed assuming quartic terms are negligible. The Zeeman term is small for $S=5/2$, Fe(III), especially compared to D, so that the position of spectral transitions (g values) will depend mainly upon the D and E values. Since the heme group gives the Fe(III) ion essentially axial symmetry (D is large),²³ electronic spin transitions occur at different energies when the magnetic field is applied perpendicular ($g=6$) or parallel ($g=2$) to the heme. Thus, we have the characteristic myoglobin spectrum (figure 8).²⁴ The asparagine mutant spectrum (figure 8) is very similar. There is no evidence of significant broadening or splitting of the myoglobin heme signal from rhombic distortion upon replacement of val68 with asparagine. The superimposability of their ESR spectra is paralleled by the superimposability of their NMR dispersion curve shapes (*vide supra*). Indeed, from this observation the possibility exists for a more general correlation between ESR spectra and NMRD profiles so that one could, within limits of the extent of difference between two proteins (e.g., site-directed mutants of a protein), predict NMRD

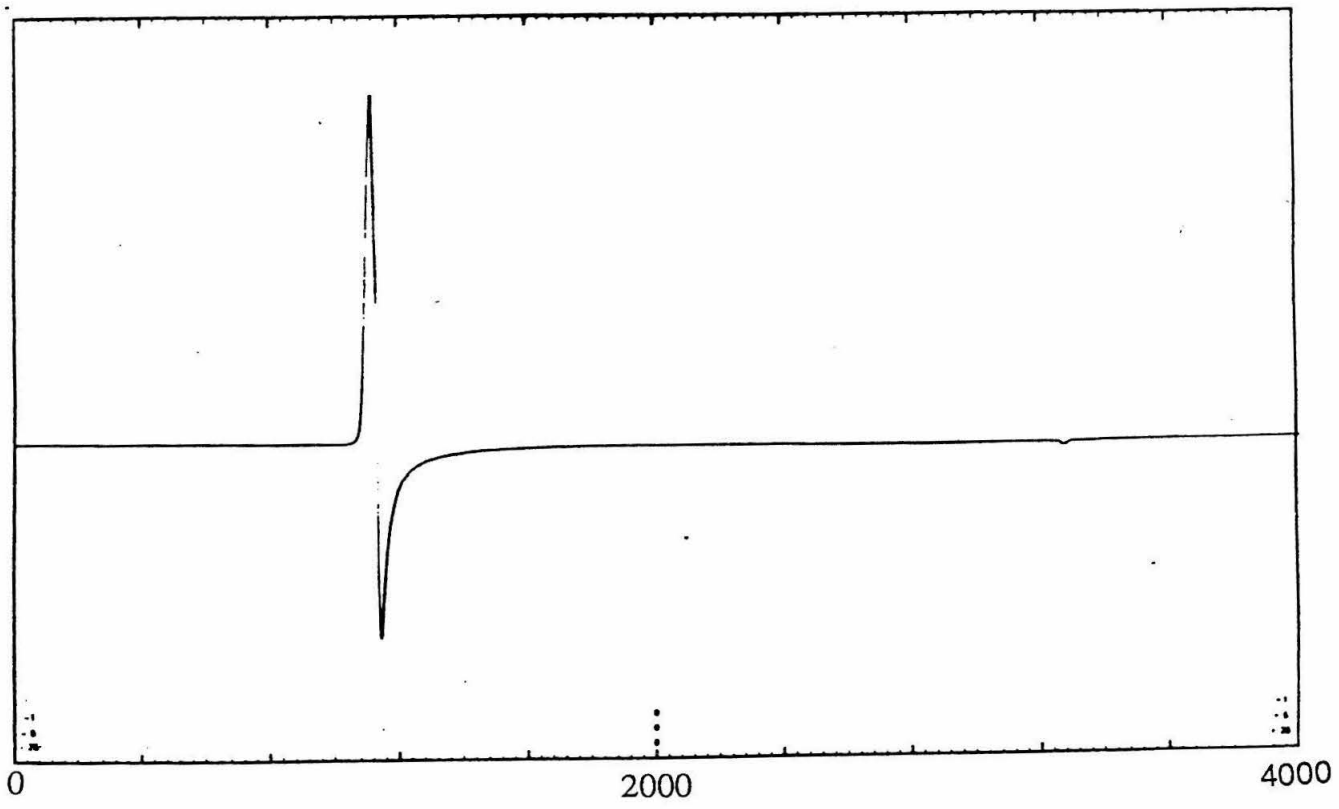
Figure 8. ESR spectra. Top spectrum: native human myoglobin 2mM, 0 to 4 kGauss, 0.128s time constant, 4 min. scan, 2.5 Gauss modulation amplitude, 100kHz modulation frequency, 3.2×10^2 receiver gain, 3.8 °K, 5mW microwave power (inset is $g=2$ signal at 20x gain). Bottom spectrum: Val68Asn myoglobin 1mM, all other things equal to top spectrum's parameters except scan time was 8 minutes with 0.250s time constant, and the temperature was 4.1 °K.

Absorption Derivative



Magnetic Field / G

Absorption Derivative



profiles and thus derive NMRD information from ESR spectroscopy, a much more sensitive technique.

The aspartate and glutamate mutants show more of a deviation from the native myoglobin spectrum (Figures 9 and 10). For a high-spin ferric ion with appreciable zero-field splitting ($2D$), the in-plane g values for the ground state doublet are, to second order in E/D and h ,

$$g_{x,y} = 6.01 \pm 24 E/D - 18.7(E/D)^2 - 12h^2$$

where E/D is the ratio of rhombic to axial ligand field strength and $(6h)^{1/2}$ indicates the admixture of the $S=5/2$ and $S=3/2$ (quartet) spin states. Figure 11 demonstrates the theoretical derivation for these parameters.²⁵⁻²⁷ Both the spectrum of the glutamate and of the aspartate mutant show a splitting in the $g=6$ transition indicating a rhombic distortion which breaks the degeneracy of the d_{xz} and d_{yz} orbitals. The effect is much more pronounced in the glutamate mutant ($E/D=0.031$) than in the aspartate mutant ($E/D=0.002$). The E/D value for the glutamate mutant is significantly lower than the E/D for fluorometmyoglobin (0.004). (One would expect a bound carboxylate to cause more rhombic distortion than a bound fluoride ion.) Thus, this additional paramagnetic anisotropy in the glutamate mutant compared to fluoromethemoglobin could explain why the NMRD profile in the former fails to disperse as completely or sharply as in the latter. Basically, the bound water(s) or proton(s) responsible for the $T_{1\rho}^{-1}$ enhancement experience spacially different paramagnetic components when there is significant ligand field distortion so that the NMR dispersion profile, being a superposition of these components, would be broader. Moreover, there seems to be evidence that the magnetic field dependence of the electronic correlation time is more significant when E/D is greater. [Examples are transferrin (large E)^{10,16, 22} and manganese proteins^{3,28} (small D).] Since our NMRD theory does not consider t_S varying

Figure 9. ESR spectrum of Val68Asp myoglobin 1mM, 0 to 4000 Gauss, 0.128s time constant, 4 min. scan, 10 Gauss mod. amplitude, 100kHz mod. frequency, 5×10^3 gain, 3.8 °K, 10mW microwave power.

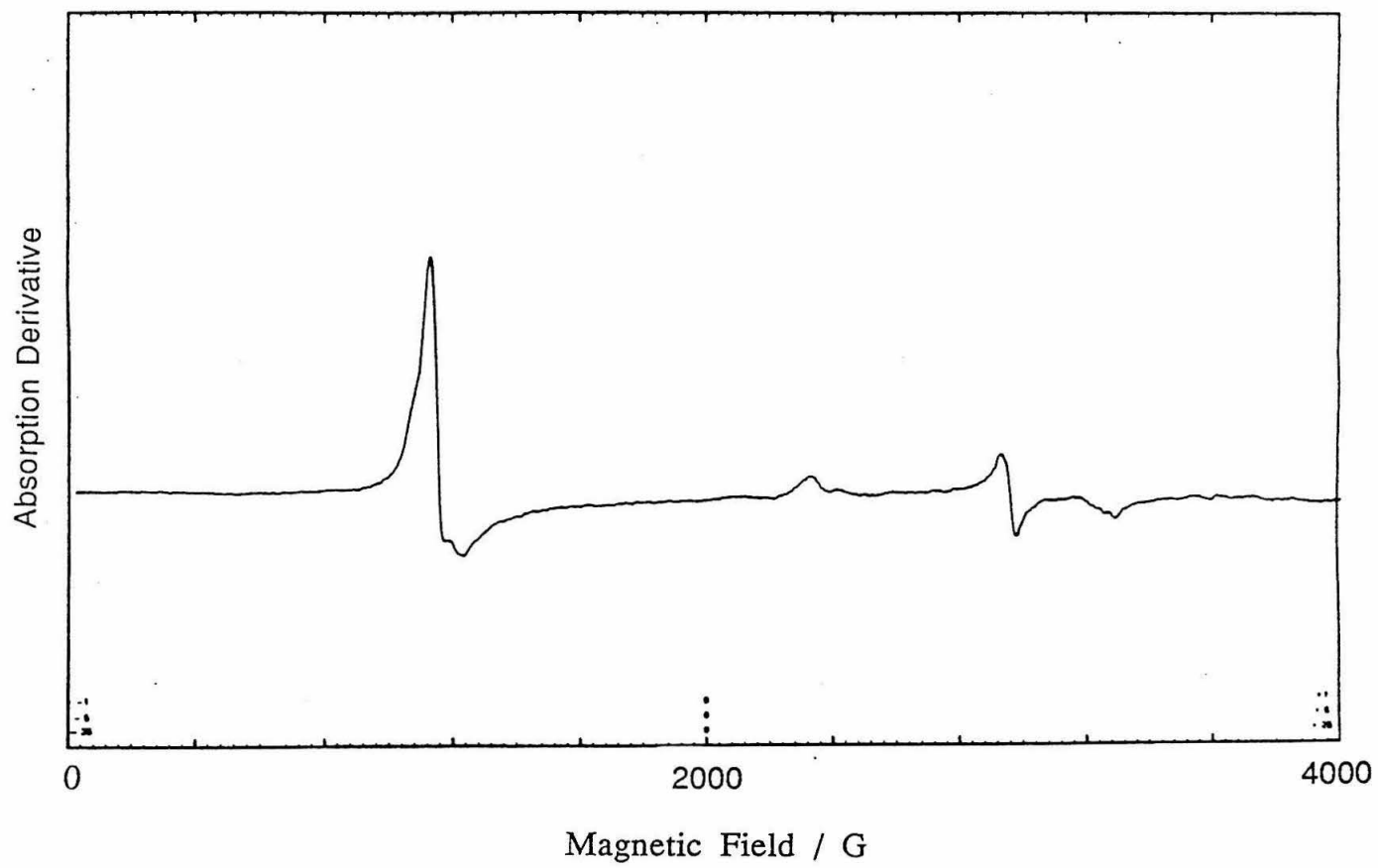
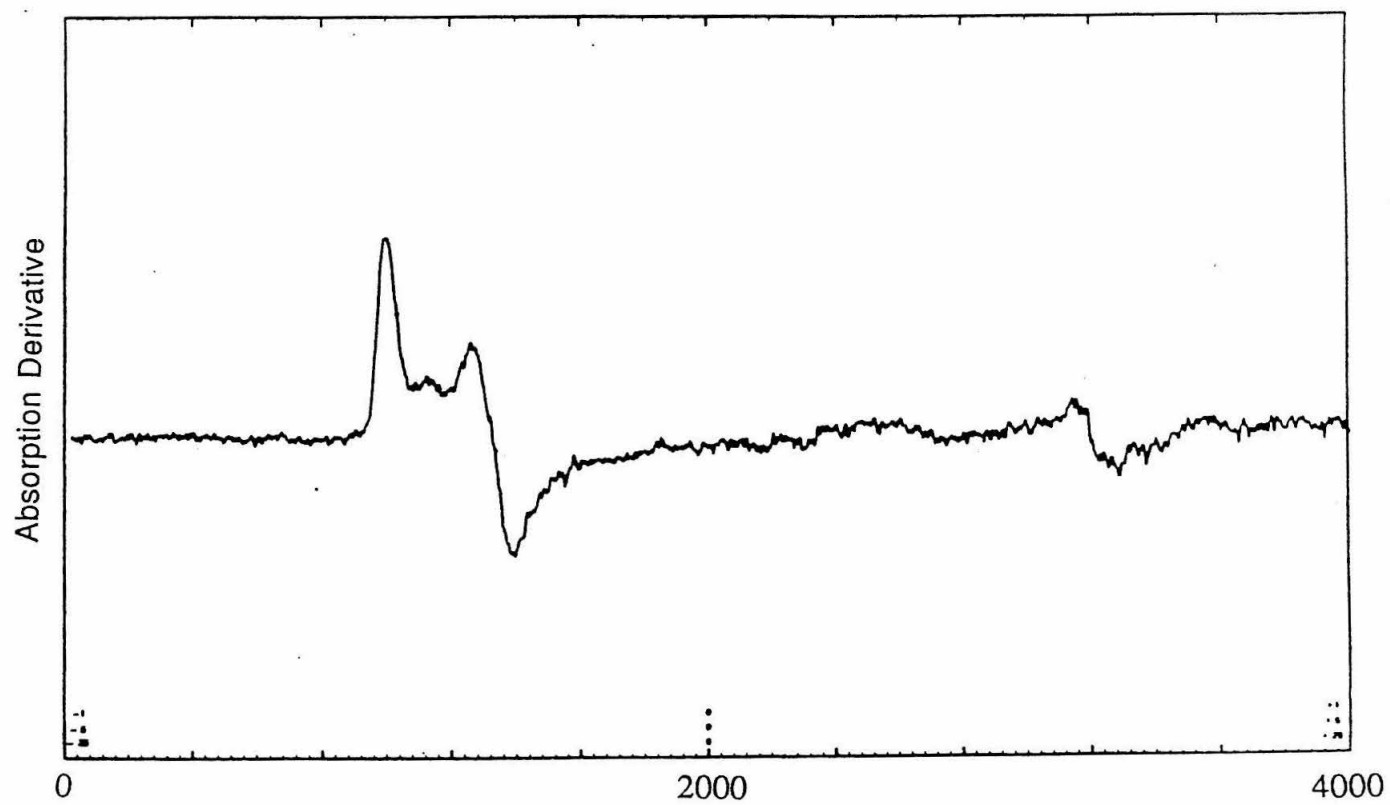
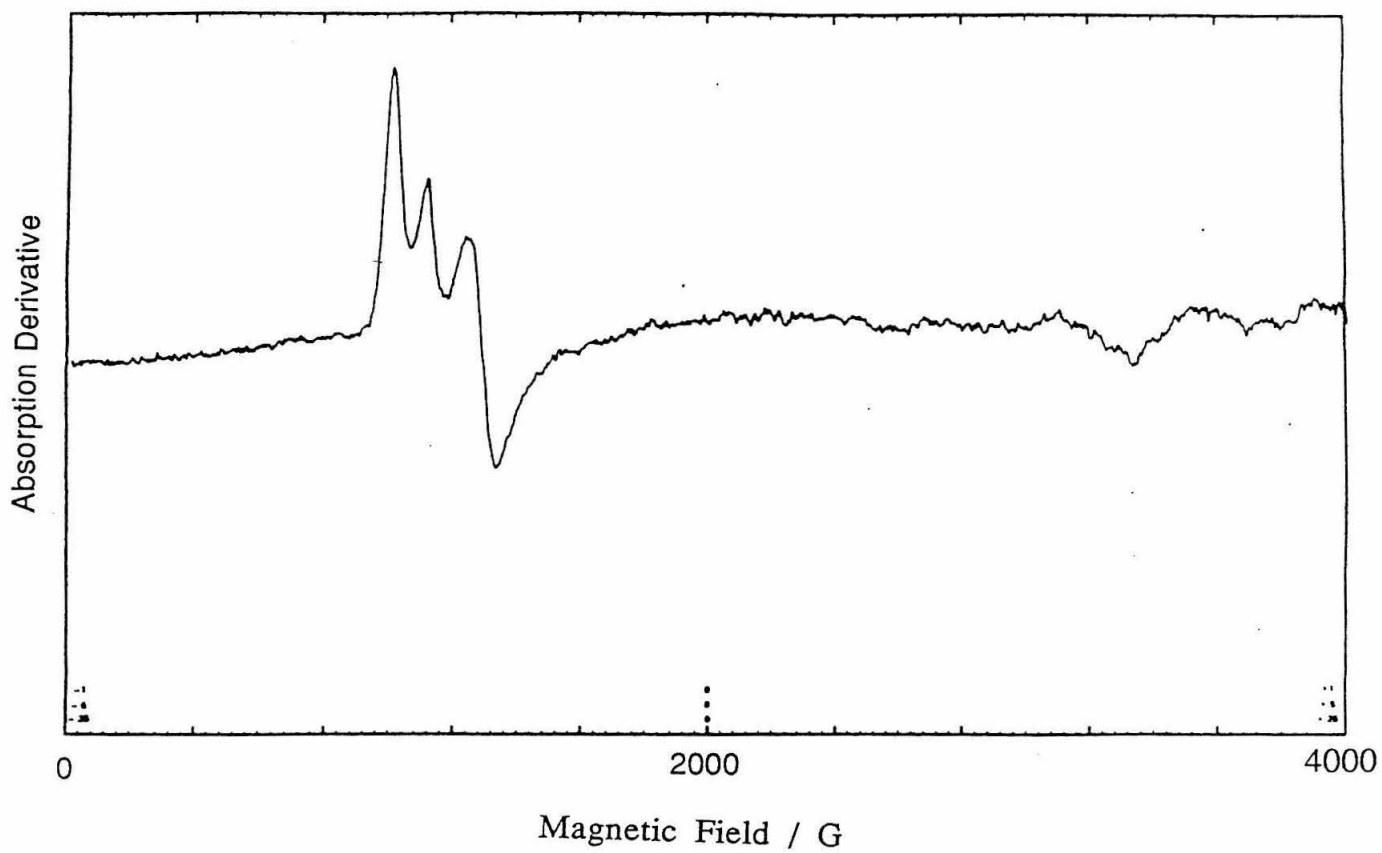


Figure 10. ESR spectra of Val68Glu myoglobin at 3.8°K (top) and 50°K (bottom). The top spectrum has the same parameters as Figure 9 except 1.6×10^4 receiver gain. The bottom spectrum has the same parameters except 2.5×10^4 receiver gain and is 2mM.

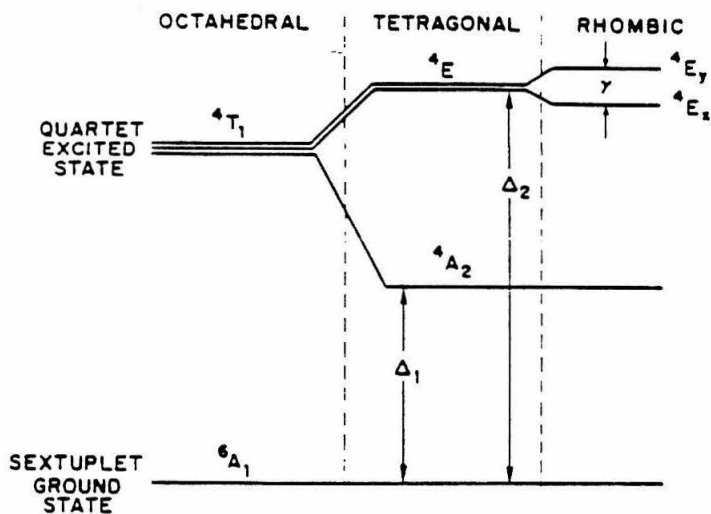


with magnetic field, this could be another reason why our fit to the glutamate mutant NMRD profile was only approximate.

It should be noted that at liquid helium temperature, three peaks appear near $g=6$ in the glutamate mutant ESR spectrum (6.5, 5.8, 5.0). The only reasonable explanation for this is a mixture of different two major states of the iron(III) center. Both are high spin, one with $E/D=0.06$ and one with E/D which appears to be approximately zero in this frozen solution. The spectrum arising from the state with $E/D=0.031$ becomes dominant at 120°K which would indicate a thermal equilibrium between the two states which strongly favors (>99%) the $E/D=0.031$ state at the temperatures of the NMRD measurements.

A thermal equilibrium of two major iron(III) spin states is also evident in the ESR spectrum of the aspartate mutant; except, in this case the two states are not both high spin, one is high spin and the other low spin ($S=1/2$). Low spin ferric heme signals have been well documented; the manifold of absorptions at $g=2.8, 2.3$, and 2.0 for the aspartate mutant undeniably fall into this category (figure 9).^{29,30} The low spin signal occurs when the energy of the Fe(III) d_{z^2} orbital is raised such that spin pairing energy is less than the potential energy difference from the ligand field effects (Figure 11). A ligand electron density (negative charge) along the Z-axis of the iron(III) (perpendicular to the heme) would dramatically raise the energy of the d_{z^2} orbital. Thus, it is probable that the structure giving rise to the low spin signal is one in which the carboxylate group of the mutant aspartate residue is either very strongly hydrogen bonded to a hydrogen of a water molecule coordinated to the heme, or the carboxyl group actually has taken a proton from the water molecule leaving a hydroxyl group coordinated to the heme. Molecular modeling has shown that either oxygen atom in the mutant aspartate residue sidechain is within the appropriate distance to hydrogen bond to hydrogens of a heme-coordinated water. (The

Figure 11. Relevant electronic information for an Fe(III) heme. The diagram and equations on top refer to a high spin system ($S=5/2$) which is progressively distorted from octahedral symmetry and is somewhat mixed with the $S=3/2$ spin manifold according to the term h . d is the effective spin-orbit coupling constant and b is an effective orbital g value for the quartet ($S=3/2$) excited state (4T_1). The diagram on the bottom represents the possible ground spin states of ferric hemes. Adapted from Refs. 25-27.



$$\eta^2 = \frac{a^2}{5} \left(\frac{1}{\Delta_1^2} + \frac{1}{\Delta_2^2} - \frac{b}{\Delta_1 \Delta_2} \right)$$

$$E/D = \frac{1}{2} \frac{\gamma}{\Delta_2} \frac{\Delta_1}{\Delta_2 - \Delta_1}$$

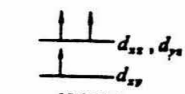
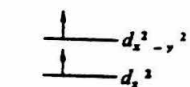
$${}^6A_1 = (d_{xy})^+ (d_{xz})^+ (d_{yz})^+ (d_{z^2})^+ (d_{x^2-y^2})^+$$

$${}^4A_2 = (d_{xy})^2 (d_{xz})^+ (d_{yz})^+ (d_{z^2})^+$$

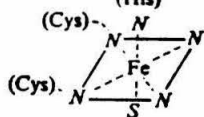
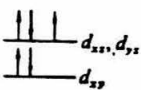
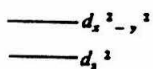
$${}^4E = (d_{xz})^2 (d_{yz})^+ (d_{xy})^+ (d_{z^2})^+$$

$$(d_{yz})^2 (d_{xz})^+ (d_{xy})^+ (d_{z^2})^+$$

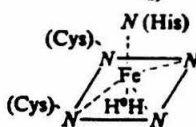
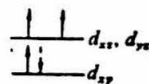
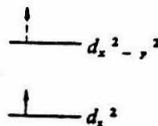
(A) High spin



(B) Low spin



(C) Quantum mechanically admixed intermediate and high spin

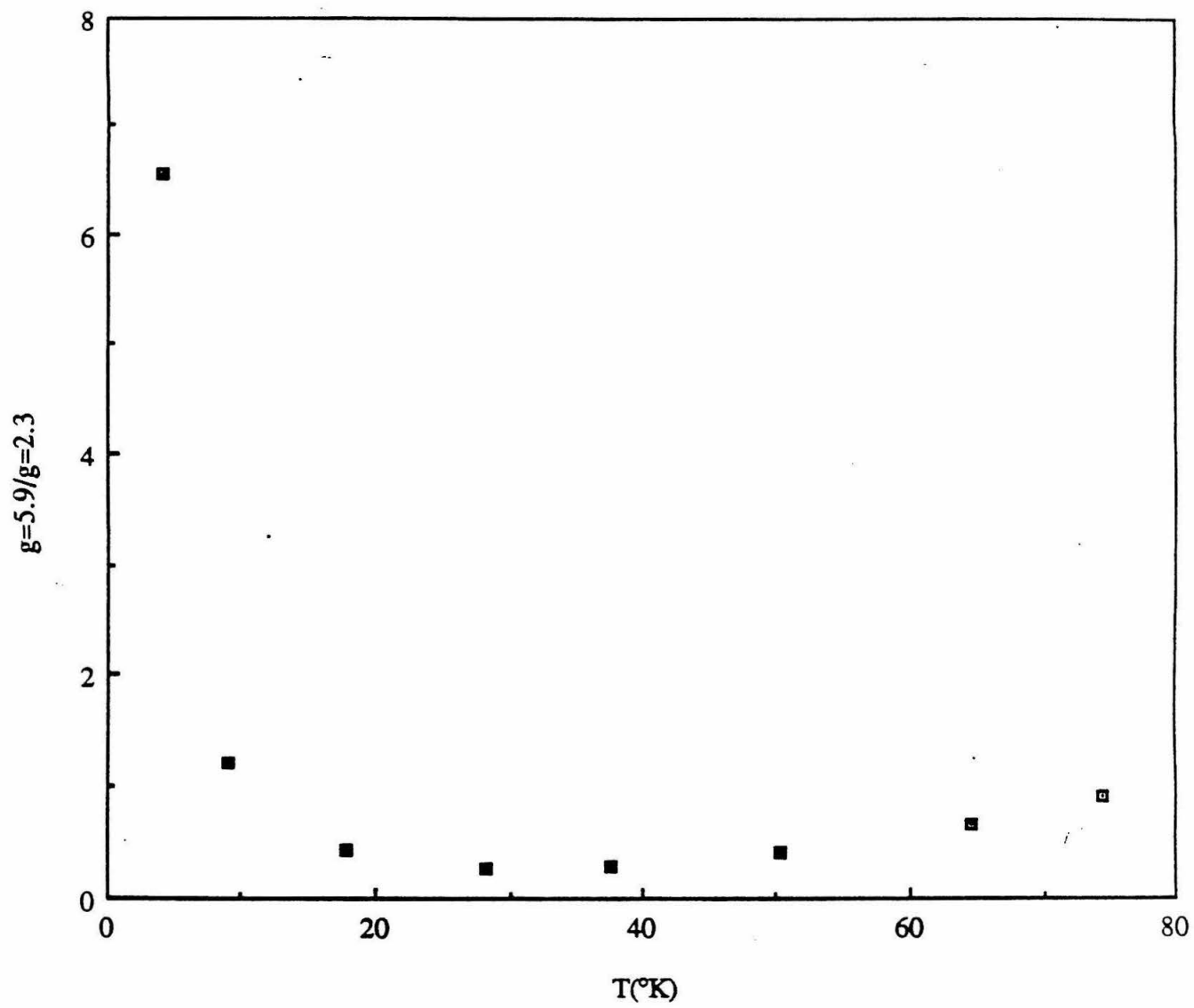


aspartate sidechain is not long enough for its carboxylate to bind to the heme itself.)

Further, the ESR spectrum of hydroxymetmyoglobin also shows a mixture of high and low spin forms. The thermal equilibrium is shifted in favor of the high spin form at higher temperatures for hydroxymetmyoglobin.²⁹ The same temperature dependence is observed for the aspartate mutant myoglobin (Figure 12). Extrapolating the ESR temperature dependence to the temperature of the NMRD experiments, there should be less than 0.1% low spin form. This is what we expected since the visible absorption spectrum at room temperature indicates no trace of low spin heme (Chapter 2). At very low temperatures (4-10°K) there is a sharp decrease in the ratio of high-spin to low spin forms with increasing temperatures. This effect is caused by a thermal saturation which is extremely precipitous for the ferric $S=5/2$ signal at very low temperatures,³¹ the $S=1/2$ signal hardly changes (<15%) in going from 4 to 10·K because it is not being thermally saturated. At temperatures above about 30°K (Figure 12) the saturation effect becomes overshadowed by a shifting of the thermal equilibrium of the two chemical forms of the protein in favor of that form which gives rise to the high spin signal. (Variable temperature ESR experiments for hydroxymetmyoglobin did not show this initial decrease in the high spin to low spin ratio; however, they did not go below 77°K.)

In another ESR experiment, $H_2^{17}O$ was added to the mutant proteins. Hyperfine coupling between the ^{17}O nucleus ($I=5/2$) and the iron (III) electrons has been observed to cause a broadening of the ferric heme signal in myoglobin.³² It was hoped that this same broadening could be observed in the mutant proteins to determine whether water was bound in the sixth coordination site of the heme in any of them. We were able to reproduce the ^{17}O hyperfine broadening of the $g=2$ signal in the native myoglobin. The $H_2^{17}O$ treated

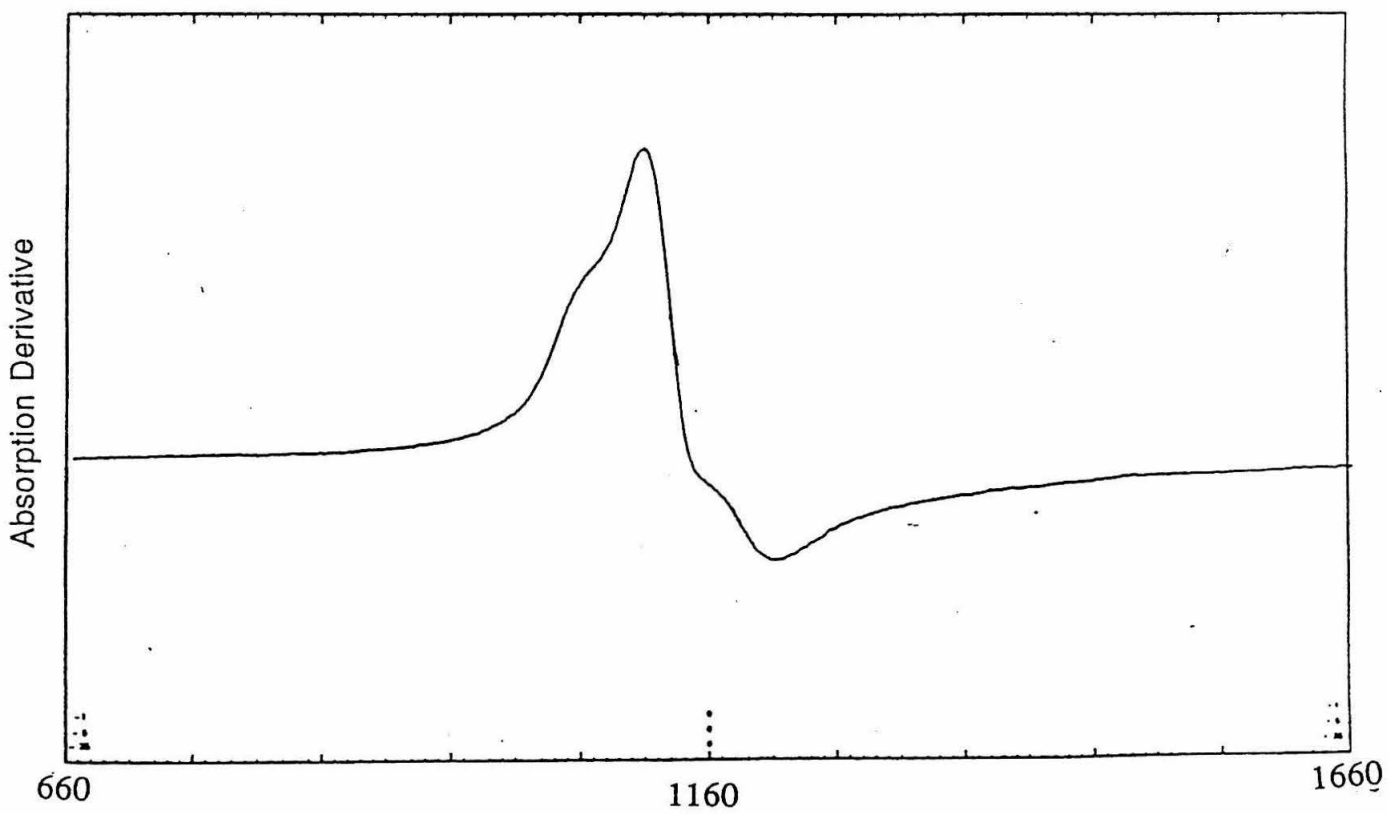
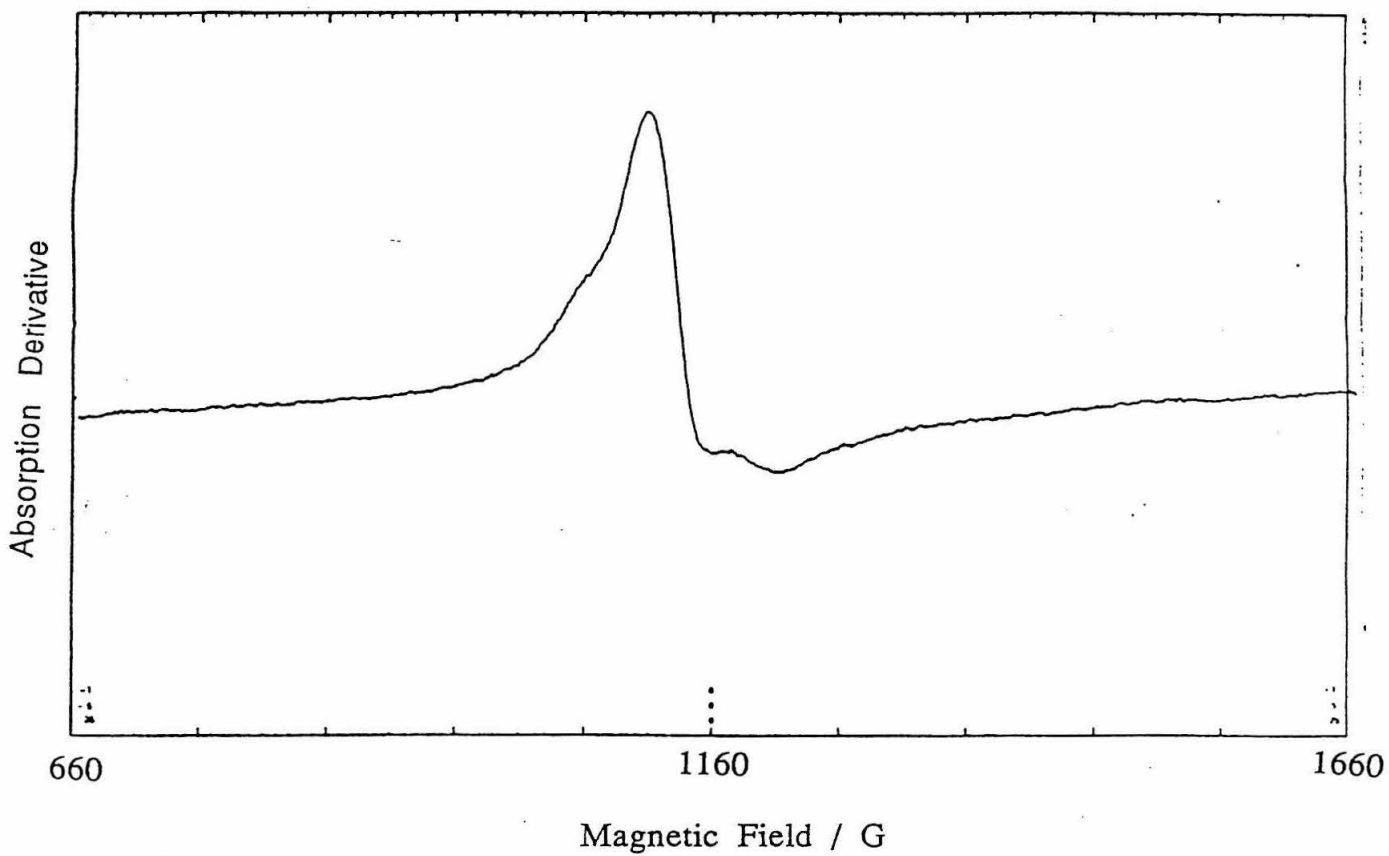
Figure 12. Temperature dependence of the ratio of the ESR signal at $g=5.9$ to that at $g=2.3$ for the Val68Asp myoglobin. Same parameters as Figure 9.



glutamate mutant showed no detectable broadening in any of its ESR signals while aspartate mutant demonstrated significant broadening of its lowest field band (figure 13). The other bands of the aspartate mutant were not broadened. It is not unexpected to see preferential broadening of one geometric component of a heme ESR signal compared to another because ligand hyperfine interactions are anisotropic.³³ However, the native myoglobin signal shows preferential broadening of its highest field ESR signal ($g=2$)³² in contrast to the aspartate mutant which shows broadening of its lowest field ($g=5.9$) signal. The reason for this difference could be that rhombic distortion, which affects only the $g=6$ signal in hemes, causes the lowest field transition to be the most susceptible to hyperfine broadening. Evidence for this hypothesis can be seen in the axial, slightly rhombic, ferric ESR spectrum, of $H_2^{17}O$ treated lipoygenases ($E/D=.01$ and $E/D=.06$) which also show the most significant broadening in its lowest field signal.³⁴

In summary, NMRD and EPR indicate that a water is bound to the ferric heme in the aspartate and asparagine mutants and a carboxylate is coordinated in the glutamate mutant. The similarity of the glutamate NMRD profile to that of fluoromethemoglobin is evidence that a water molecule hydrogen bound to a coordinated carboxylate oxygen is the most significant contributor to the paramagnetic relaxivity (T_{1P}^{-1}). The fit of the dispersion data, which indicates hydrogen bound approximately 4\AA away from the Fe(III) undergoing t_S limited relaxation, supports the above assertion. Further, the magnitude of the inverse thermal activation of the T_{1P}^{-1} of the glutamate mutant is equal to that of fluoromethemoglobin. In contrast, the aspartate and asparagine mutants have dispersion shapes similar to that of native myoglobin which has a ferric-coordinated water molecule, and all of these proteins have thermally activated T_{1P}^{-1} . Also, the ESR spectra of the asparagine and

Figure 13. ESR spectra (660-1660 Gauss) of H_2^{16}O (top) and H_2^{17}O (bottom) treated Val68Asp myoglobin. Same parameters as Figure 9 except that the concentration for both samples was $\approx 2\text{mM}$.



aspartate mutants and native myoglobin are all very similar and show much less rhombic distortion than the glutamate mutant spectrum. This ESR result is theoretically consistent with our Fe(III) bonding model since a bound carboxylate is less symmetric than a bound water molecule. Moreover, the ESR spectrum of the aspartate mutant is very similar to that of hydroxymetmyoglobin ($E/D \approx 0.002$ with a high/low spin equilibrium) suggesting an interaction between the carboxylate from the aspartate residue and a hydrogen from a water molecule bound to the heme. Finally, the deviations of the NMRD profiles from the present theory for $S=5/2$ ions can be accounted for in the asymmetry and accompanying ligand field splitting and also the slight admixture of the $S=5/2$ state with the $S=3/2$ state. ($h \approx 0.1$ for all the mutants and the native protein.)

References

1. Davidson, D. and Gold, R., *Biochim. Biophys. Acta* 26, 370 (1957).
2. Wishnia, A., *J. Chem. Phys.* 32, 871 (1960).
3. Brewer, C. F., Brown, R. D., III, and Koenig, S. F., *Biochem.* 22, 3961 (1983).
4. Mildvan, A. S., Eastabrook, R. W., and Palmer, G., in *Magnetic Resonance in Biological Systems*, Ehrenberg, E. G., Malmstrum, B. G., and Vanngard, T. (Eds.), Pergamon Press, p.175 (1967).
5. Bertini, I. *et al.*, *Inorg. Chem.* 28, 352 (1989).
6. Koenig, S. H. and Brown, R. D., *Handbook of NMR in Cells*, CRC Press (1987).
7. Bertini, I. and Luchinat, C., *NMR of Paramagnetic Molecules in Biological Systems*, Benjamin /Cummings Inc. (1986).
8. Luz, Z. and Meiboom, S., *J. Chem. Phys.* 40, 2686 (1964).
9. Daszkiewicz, O. K. *et al.*, *Nature* 200, 1006 (1963).
10. Koenig, S. H. *et al.*, *Biochem.* 17, 4348 (1978).
11. Koenig, S. H., Brown, R. D., III, and Lindstrom, T. R., *Biophys. J.* 34, 397 (1981).
12. Bennet, H. F. *et al.*, *Magn. Reson. Med.* 4, 93 (1987).
13. Koenig, S. H. and Brown, R. D., III, *Ann. N. Y. Acad. Sci.* 222, 752 (1973).
14. Koenig, S. H. and Schillinger, W. E., *J. Biol. Chem.* 244, 6520 (1969).
15. Gupta, R. K. and Mildvan, A. N., *Ibid.* 250, 246 (1975).
16. Koenig, S. H., Baglin, C. M., and Brown, R. D., III, *Magn. Reson. Med.* 2, 283 (1985).
17. Sternlicht, H., *J. Chem Phys.* 42, 2250 (1965).
18. Deatherage, J. F., Loe, R. S., and Moffat, K., *J. Mol. Biol.* 104, 723 (1976).
19. Lumry, R. *et al.*, *J. Phys. Chem.* 65, 837 (1961).
20. Dowsing, R. D. and Gibson, J. F. , *J. Chem. Phys.* 50, 294 (1969).
21. Blumberg, W. E., in *Proceedings of the Second International Conference on Magnetic Resonance in Biological Systems*,Pergamon Press, p. 119 (1967).
22. Pinkowitz, R. A. and Aisen, P., *J. Biol. Chem.* 247, 7830 (1972).

23. Palmer, G., in *Iron Porphyrins*, Part II, Lever, A. B. P. and Gray, H. B. (eds.), Addison Wesley, p. 52 (1982).
24. *Ibid.* p. 51.
25. Brill, A. S., Fiamingo, F. G., and Hampton, D. A., *Frontiers in Biological Energetics* 2, 1025 (1978).
26. Maltempo, M. M. and Moss, T. H., *Quarterly Reviews of Biophysics* 9, 181 (1976).
27. Griffith, J. S., *Proc. Roy. Soc. A*235, 23 (1956).
28. Schulz, C. et al., *Inorg. Chem.*, in press.
29. Ehrenberg, A., *Arkiv For Kemi* 19, 119 (1962).
30. Ehrenberg, A. and Estabrook, R. W., *Acta Chem. Scand.* 20, 1667 (1966).
31. *Ibid.* 23, p.68.
32. Vuk-Pavlovic, S. and Siderer, Y., *Biochem. Biophys. Res. Comm.* 79, 885 (1977).
33. Goodman, B. A. and Raynor, J. B., *Adv. Inorg. Chem. Radiochem.* 13, 135 (1970).
34. Nelson, M. J., *J. Am. Chem. Soc.* 110, 2985 (1988).

CHAPTER 4
KINETICS OF
RUTHENIUM-MODIFIED DERIVATIVES

Electron transfer processes are of fundamental importance in a wide variety of fields. In biology these reactions occur in energy uptake events like photosynthesis¹ and oxidative phosphorylation.²⁻⁴ Often charge transfer can occur over long distances ($>10\text{\AA}$) with considerable rates (e.g. picoseconds in photosynthetic reaction centers).⁵ To further understand and possibly mimic these systems, the relative importance of factors which influence the rate must be clarified.

Semi-classical models are convenient for representing the physical principles involved in electron transfer and are, therefore, used quite frequently.⁶ For intramolecular electron transfer the most general form of the rate constant is given by

$$k_{et} = \nu_n \kappa_{el} \kappa_n \quad (1)$$

In terms of activated complex theory, ν_n , the nuclear vibrational frequency, corresponds to the frequency of approach to the activation barrier, κ_{el} is the electronic transmission coefficient which is the probability of reaction at the height of the activation barrier (activated complex), and κ_n is the nuclear factor or probability of forming the activated complex.

The electronic transmission coefficient is proportional to the donor/acceptor wave function overlap. At long range (non-adiabatic limit) the overlap is limited to the tails of the respective wave functions so that the electronic term can be approximated by using a negative exponential weighted by a coupling term β .

$$\kappa_{el} = \exp^{-\beta(r-\rho)} \quad (2)$$

The spatial separation of donor and acceptor is r , and ρ is the the combined van der Waals radii of the donor/acceptor pair. Included in β are orientational effects which depend upon orbital symmetry, molecular configuration, and intervening medium.⁷

Using straightforward geometric arguments and the classical harmonic oscillator approximation for nuclear motion, the Marcus equation is obtained:⁶

$$\kappa_n = \exp[-(\Delta G^\ddagger/RT)] = \exp[-(\lambda + \Delta G^\circ)^2/4\lambda KT] \quad (3)$$

ΔG° , also known as the driving force, is the redox potential difference between donor and acceptor. λ is the free energy necessary to change the orientation and microscopic geometry of the donor/acceptor pair and medium to the equilibrium nuclear position for the potential energy surfaces of reactant and product--the activated complex. λ , the reorganizational energy, can be separated into two components:

$$\lambda = \lambda_{in} + \lambda_{out} \quad (4)$$

an inner-sphere contribution which includes the internal displacement of bonds in the donor and acceptor, and an outer-sphere contribution which is the free energy of polarization of solvent to its "activated" position before electron transfer can occur. Using the dielectric continuum approximation for solvent, one obtains the following expression for the outer sphere reorganization energy:

$$\lambda_{out} = (\Delta e)^2 \left[\frac{1}{2a_1} + \frac{1}{2a_2} - \frac{1}{r} \right] \left[\frac{1}{D_{op}} - \frac{1}{D_s} \right] \quad (5)$$

where a_1 and a_2 are the radii of the two spherical reactants, r and Δe are their respective separation and charge to be transferred, and D_{op} and D_s are the solvent's optical and static dielectric constants. Inner sphere reorganization can be calculated from the parameters of the inner shell vibrational modes:

$$\lambda_{in} = 1/2 \sum_{jk} k_{Hjk} Q_j Q_k \quad (6)$$

where k_{Hjk} , the Hook's law force constant, can be approximated by its value before, f_r , and after, f_p , electron transfer.

$$k_H = 2f_r f_p / (f_r + f_p) \quad (7)$$

This relation holds for each subscript in equation 6. $Q_{j,k}$ is the displacement of the equilibrium positions of the vibrational coordinates caused by electron transfer.³

In general then there are two factors which influence the rate of intramolecular electron transfer: electronic and nuclear. The former is a function of distance, donor/acceptor symmetries, orientation and medium; in the non-adiabatic limit it is non-energetic. The latter depends upon temperature, driving force, and reorganizational parameters; it is always energetic. The quantum mechanical expression (derived from radiationless transition theory) of the electron transfer rate constant is a compact representation of these concepts:

$$k = \frac{2\pi}{h} H_{ab}^2 (FC) \quad (8)$$

where H_{ab} is the electronic coupling between reactants and products, and (FC) is the thermally averaged vibrational overlap of initial and final states.

A serious obstacle in the experimental verification of these theories is that it is difficult to vary only one factor at a time. For example, the use of rigid organic bridges simplifies analysis¹¹⁻¹⁴ because a fixed donor/acceptor spacing eliminates the need for a summation over an infinite number of distances; moreover, the work involved in the formation of a precursor complex need not be considered. However, a fundamental difficulty in applying the results obtained from these complexes to biological electron transfer is that there is often no short covalent path between donor and acceptor in biological systems.¹⁵ Theory predicts an enhanced electronic coupling in through bond (including sigma) pathways compared to through "space."¹⁶⁻¹⁷ Experimental evidence supports this assertion.^{15,18,19}

Other models of biological electron transfer include protein-small molecule systems,²⁰ protein-protein complexes²¹⁻²² and semi-synthetic multi-site metalloenzymes.^{18,19,23} This last method has the obvious advantage of being intramolecular, as well as being amenable to through “space” study and systematic changes in the factors responsible for determining k_{et} . Specifically, the approach in the Gray group has been to attach a transition metal complex which is relatively stable in two oxidation states $a_4LRu(2+/3+)$ ($a=NH_3$, pyridine, pyrazine, or isonicatinamide) to the imidazole of a solvent accessible histidine residue of a redox active protein. The two metal centers can then act as a donor/acceptor pair. Several measurements¹⁸ (UV-visible, CD, EPR and X-ray crystallography)²⁴ have confirmed that this method is only locally perturbative so that the environment of the native protein’s active site and its basic tertiary structure remain unchanged. Therefore, physical parameters of the native active site can be used in the analysis of electron transfer data, and the geometry of the donor, acceptor and intervening medium can be readily determined through local energy minimization of crystallographically determined coordinates²⁵ of the unmodified protein or by direct crystallography at the modified protein.²⁴

Kinetic studies have now been performed on several ruthenium-modified metalloproteins.¹⁸ This technique has been used to elicit information concerning medium effects, driving force, distance dependence and reorganization energy on several electron transfer proteins including cytochrome c,²⁶ azurin,²⁷ and high potential iron-sulfur proteins.²⁸ Moreover, studies of the oxygen carrier sperm whale myoglobin have been particularly productive because it has been the most thoroughly characterized protein prior to electron transfer studies, has several modifiable sites and contains a prosthetic group which is easily replaced.¹⁹ The most extensive experiments

with respect to the distance dependence and reorganization energy of electron transfer have been performed on this protein. Moreover, recent experiments with porphyrin substitutions have allowed a detailed analysis of donor/acceptor coupling in terms of H_{ab} and β , the nuclear frequency factor ν_n , and a reanalysis of λ .²⁹ With such a well defined system it should be possible to assign factors that control the rate of electron transfer to specific chemical and physical phenomena with a level of accuracy that has not yet been obtained for biological models.

Therefore, this system would be ideal for site-directed mutagenesis studies. But only human myoglobin can be produced genetically in a form that is identical to its natural counterpart. Human myoglobin is quite similar to sperm whale myoglobin. The sequence homology is 85%; it is >95% if one considers homology between residues of similar polarity (table 1). Moreover, excluding human and sperm whale from an evolutionary analysis of the residues that differ between them, one still finds that these residues are non-conserved. Further, >80% of the differences are on the protein exterior and, the optical and redox properties of the proteins are very similar (*vide infra*).

It is then assumed that the following is a good structural model for human myoglobin. Starting with a sperm whale peptide backbone, the sperm whale residues were replaced with those in the human sequence, then the sidechains were aligned and locally perturbed to find energy minima through 360 degrees of dihedral angle in the $C_\alpha - C_\beta$ bond in 20 degree increments. The graphics indicate that there is no significant difference in the respective environments or positions between the human and corresponding sperm whale residues His48 and His81. Therefore, ruthenium modification was predicted to work--as it did (*vide infra*).

TABLE 1

Different Residues of Human and Sperm Whale Myoglobin

<u>Residue Number</u>	<u>Human</u>	<u>Sperm Whale</u>
1	glycine	valine
4	aspartate	glutamate
* 12	asparagine	histidine
15	glycine	alanine
21	isoleucine	valine
22	proline	alanine
27	glutamate	aspartate
28	valine	isoleucine
35	glycine	serine
45	lysine	arginine
51	serine	threonine
* 53	aspartate	alanine
66	alanine	valine
74	glycine	alanine
86	isoleucine	leucine
101	valine	isoleucine
110	cysteine	alanine
* 113	glutamine	histidine
* 116	glutamine	histidine
118	lysine	arginine
* 122	aspartate	asparagine
142	methionine	isoleucine
144	serine	alanine
* 145	asparagine	lysine
151	phenylalanine	tyrosine

(*) Indicates a possible change in charge.

We believe that the Val68 mutants would be interesting model compounds for electron transfer studies. The influence of these polar and charged heme-pocket mutations on the redox thermodynamic properties are quite dramatic (Chapter 2). Since the reduction potentials are changed in these mutant proteins compared to native myoglobin (lowered 200mV in both Val68Glu and Val68Asp), we will be changing the driving force for heme to ruthenium electron transfer in the corresponding ruthenium modified proteins. Moreover, the effect of different structural perturbations on intramolecular protein electron transfer can be addressed. A number of biochemical (IEF, ligand binding studies, and electrochemistry) and spectroscopic (UV-vis, CD, NMR, NMRD, and ESR) techniques have been used to clarify the interaction between the heme and the new residue side chains in the Val68 myoglobin mutants (Chapters 2 and 3). Some results relevant to this kinetic study are that the carboxylate sidechain of the glutamate in Val68Glu is bound to the ferric heme while the aspartate sidechain in Val68Asp is not. Instead, a water molecule is bound to the ferric heme in Val68Asp as in native myoglobin. The sixth coordination site is occupied by an imidazole nitrogen from the sidechain of His93 in all these proteins.

Upon reduction the heme becomes five-coordinate in the mutant myoglobins and the native protein; further, the mutant carboxylate sidechains in both Val68Asp and Val68Glu are neutralized by proton uptake in the ferrous myoglobins. Thus, specific changes in inner sphere (e.g., releasing an iron bound water molecule upon electron transfer) and outer sphere (e.g., change in protein dielectric change when a polar residue is placed in the protein interior) reorganization energy will be analyzed in these mutant proteins.

Experimental

All computer graphics and related calculations were performed using BIOGRAF.CAMD version 123 on a DEC Microvax. Results were displayed on an Evans and Sutherland 340 terminal.

Pentaamine ruthenium modification was performed on 30mg of the Cys110Ala derivative using the same methods used for sperm whale myoglobin.¹⁵ Time, concentration, and pH assays were performed: the optimal conditions for single modification of His48 were determined to be 0.1M NaPi, 25x (NH₃)₅Ru(II)H₂O and 15 minutes reaction time. For the His81Gln mutants this reaction was performed for 30 minutes. Excess Co(phen)₃(ClO₄)₃ was prepared in advance and added to keep the metal centers oxidized. The oxidant and excess ruthenium complex were removed using a gel filtration column (G-25, 3-15cm). The products were tentatively identified and purified using analytical IEF (LKB) and FPLC (Pharmacia). Cation (Mono S) exchange was used for the native protein and the Cys110Ala mutant. The His81Gln mutants did not bind well to cation exchange, but did bind to anion exchange (Mono Q).

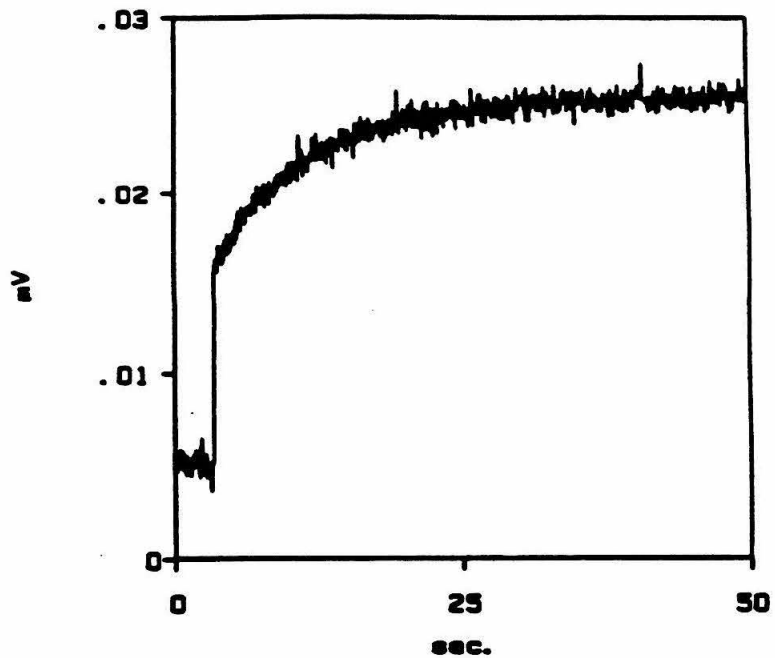
PMR spectra of the derivatized proteins were acquired using a Bruker WM500 spectrometer. Typically 500-600 scans were needed for most samples of concentration 0.5-1.0mM. The samples were prepared by ultrafiltration and addition of D₂O (99.9%, Aldrich) using YM10 Centricons. The pH was adjusted with 0.05M DCl or NaOD and was uncorrected for deuterium isotope effects. Differential Pulse Polarography was performed as previously described at protein concentrations of 2mM.³⁴ Spectroelectrochemistry was performed as described in Chapter 2.

Flash photolysis was performed in a 15cm pathlength water-jacketed cell. 7.25mM EDTA, 650μM Ru(Bpy)₃⁺² reagents in the 10ml flash solution.

Figure 1. Dideoxy sequencing gel of M13 sst containing His → Gln mutations at codons 48 and 81. Klenow fragment was used along with ^{35}S as the tracer isotope. The His48Gln reaction was primed at codon 21 while the His81Gln reaction was primed at codon 68.

Figure 2. Transient absorption traces after flash photolysis of singly ruthenium-modified myoglobin. The top trace is of the first FPLC peak and the bottom of the second FPLC peak; the contents are believed to be the His48 and His81 modified proteins, respectively. Flash sample preparation given in the experimental section (as with all other flash traces).

Sample from First FPLC Peak



Sample from Second FPLC Peak

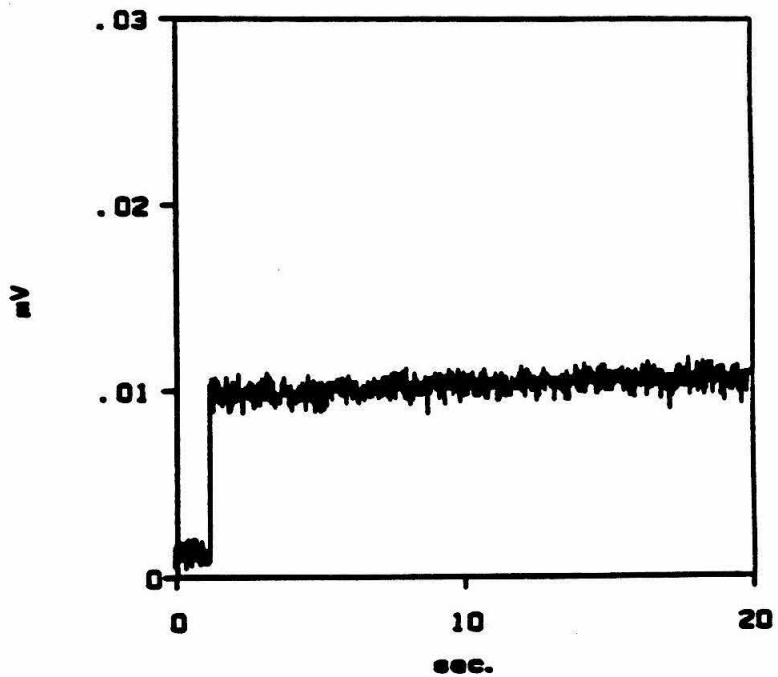
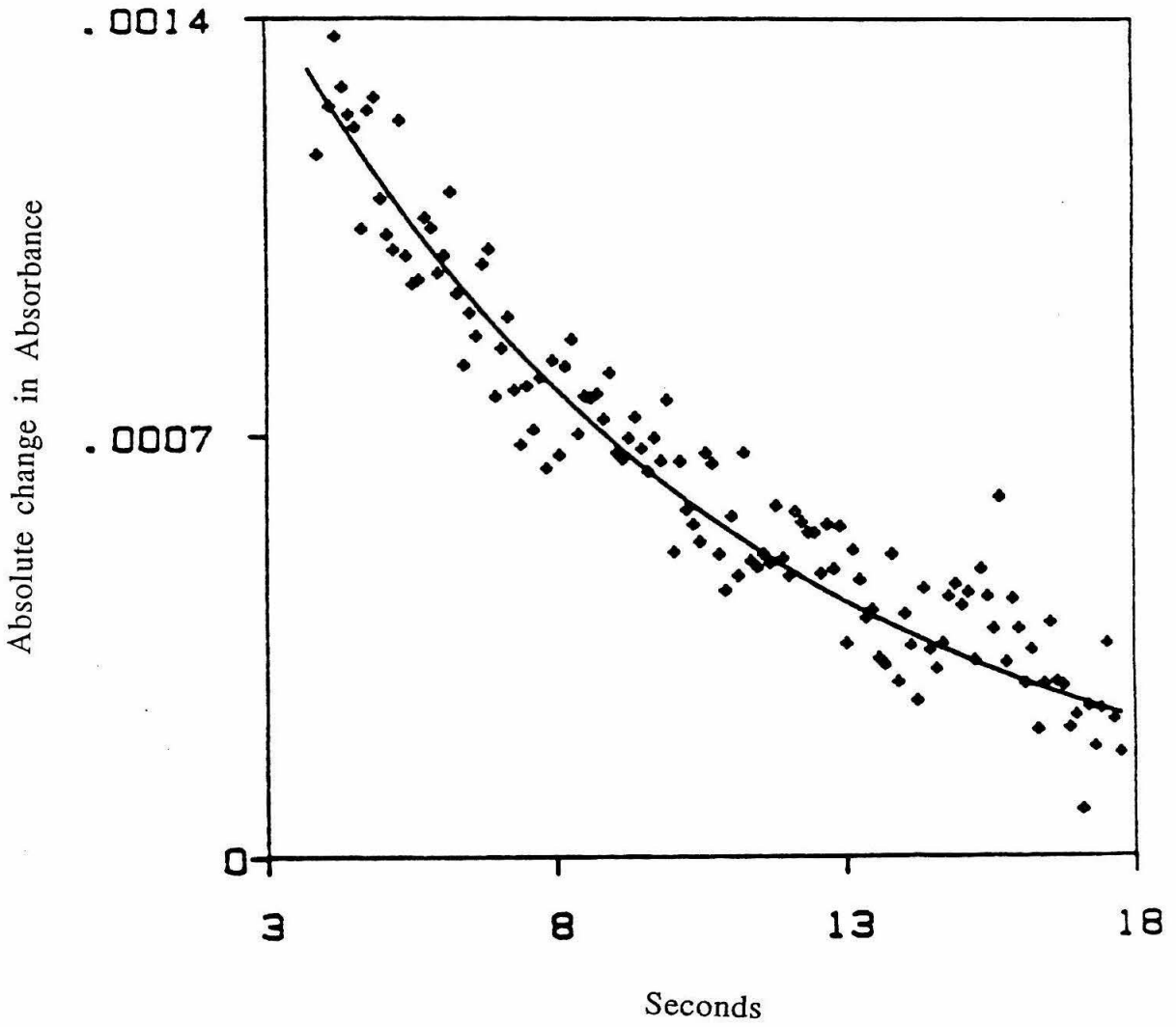


Figure 3. Two parameter fit of top flash trace in Figure 2. $k_{obs}=0.150\pm 0.020$, correlation coefficient=0.948.



The specific protein concentrations (2-15 μ M) are indicated in the figure legends. The flash solution was first rigorously degassed by alternate exposure to vacuum (10^{-3} Torr, 30 seconds) and argon gas (5 min.) 3-4 times while stirring. The protein was then added and the solution was degassed again but less rigorously (4 cycles with only 3 second exposure to vacuum each time).

The probe and flash lamps were allowed to warm up for greater than 30 minutes prior to the run. Absorbance at 555nm was monitored, and rates were obtained using the flash apparatus described previously.³⁰ An IBM compatible computer instead of the biomation, a 100x amplifier and fiber optics for directing the probe beam had been added as was a polyurethane pad under the optics (to reduce vibrational noise).

After the flash experiment the proteins could be ultra-filtered (YM10 Centricons, Amicon Co.) and repurified on FPLC for reuse.

The recombinant proteins were purified from *E. coli* AR68 which had been grown up as previously described. The cells were harvested at 5°C through a continuous flow centrifuge at a rate of 100L/hr. Cell paste was immediately frozen in LN₂ (popcorn) and stored in a CO₂ freezer at -70°C. The previously published, purification procedure was followed with the following modifications.³⁴ The protease inhibitor PMSF was not used. Cells were lysed using an ultrasonicator; 70ml volumes of the cell suspension were exposed (5 times at 400W) to ultrasound for 2 minute intervals with 3 minute periods in between. It was important that the suspension remain on ice throughout this procedure. The Triton X-100 treated pellet should be raised to pH 8.8 when the 8M urea buffer is first added. The suspension should turn to a lighter tan color once all of the cells have been lysed. The dialysis tubing was from Spectrum Medical Industries (Spectrapor, MW cutoff 6000-8000). The yellow supernatant resulting from the centrifugation of the urea extract need not have any DTT in

the subsequent dialysis buffer since Cys110 was replaced with Ala. It is essential not to concentrate the dialysate before the trypsin digest as the reconstitution/digest yield is better when the initial protein solution is dilute (~0.75mg/ml). For the second digest the protein can be concentrated beforehand using YM10, Amicon ultrafiltration membranes. Moreover, the Zn mesoporphyrin IX (ZnmPIX) reconstitution was allowed to proceed for 6 hrs at 16°C before trypsin was added. ZnmPIX was prepared as previously described.³⁴ It is important that the ZnmPIX or its protein derivatives not be exposed to light. A three-fold excess of ZnmPIX was used in the reconstitution, and a 25cm length of DE-52 column was used in the initial purification. The ZnmPIX-substituted and the heme-substituted, charged, heme-pocket mutant proteins were eluted off the second DE-52 column with 100mM and 60mM Tris•HCl pH 9.0 at 4°C (pH 8.75 at 25°C), respectively. The most successful method of month-timescale storage of proteins was in 100mM Tris•HCl, pH 7.0 at 4°C (i.e., the ammonium sulfate precipitate need not be formed). The protein concentration should be above 0.5mM. Flash freezing in the LN₂ and storage at -70°C is preferable for long term storage.

I thank Prof. P. B. Dervan for allowing me to use the Beckman System 1 Plus DNA Synthesizer in his lab to construct (phosphoramidite method) 18-mer oligonucleotides. The oligos were purified using polyacrylamide (20%) gel electrophoresis and subsequent dialysis. Melting temperature, oligo binding data, and restriction sites were calculated or assigned using the University of Wisconsin Genetics Computer Group software on a DEC Vax 8550 at Stanford University (Cell Biology). The Kunkel procedure was used for mutagenesis with several minor modifications published elsewhere and described in the results and discussion section. Sequencing (Sanger) reagents were obtained from

Amersham. All non-restriction enzymes were obtained from New England Biolabs.

Site-Directed Mutagenesis

Non-selective reaction of $a_4LRu(II)H_2O$ with residues other than histidine (e.g., cysteine) or multiple modification of histidines are technical drawbacks of the ruthenium modification. Site-directed mutagenesis was used to eliminate these problems for human myoglobin. First, the mutation Cys110Ala was cloned into the Val68Asp variant of human myoglobin. The former mutation had been constructed in the native gene and cloned into the Val68Glu and Val68Asn proteins previously for another technical reason: the prevention of dimer formation during protein purification and electrochemistry. Secondly, the two surface histidines--residues 48 and 81--were individually changed to glutamine via the Kunkel procedure in the native protein and cloned into all of the Cys110Ala proteins. The histidine to glutamine mutations were used to increase yields of desired modification, facilitate NMR identification of modified residues and construct a base protein with no surface histidines (to which we can later mutate histidines at predetermined sites for distance dependence studies).

Uracil-containing single-stranded template (sst) was isolated from the RZ1032 (*dut⁻ ung⁻*) strain of *E. coli* after infection with the non-amber vector m13mp11mbca. The mismatched oligonucleotides were then separately hybridized to the human myoglobin gene in the sst. The complement to the sst was then synthesized by extending the mismatched oligonucleotide with deoxynucleotides using Klenow fragment (5'-3' polymerase and 3'-5' exonuclease). The uracil-free complement was circularized using T4 ligase. The double-stranded molecules were then transformed into supercompetent cells DH5a or directly into JM101. Both of these strains of *E. coli* are *dut⁺ ung⁺*;

therefore, the uracil-containing template was destroyed. Plaques were picked, grown up and the concentrated phage supernatant blotted onto nitrocellulose paper. The filter was exposed to the appropriate ^{32}P labeled oligonucleotides and then washed above the pre-calculated "melting" temperature of the mismatched oligonucleotides (55°C for His48Gln and 64.5°C for His81Gln). Positive plaques underwent a second screening for purification. Dideoxy sequencing confirmed the mutations (figure).

48 mutation		81 mutation
CAAGTTCGTGGACTTCAG	nonsense strand	CTTCCCCGTAGTACTCCG
GTTCAAGCA_CTGAAGTC	mismatched 18-mer	GAAGGGGCA_CATGAGGC
A		A

A BamH1/Afl2 restriction digest of the His48Gln mutant m13 and Afl2/Hind3 digests of the His81Gln mutant m13 were cloned into the complementary digests of the expression vectors pMb4(x) which are variants of PLclIFXB the expression vector used for β -globin.³²

Thus, four new mutant proteins were constructed:

His81Gln, Cys110Ala
 Val68Asp, His81Gln, Cys110Ala
 Val68Glu, His81Gln, Cys110Ala
 His48Gln, Cys110Ala

The pMb4 vectors were transformed into strain AR68 which has a temperature sensitive mutation in the λcl gene. (pMb4 expression is under control of the λ_{P_L} promoter.) pMb4 also codes for the first 31 amino acids of the λ phage cII protein and the tetrapeptide ile-glu-gly-arg. The latter peptide is the recognition site for the protease factor X; although, purification has been optimized using trypsin to degrade the part of the fusion protein that is not myoglobin.

Results and Discussion

To compare human and sperm whale myoglobin as semisynthetic models of electron transfer, pentaammine ruthenium derivatives of the human myoglobin Cys110Ala mutant were made and the electron transfer rates compared to the rates for the corresponding sperm whale derivatives. An analytical IEF (pH=6-10) for the products, after conditions were optimized for single modification, showed one minor band at 6.62 and three major bands at 7.25, 8.15, and 9.03. The first two bands were determined to be the reduced and oxidized forms of the starting protein, respectively. Of the two other bands the lower was assumed to be singly modified product while the higher was assumed to be doubly modified. In support of this hypothesis, both bands increased in intensity when more $a_5Ru(II)H_2O$ was added and when the reaction was allowed to proceed for a longer time. Moreover, it is known that for sperm whale myoglobin the pI increases approximately one unit for each ruthenium complex that is attached.³³

The protein reaction mixture was run on an FPLC cation exchange column. The 8.15 IEF band split into two peaks; whereas, the 9.03 IEF band came off as one peak. Absorbance at both 280 and 405nm were monitored and gave the same results. Flash photolysis was performed on the unmodified protein and the material corresponding to the first and second peaks of the 8.15 IEF band, respectively. In the flash photolysis experiments of these proteins $Ru(bpy=bipyridine)_3+2^*$ (*=photoexcited) acts as strong reductant of both the heme and the pendent ruthenium complex. Since the ruthenium complex is significantly more solvent accessible, it is much more frequently reduced than the heme. Thus, even though the driving force for the reaction favors the heme (II) to ruthenium (III) electron transfer, the signal from ruthenium (II) to heme (III) dominates the relaxation kinetics. The component corresponding to the first

FPLC peak exhibited measurable electron transfer; the component from the second did not. The trace of the second peak is identical with that of the native protein which, of course, was expected not to show kinetics (flat trace). The observed rate constant (k_{obs}) of the first peak was determined by a monophasic exponential fit to be 0.150s^{-1} (correlation coefficient=0.948). See Figure 2. This rate did not change over the range of protein concentrations $3\text{-}10\mu\text{M}$; therefore, bimolecularity was ruled out. Thus, it would appear reasonably safe to assign the first peak to the His48 derivative and the second peak to the His81 since from the analytical and kinetic data we know that they are the only singly modified products; we also know with reasonable certainty that 48 and 81 are the only surface histidines from the computer generated model of human myoglobin, and we know that for sperm whale myoglobin the His48 derivatives elutes before the His81 on cation exchange columns.³³ Finally, one would expect the electron transfer rate for the $\text{a}_5\text{Ru(II)His81Mb}$ derivative to be far too slow to be observed¹⁸ on our apparatus, which is the case.

The electron transfer k_{obs} for $\text{a}_5\text{Ru(II)HisSWMb}$ is 0.06s^{-1} which is 2.5 times smaller than that of its human counterpart. Although the difference in rates is clear, we believed that it is small enough to justify the use of the sperm whale myoglobin peptide backbone as a functional model for human. Later, the crystal structure of human myoglobin demonstrated that our assumption was sound.³⁴ Assuming the same β for sperm whale and human myoglobin, a change in edge-to-edge distance of only 1\AA between the histidine imidazole and heme would account for the difference in rates. Further, the $T_{1\rho}^{-1}$ for sperm whale myoglobin is 34% greater at low magnetic fields (0.02MHz) than that for human while the shapes of the dispersions are identical. This result suggests that the sperm whale heme pocket is more solvent accessible than the human counterpart. One would then expect a greater reorganization energy because

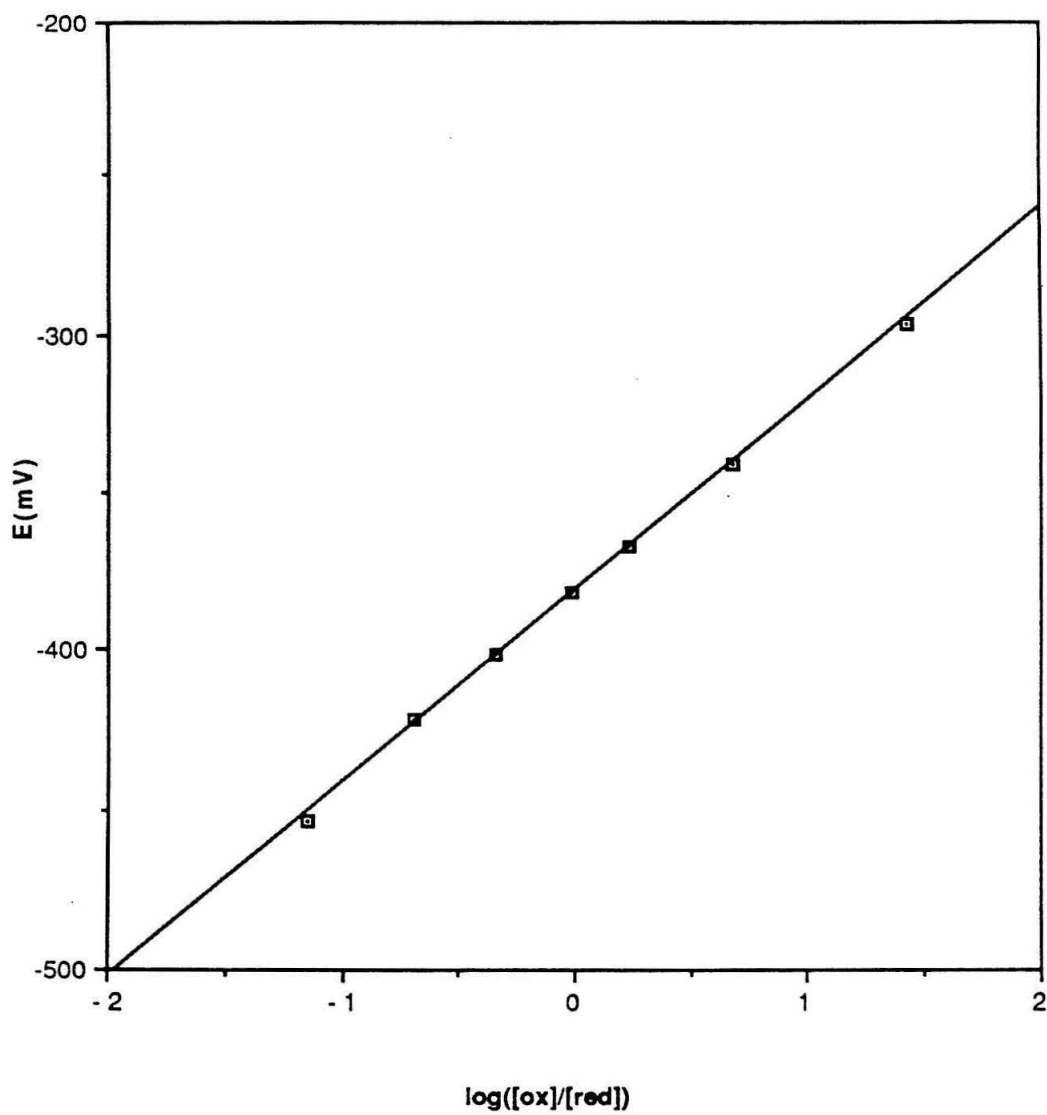
of a higher dielectric environment surrounding the sperm whale heme center, and thus a slower electron transfer rate.

His81Gln Mutants

Extensive characterization was performed on the His81Gln mutants to determine if this mutation perturbed the structure of the protein and if the protein was modified at His48 after being exposed to $(\text{NH}_3)_5\text{Ru}(\text{II})\text{H}_2\text{O}$. First, the protein was run on a copper affinity column (Monsanto Co., laboratory of Dr. Barry Haymore) which binds proteins according to the number of surface exposed histidines on them. The results using this technique were that the His81Gln protein bound to the column as if it had one surface histidine, while the corresponding ruthenium modified protein bound as if it had no surface histidines, as expected.

Spectroelectrochemistry of $(\text{NH}_3)_5\text{RuMb}(\text{Val68Glu}, \text{His81Gln}, \text{Cys110Ala})$ was performed. The UV-visible spectrum of this ruthenium modified protein was the same as the corresponding unmodified protein and the same as the unmodified protein without the His81Gln mutation. (This observation was true for all the proteins used in this chapter.) The spectroelectrochemical Nernst plot (figure 4) of $(\text{NH}_3)_5\text{RuMb}(\text{Val68Glu}, \text{His81Gln}, \text{Cys110Ala})$ gave an E° of $-135.3 \pm 2.5 \text{ mV}$ vs. NHE for the heme, which was within experimental error of the value of the unmodified Val68Glu, Cys110Ala protein (Chapter 2). These results indicate that there was no significant perturbation of the heme environment upon ruthenium modification of His81Gln mutation. Differential Pulse Polarography (DPP) was performed on the ruthenium modified His81Gln protein to determine the reduction potential of the pendent $(\text{NH}_3)_5\text{Ru}^-$. These experiments gave $92.3 \pm 5.0 \text{ mV}$ vs. NHE for the ruthenium reduction potential within experimental error of that for the ruthenium in $(\text{NH}_3)_5\text{RuHis48}$ Sperm Whale Mb.³⁵

Figure 4. Nernst plot of spectroelectrochemical data for $(\text{NH}_3)_5\text{RuHis48}(\text{Val68Glu}, \text{His81Gln}, \text{Cys110Ala})\text{Mb}$ at 25°C . $E^\circ = -135.3 \pm 2.5\text{mV}$ vs. NHE, $RT/nF = 58\text{mV}$, correlation coefficient = 0.998.

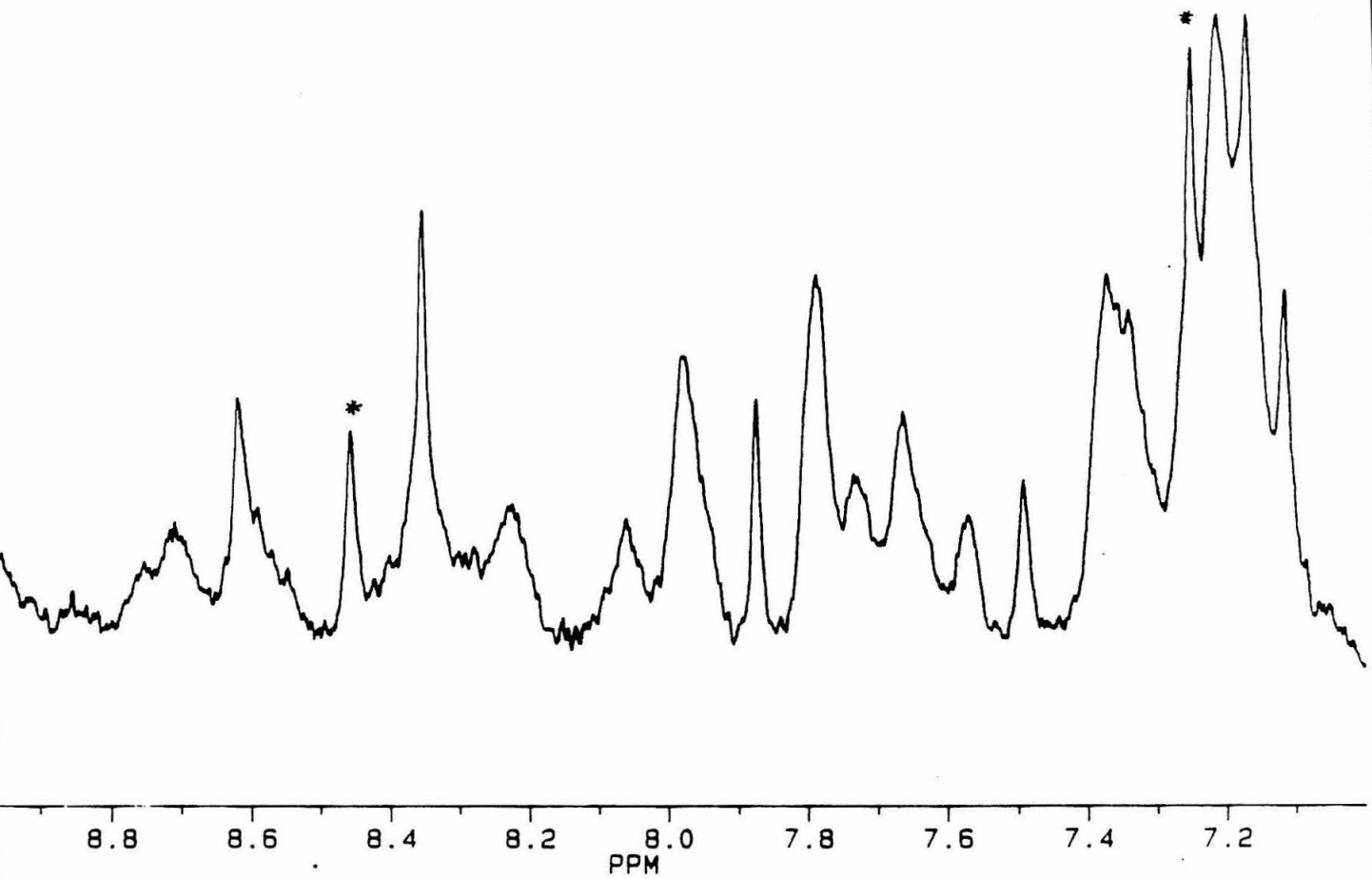


Next, Proton NMR was performed to ascertain the site of ruthenium modification. Specifically, the C-2 and C-4 imidazole proton resonances of the histidines in $(\text{NH}_3)_5\text{Ru}(\text{III})$ -modified and unmodified proteins were observed between 7 and 9 ppm. If a $(\text{NH}_3)_5\text{Ru}(\text{III})^-$ were covalently attached to a histidine, the hydrogen resonances of the imidazole of that histidine would be broadened and/or shifted out of the spectral window (7-9 ppm) by the ruthenium paramagnet. This procedure was previously used with sperm whale myoglobin³⁵ and cytochrome c.³⁶ Seven histidines are observable in the NMR spectrum of sperm whale myoglobin;³⁷ three of these (12,113, and 116) are not present in human myoglobin. The mutation His81Gln further simplified the spectra so that His36, 48, and 119 are the only NMR observable histidines remaining. The original assignments of these histidine C-2 proton resonances for sperm whale myoglobin³⁷ were shown to be incorrect.³⁵ By interpreting the original sperm whale and human myoglobin pH titration/C-2 histidine NMR data in light of the corrections, one obtains the following:

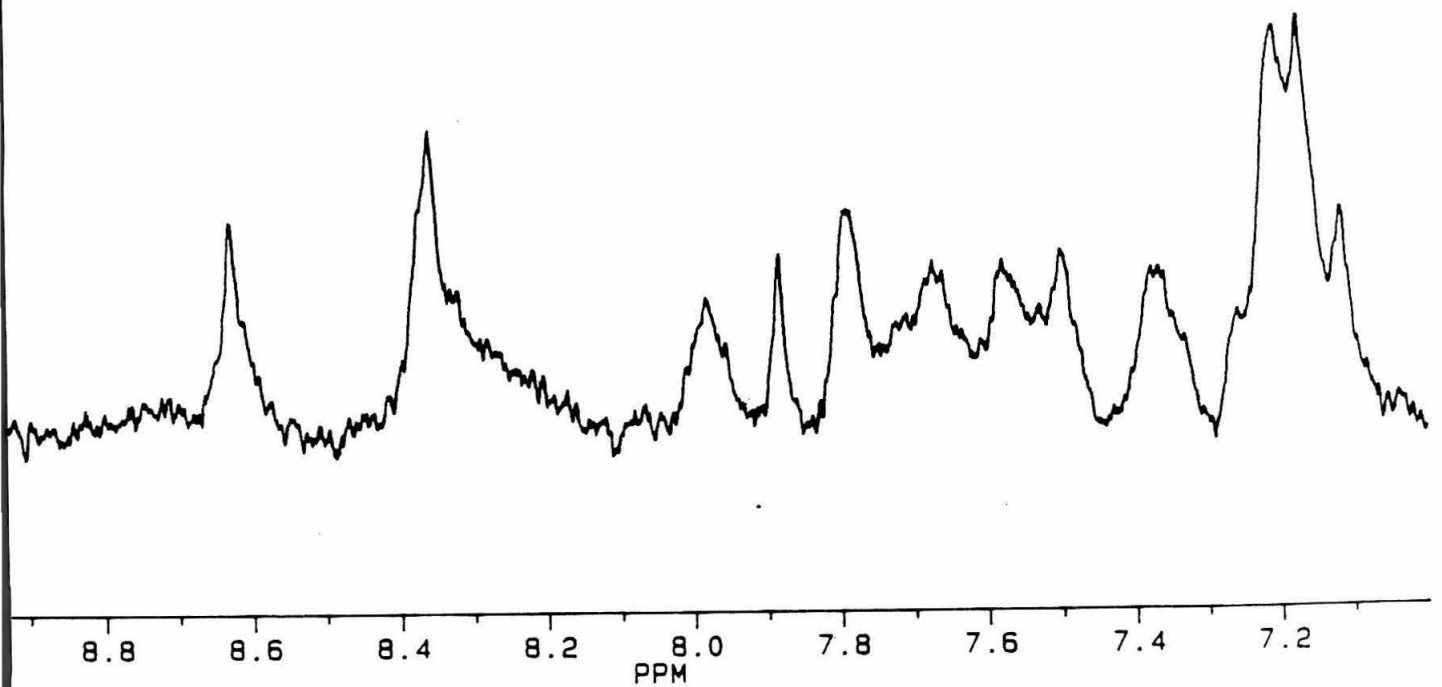
<u>Residue</u>	<u>pKa</u>	<u>Relative C-2 proton positions at pH 5.0</u>
36	7.8	lowest ppm
48	5.6	middle ppm
119	6.3	highest ppm

It was then concluded that His48 was being modified in our His81Gln mutants (figure 5). Over the pH range tested (4.7 to 5.6) the middle peak at pH 5.0 moved extensively (to lower ppm at higher pH) as expected from its predicted pK_a of 5.6. Moreover, the highest ppm peak at pH 5.0 shifted very slightly and the lowest ppm peak at pH 5.0 did not move at all over the pH range tested. In the ruthenium modified proteins tested, the His48 peak (i.e. middle peak at pH 5.0 in the unmodified protein) disappeared; the remaining peaks exhibited the same pH titration behavior (very little sensitivity to change in pH) as the peaks at

Figure 5. Proton NMR of (His81Gln, Cys110Ala) human Mb (top trace) and $(\text{NH}_3)_5\text{Ru}^-$ His48(His81Gln, Cys110Ala) human Mb (bottom trace). Samples are 1 mM protein in D_2O , pH=5.0. 600 acquisitions were made with 2 Hz line broadening on a Bruker 500 MHz spectrometer. Note the disappearance of the middle C-2 histidine peak in the ruthenium modified derivative. This peak corresponds to His48 (see text). The broad peaks in the region 8.2-9.1 ppm typically appear in the unmodified protein spectrum but not in the modified protein spectrum. They most likely correspond to resonances from protons spatially near the His48. These peaks do not shift in the pH range tested (4.5-5.7).



Human Myoglobin without his81



(NH) Bu-his48/Human Myoglobin without his81

the corresponding ppm's in the unmodified protein.

The k_{obs} for electron transfer in $(NH_3)_5RuHis48Mb(His81Gln, Cys110Ala)$ was 0.14 ± 0.01 . This rate is within experimental error of that observed for $(NH_3)_5RuHis48Mb(Cys110Ala)$ demonstrating that the mutation His81Gln does not affect the electron transfer rate. The k_{obs} 's for $(NH_3)_5RuHis48Mb(Val68Glu, His81Gln, Cys110Ala)$ and $(NH_3)_5RuHis48Mb(Val68Asp, His81Gln, Cys110Ala)$ were 0.30 ± 0.03 and 0.85 ± 0.05 , respectively. The rates were measured using the same flash reagents as before. The photoexcited $Ru(bpy)_3^{2+}$ acted again as a reductant to both the heme and the pendent ruthenium. However, for the charged heme-pocket mutants electron transfer occurred solely from heme to ruthenium because of the large driving force in this direction (0.22eV for both Val68Asp and Val68Glu). Thus, we saw an initial increase in absorbance at 555nm from initial reduction of the heme and then a transient decrease ($k_{obs}=k_{et}$) caused by intramolecular oxidation of the heme by the pendent ruthenium. The signal-to-noise in these charged, heme-pocket mutants is worse than in the uncharged protein because relatively little of the buried heme is reduced. The rates of electron transfer changed very little (<10%) over the protein concentration range (2-15 μ M) confirming intramolecularity.

A most significant result is that even though the driving forces for heme to ruthenium electron transfer are the same for the aspartate and glutamate mutants, the rate of the former is nearly three times that of the latter. Since there are only minor differences in the electronic properties of these two proteins (Chapter 2), the most probable explanation for the disparity in rates is a difference in reorganization energy. One possible indication of a difference in reorganization energy is the difference in entropy of reduction (ΔS_{rc}°) for these two proteins. As shown in Chapter 2, the entropy of reduction of the glutamate

Figure 6. Transient absorption trace after flash photolysis of $(\text{NH}_3)_5\text{Ru}(\text{III})\text{His48}$ (His81Gln, Cys110Ala) human Mb. Protein concentration was $6\mu\text{M}$, flash reagent concentrations described in the text.

tz38.001 6mM 1st flash

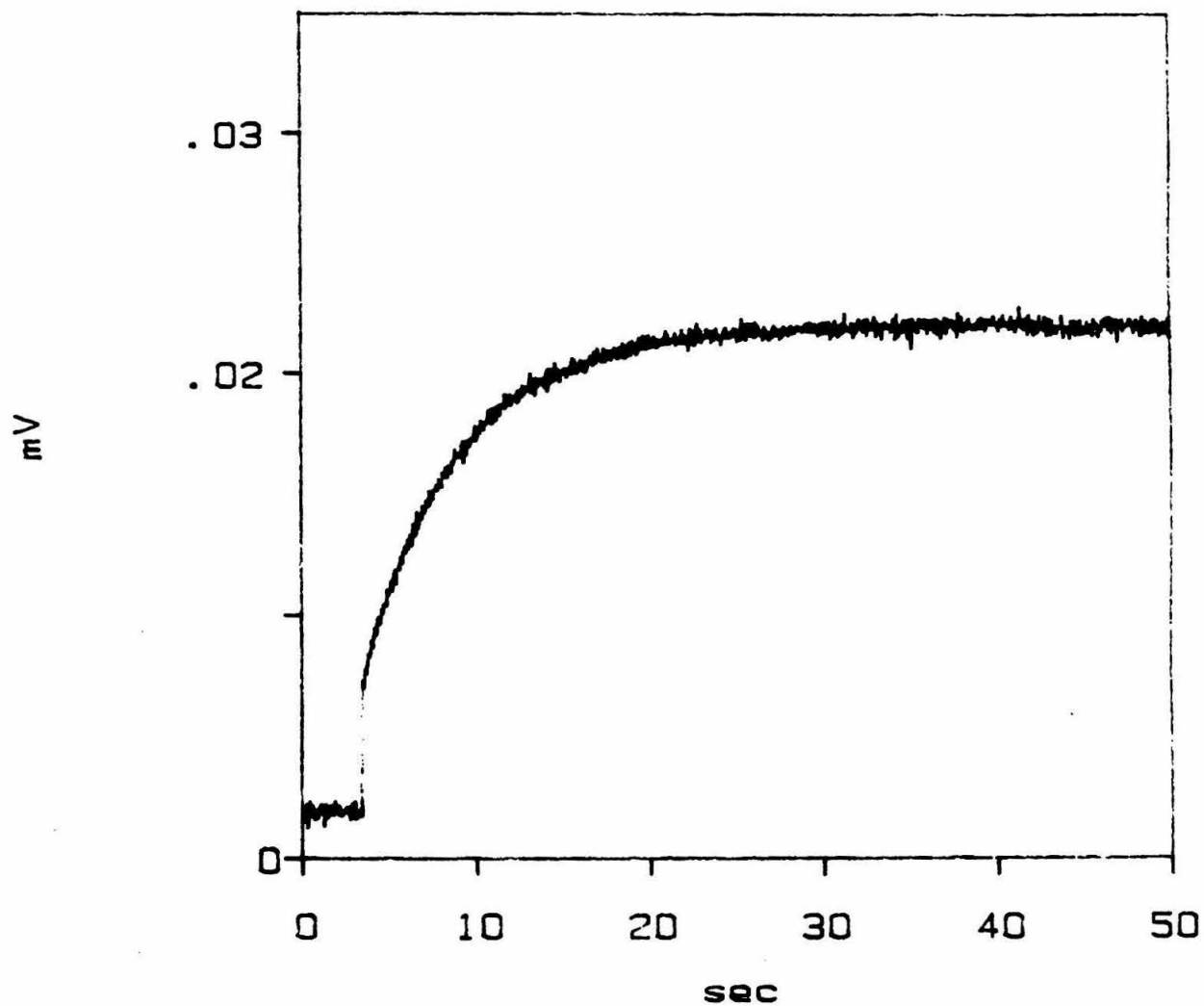


Figure 7. $t + \tau$ fit of data in Figure 6. $k_{\text{obs}}=0.14 \text{ s}^{-1}$, correlation coefficient=0.997. Two and three parameter fits gave the same rate.

t+T Fit of Modified Human Myoglobin (-81)

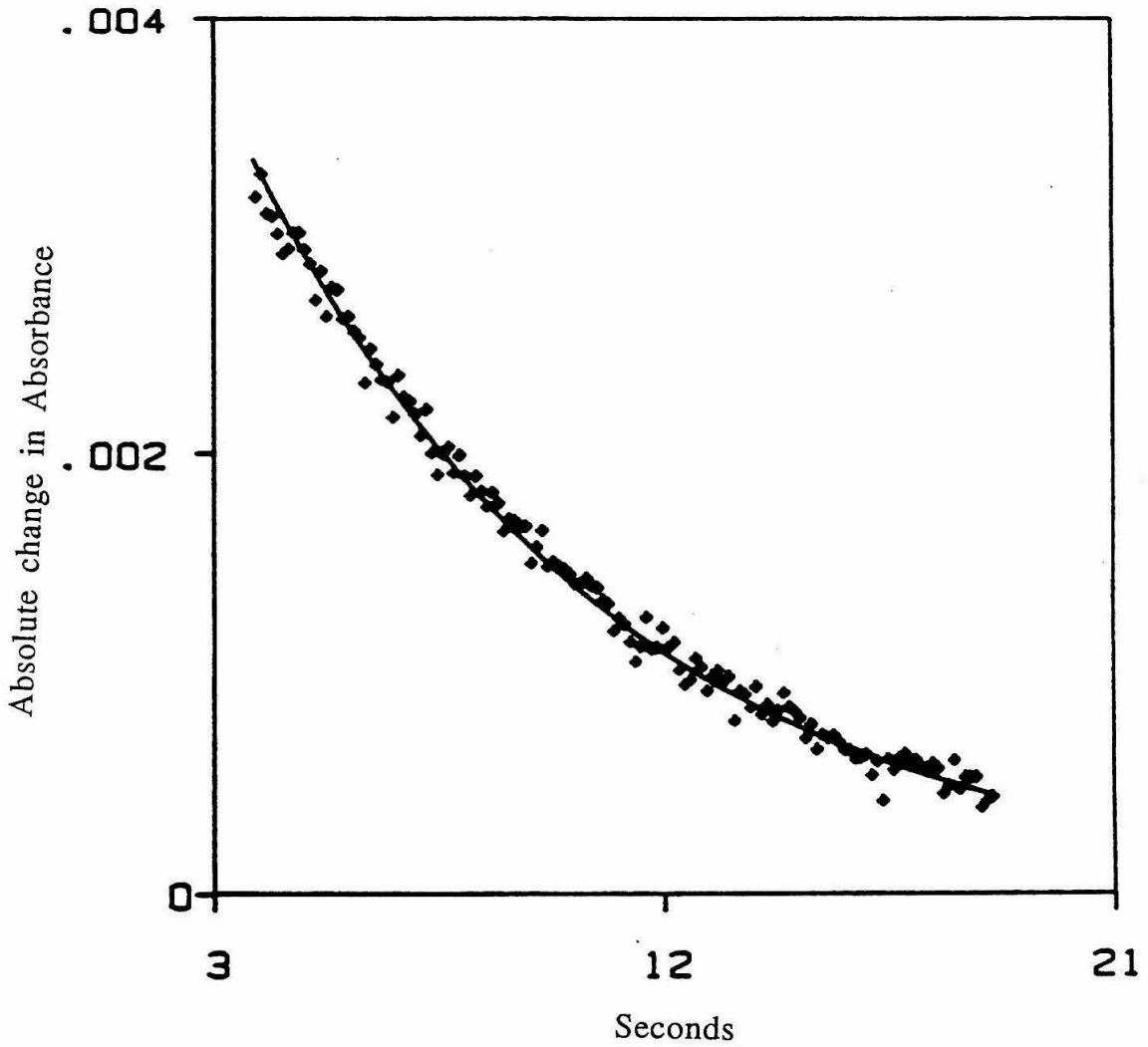
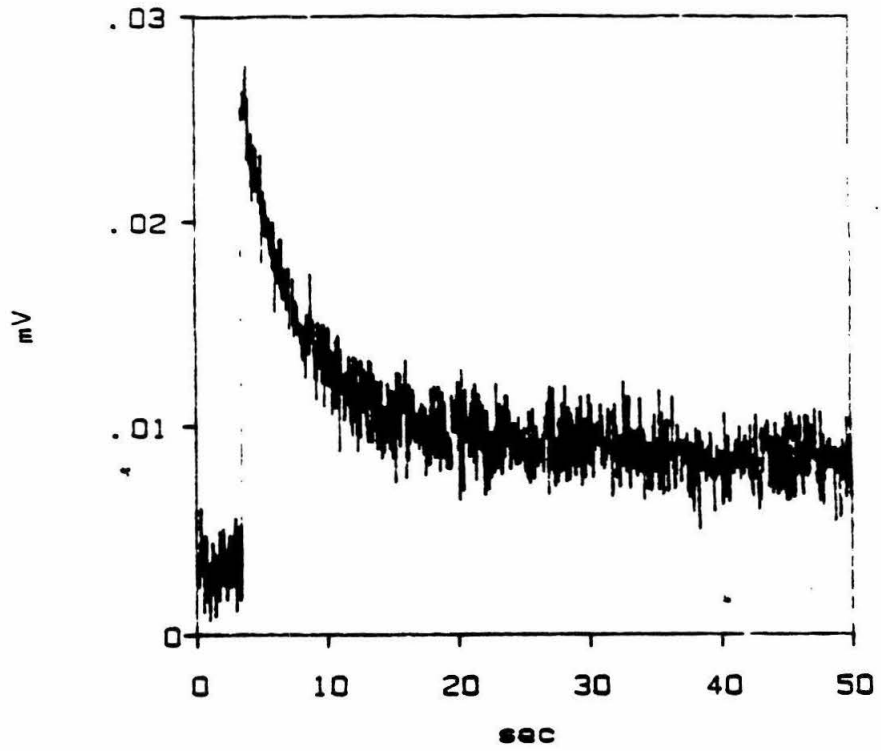


Figure 8. Transient absorption traces after flash photolysis of $(\text{NH}_3)_5\text{Ru}$ —His48(Val68Glu, His81Gln, Cys110Ala) human Mb (top trace) and $(\text{NH}_3)_5\text{Ru}$ —His48(Val68Asp, His81Gln, Cys110Ala) human Mb (bottom trace). Note the change in horizontal scale for the two traces. Same conditions as described previously. Protein concentrations were $3.5\mu\text{M}$.

(NH₃)₅Ru-his48(Glutamate Mutant)



(NH₃)₅Ru-his48(Aspartate Mutant)

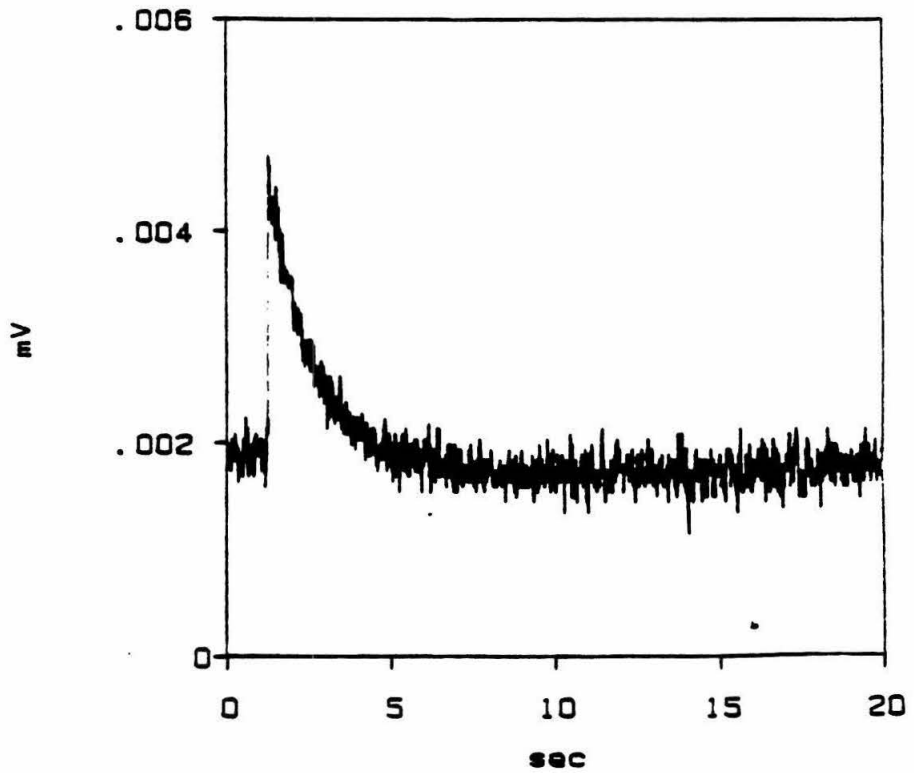


Figure 9. Three parameter fit of top trace in Figure 8. $\chi^2=6 \times 10^{-10}$, 4.7 half-lives, $k_{\text{obs}}=0.30 \text{ s}^{-1}$.

.0021

val68glu Mb his48Rua5

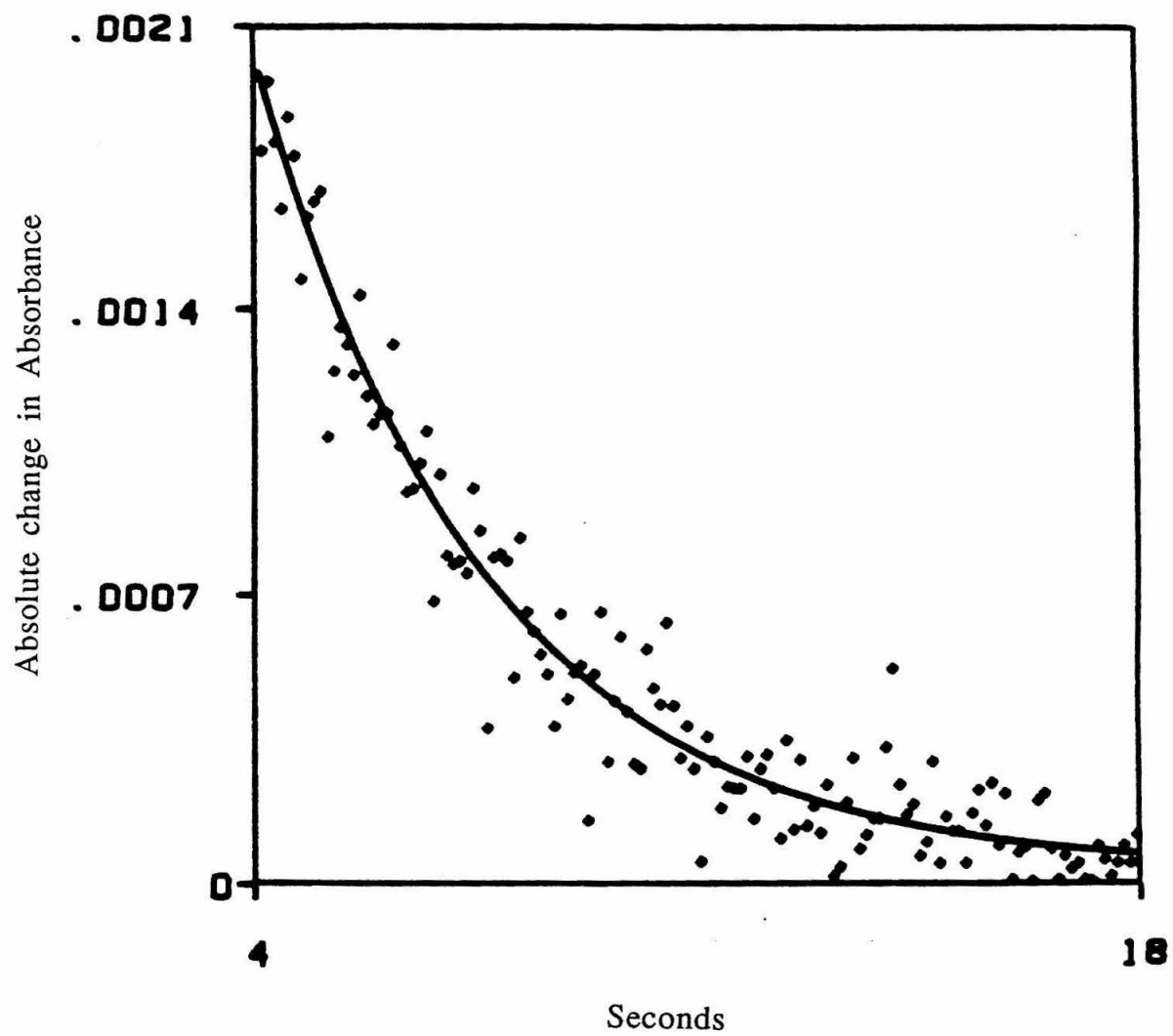
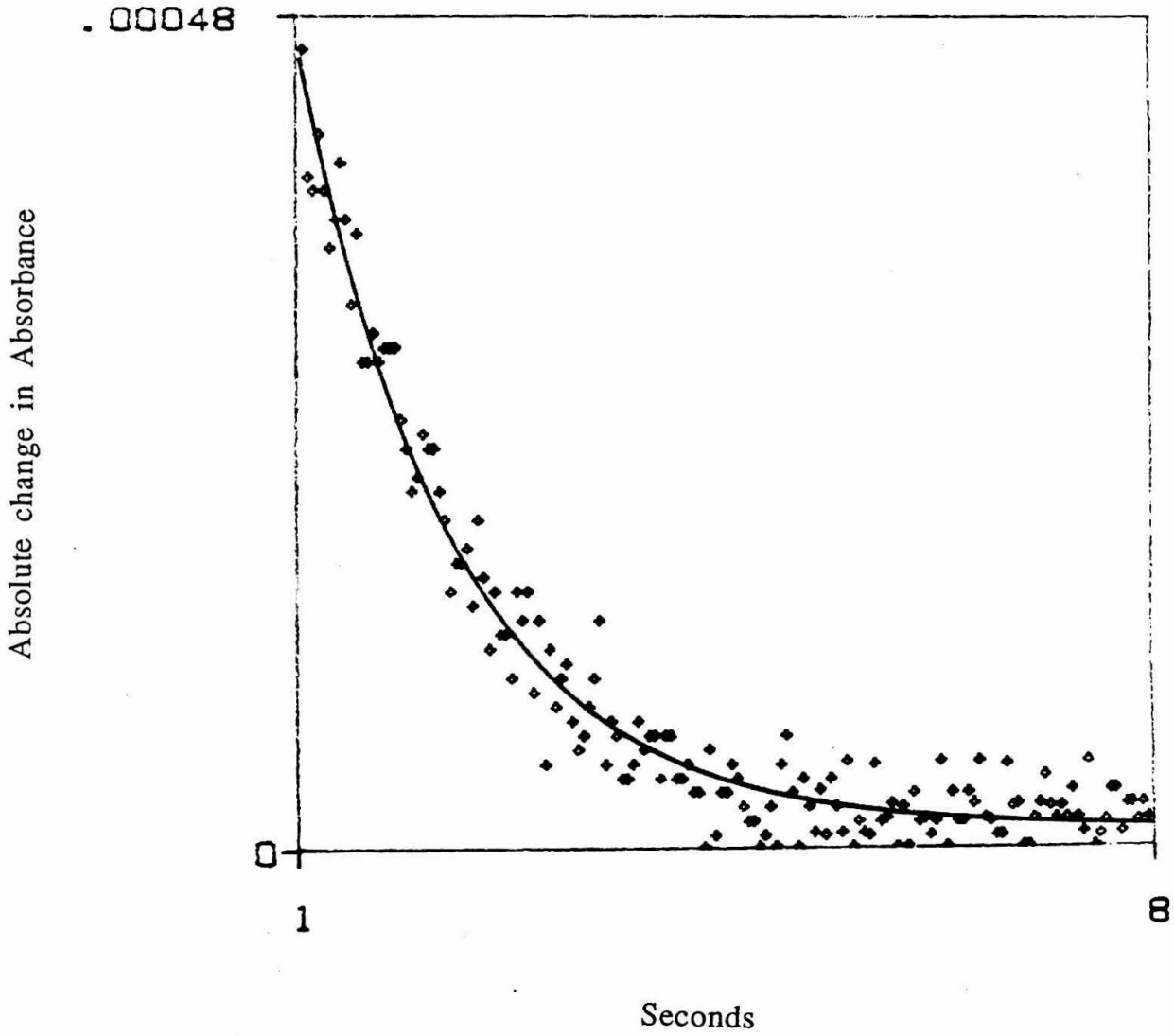


Figure 10. Three parameter fit of bottom trace in Figure 8. $\chi^2=3 \times 10^{-10}$, 5.7 half-lives, $k_{\text{obs}}=0.87 \text{ s}^{-1}$.

tz329.003 aspru 25.0C



mutant is 11.5eu less than that of the aspartate heme-pocket mutant.

Studies of small inorganic complexes suggest a correlation between ΔS_{rc}° and the self-exchange rate k_{ex} of these complexes. Empirically, k_{ex} is lower when ΔS_{rc}° is smaller in a comparison of several inorganic complexes.³⁸ A physical explanation of this phenomenon can be obtained from an analysis of the potential wells of the reactants and products of electron transfer. The absolute entropy of the reactants or products affects the depth or shallowness of their respective potential well on the reaction coordinate. If the absolute entropy of a state is large, it will, most likely, have more motional freedom and thus its potential well will be shallow. The inverse also applies: smaller entropy will imply less motional freedom and a steeper potential well. Since the reorganization energy of electron transfer is determined by where the reactant and product potential curves intersect, shallower potential wells (greater absolute entropy) give lower reorganization energy. It follows then that if one assumes equal entropy for the initial (oxidized) states for two complexes, the one with the greater entropy of reduction (ΔS_{rc}°) will have a smaller reorganization energy and a faster electron transfer rate (all other things being equal). An example is the difference in k_{ex} for $Ru(NH_3)_6$ ($800 M^{-1}s^{-1}$) and $Ru(H_2O)_6$ ($60 M^{-1}s^{-1}$); the former compound's ΔS_{rc}° is 12eu less than the latter.³⁹

A perusal of measured ΔS_{rc}° and k_{ex} (estimated and measured) data⁴⁰ of heme proteins shows that a rough correlation of the type just discussed exists.

<u>Metalloprotein</u>	ΔS_{rc}°	k_{ex}
Sw myoglobin	-24±1	1
cytochrome b ₅	-21±2	3×10 ³
cytochrome c ₅₅₁	-16±2	10 ⁶
cytochrome c	-15±1	10 ⁴
cytochrome c ₂	+10±1	slow
cytochrome c'	-8±1	≈10 ⁵

The glutamate and aspartate mutant data seem to support the above theory since an 11.5eu decrease in ΔS_{rc}° is accompanied by a three-fold decrease in k_{et} . The greater ΔS_{rc}° for the aspartate mutant corresponds to the fact that a water molecule is released from the heme site upon reduction as opposed to a protein carboxyl group for the glutamate mutant. The faster electron transfer from ferrous heme to ruthenium(III) for the aspartate mutant could be explained by it being energetically more favorable for a water molecule to be oriented properly to achieve the activated complex for electron transfer than a protein carboxylate. Another possibility is that there is a greater protein conformational change (and thus greater reorganization energy) upon electron transfer in the glutamate mutant, because the peptide backbone itself has to move somewhat when the carboxyl group of the glutamate binds to or is released from the heme iron, whereas a similar process does not occur for the aspartate mutant.

We know that for both of these mutants reduction of the heme is concomitant with proton uptake (chapter 2). To determine how closely proton uptake is tied to the formation of the activated complex, electron transfer experiments were done in D₂O buffer. If proton transfer is a rate-determining step in electron transfer, a kinetic isotope effect in D₂O should be seen as evidenced by a smaller k_{et} . As it turns out, no kinetic isotope effect is observed for either of the proteins. The most plausible explanations are that the proton

transfer is sufficiently faster than electron transfer or that the deuterium isotope effect is inherently too small to be observed. (Secondary deuterium isotope effects are usually small and are often small enough to be in the error of this experiment.) Another possibility is that proton transfer is part of a pre-equilibrium in the electron transfer reaction.

Another experiment we performed was measurement of the forward and recombination electron transfer rates of the photoexcited, zinc porphyrin substituted, ruthenium modified (Val68Glu, His81Gln, Cys110Ala myoglobin). From previous experiments we know that the Glu68 carboxyl group is protonated in the zinc porphyrin protein. Further, the carboxyl group of Glu68 is not coordinated to the zinc ion; as evidence for this assertion we note that the UV-visible absorption spectrum of this protein is identical to the zinc porphyrin substituted native sperm whale myoglobin (spectra not shown). The forward and recombination electron transfer rates of the zinc Glu68 protein [$7.2(3) \times 10^4 \text{ s}^{-1}$ and $1.4(3) \times 10^5 \text{ s}^{-1}$, respectively] are nearly identical to those of zinc native sperm whale myoglobin [$7.0(5) \times 10^4 \text{ s}^{-1}$ and $1.5 \times 10^5 \text{ s}^{-1}$, respectively] indicating that placement of the very polar carboxylic acid in the heme pocket has little effect on the electron transfer rate. One would expect a highly polar residue to increase the dielectric constant (and consequently the reorganization energy upon electron transfer) of the protein medium immediately surrounding the porphyrin. This protein microenvironment immediately surrounding the porphyrin has been suggested to be the most important factor in determining the effective dielectric constant of a redox active prosthetic group.³¹ Our results would obviously argue against this suggestion. One could argue that an expected decrease in rate from an increase in reorganization energy is offset by an increase in rate from an increase in driving force, since the polar Glu68 carboxyl would stabilize the polar radical cation formed from forward electron

transfer, thus making the ΔG° for the zinc porphyrin excited state forward electron transfer greater. However, for this argument to be consistent, the recombination electron transfer [Ru(II) \rightarrow Zn porphyrin⁺] rate would have to be much slower than the corresponding recombination rate in zinc substituted native myoglobin since the driving force would now be less compared to the zinc native myoglobin while reorganization energy would still be greater; but the Glu68 rate for the recombination reaction is identical to that of the zinc native myoglobin. One can then conclude that in this case the placement of a polar group in the interior of a protein near the prosthetic group has little effect on λ_{out} . Thus, when analyzing the environment responsible for λ_{out} in proteins, one should not only consider the protein immediately surrounding the electron group but also more distant parts of the protein and surrounding solvent layers.

References

1. Govindjee (ed.), *Photosynthesis: Energy Conversion by Plants and Bacteria*, Academic Press (1982).
2. Hatefi, Y., *Annu. Rev. Biochem.* 54, 1015 (1985).
3. DeVault, D., *Quantum Mechanical Tunneling in Biological Systems*. ed. 2, Cambridge Univ. Press (1984).
4. Vanderkooi, J. M., *Curr. Top. Bioenerg.* 13, 159 (1984).
5. Michel-Beyerle, M. E. (ed.), *Antennas and Reaction Centers of Photosynthetic Bacteria*, Springer-Verlag (1985).
6. Marcus, R. A. and Sutin, N., *Biochim. Biophys. Acta.* 811, 265 (1985).
7. Marcus, R. A. and Sutin, N. *Inorg. Chem.* 14, 213 (1975).
8. Sutin, N., *Acc. Chem. Res.* 15, 275 (1982).
9. Hush, N. S., *Coord. Chem. Revs.* 64, 135 (1985).
10. Gray, H. B., *Chem. Soc. Revs.* 17, 17 (1986).
11. Closs, G. L. and Miller, J. R., *Science* 240, 440 (1988).
12. Hush, N. S., Paddon-Row, M. N. *et al.*, *Chem. Phys. Lett.* 8, 117 (1985).
13. Leland, B. A. *et al.*, *J. Phys. Chem.* 89, 5571 (1985).
14. Joran, A. D. *et al.*, *Nature* 110, 508 (1987).
15. Axup, A. W. *et al.*, *J. Am. Chem. Soc.* 108, 435 (1988).
16. Beratan, D., *J. Am. Chem. Soc.* 108, 4321 (1986).
17. Beratan, D.; Onuchic, J. N.; Hopfield, J. J. *J. Chem. C. Phys.* 86, 4488 (1987).
18. Mayo, S. L. *et al.*, *Science* 233, 948 (1986).
19. Axup, A. W., *Ph. D. Dissertation* California Institute of Technology (1987).
20. Wherland, S., and Gray, H. B. *Biological Aspects of Inorganic Chemistry* Dolphin, D., ed., Wiley, 289 (1977).
21. Guarr, T. and McClendon, G. *Coord. Chem. Revs.* 68, 1 (1985).

22. McGourty, J. L., Blough, N. V. and Hoffman, B. M. *J. Am. Chem. Soc.* 105, 4470 (1983).
23. Crutchley, R. J., Ellis, W. R. and Gray, H. B. *J. Am. Chem. Soc.* 107, 5002 (1985).
24. Petsko, G. A. and Ringe, D., to be submitted.
25. (a) Shih, H. H.-L., Brady, J., Karplus, M. *Proc. Natl. Acad. Sci., U.S.A.* 82, 1697 (1985).
(b) Gelin, B. R. and Karplus, M. *Biochemistry* 18, 1256 (1979).
26. (a) Winkler, J. R., *et al.* *J. Am. Chem. Soc.* 104, 5798 (1982).
(b) Yocum, K. M., *et al.* *Proc. Natl. Acad. Sci., U.S.A.* 79, 7052 (1982).
(c) Nocera, D. G., *et al.* *J. Am. Chem. Soc.* 106, 5145 (1984).
27. (a) Kostic, N. M., *et al.* *J. Am. Chem. Soc.* 105, 7765 (1983).
(b) Kostic, N. M., *et al.* *Proc. Natl. Acad. Sci., U.S.A.* 81, 6554 (1984).
28. Cowan, J. A., unpublished results.
29. Cowan, J. A. and Gray, H. B. *Chemica Scripta* 28A, 21 (1988).
30. Milder, S. J., *et al.* *J. Am. Chem. Soc.* 102, 6762 (1980).
31. Kunkel, T. A. *Proc. Natl. Acad. Sci., U.S.A.* 82, 48 (1985).
32. Nagai, K. and Thogerson, M. C. *Nature* 309, 810 (1984).
33. Crutchley, R. J., unpublished results.
34. Hubbard, S. R., Hendrickson, W. A., Lambright, D. G., Boxer, S. G., in press.
35. Karas, J. L., *Ph. D. Thesis*, California Institute of Technology (1989).
36. Selman, M., *Ph. D. Thesis*, California Institute of Technology (1989).
37. Botelho, L. H., *Ph. D. Thesis*, University of Indiana (1976).
38. (a) Weaver, J. M. *J. Phys. Chem.* 83, 1748 (1979).
(b) Weaver, M. J. *J. Phys. Chem.* 84, 568 (1980).
(c) Bottcher, W., Brown, G. M., Sutin, N. *Inorg. Chem.* 18, 1447 (1979).
(d) Hupp, J. T. and Weaver, M. J. *J. Phys. Chem.* 88, 1860 (1984).
39. Yee, E. L. and Weaver, M. J. *Inorg. Chem.* 19, 1077 (1980).
40. (a) Dixon, D. W. and Hong, X. submitted in the *Conference Proceedings of the 1989 Biennial Inorganic Electron Transfer in Biology and Solid State* (1989).

- (b) Ellis, W. R., *Ph. D. Thesis*, California Institute of Technology (1987).
- (c) Bradic, Z. *et al.* in *Frontiers in Bioinorganic Chemistry*, Xavier, Wernheim, FRG, p. 336 (1986).

41. Blackbourn, R. L. and Hupp, J. T. *J. Phys. Chem.* 92, 2817 (1988).

CHAPTER 5
KINETICS OF BrCN-MODIFIED,
L(NH₃)₄RU—(HIS48) SPERM WHALE MYOGLOBIN

Introduction

The factors which control the rates of electron transfer in biological systems are the focus of substantial interest.¹ Understanding how a prosthetic group (often an inorganic complex) and a protein interact to carry out electron transfer in the most physiologically efficient means is a significant problem. The protein surrounding a prosthetic group can accomplish this by providing a favorable (and/or controllable) medium,² orientation,³ and intervening distance⁴ between the electron transfer group and its partner, thereby affecting the electronic coupling between the two centers. Further, the protein can affect the electron transfer (ET) rate through the perturbation of nuclear factor.⁵ For instance, electron transfer would be expected to go faster through a protein matrix than through aqueous solvent, because the protein has a lower bulk dielectric constant which would, in turn, result in a lower outer sphere reorganization energy. Similarly, proteins affect the driving force of electron transfer by providing ligands or environments of varying polarizations for the prosthetic group which change its midpoint potential. Through analogous perturbations the protein can also alter the state of a potential paramagnet. Protein conformational change linked to electron transfer has also been suggested as a mechanism through which rates can be affected.⁶ Another factor is control of geometric and/or chemical change at the electron transfer center by the protein. This minimization of local structural change concomitant with ET is thought to be common to all of the four main classes of electron transfer proteins:⁷ flavoproteins, iron-sulfur proteins, copper proteins, and hemoproteins.

In this chapter we systematically address this problem of geometry specifically relevant to the last class of proteins mentioned. We use cyanogen bromide (BrCN) modified myoglobin⁸ as a model electron transfer system. X-

ray crystal structures of sperm whale metmyoglobin (Mb) have shown that the distal histidyl imidazole (His64) is hydrogen bonded to the Fe(III)-coordinated water molecule.⁹ When metMb is treated with BrCN, the distal histidine is cyanated and the hydrogen bond to the coordinated water is broken, so that the water molecules dissociates from the heme leaving it pentacoordinate.⁸ NMR,⁹ IR,¹⁰ and UV-visible^{8,10} absorption spectroscopy have all been used to confirm this assertion. Further, the reduction potential of BrCN-modified Mb is 180mV¹¹ vs. NHE, which is similar to those of monomeric hemoglobins and myoglobins which lack a distal histidine and a heme-coordinated water molecule.¹²

The reduced form of native Mb is known from its crystal structure to be pentacoordinate¹³ when exogenous ligands are not present. Thus, the BrCN-modified Mb (BrCN-Mb) heme does not undergo coordination change upon electron transfer, unlike the native myoglobin heme which changes from six to five coordinate upon reduction. These systems are then ideal for studying the effect of geometric change upon the electron transfer rate of a heme in a protein. In fact, bimolecular rate studies of the reduction of BrCN-metMb by a number of small molecules have been performed.¹⁴ After applying the Marcus cross-relation to the results, a self-exchange rate of $10^4 \text{ M}^{-1}\text{s}^{-1}$ was derived which was much greater than that for native Mb, $1 \text{ M}^{-1}\text{s}^{-1}$. This difference was attributed to the lowering of reorganization energy (λ) for the BrCN-Mb.

To clarify further and quantitate this effect, we performed intramolecular ET studies on BrCN-modified $(\text{NH}_3)_4\text{LRu His48Mb}$ [$\text{L}=\text{NH}_3$ or isonicotinamide (isn)]. The major advantages of this system over bimolecular reduction are (i) the need to consider the energy of formation of a precursor complex is eliminated and (ii) the effect of BrCN modification on both the reduction and *oxidation* of the heme can be measured. Further, BrCN, ruthenium-modified Mb data will help better compare results of our previous data on native

ruthenium-modified Mb (RuMb) and photoactive porphyrin-substituted RuMb, because the former undergoes a coordination change upon ET whereas the latter does not.

Experimental

The modification, purification and characterization of RuMb derivatives has been described previously.¹⁵ All experiments were performed in $\mu=0.1$ M sodium phosphate buffer, pH 7.0. [The pH was readjusted to 7.0 after the addition of $(\text{Na})_2\text{EDTA}$ to the flash mixture.] The flash cell solution was 65mM $\text{Ru}(\text{bpy})_3^{2+}$ and 6.5mM $(\text{Na})_2\text{EDTA}$. The solution was degassed without protein as described (chapter 4). During that procedure a three-fold excess of freshly mixed BrCN was added to the RuMb in a small volume (100 μL) and the cyanation reaction was allowed to complete (3-5 minutes) after which the BrCN-RuMb was quickly added to the flash cell and degassed (1-2 sec. vacuum exposure/20 sec. argon, 5 times) while stirring. The flash cell and its contents were then allowed to equilibrate to the temperature of a water bath for 15 minutes. The entire preparation time after addition of BrCN took 25 minutes so that the amount of BrCN-RuMb which reverted to RuMb or byproducts was negligible.¹⁴ BrCN-Mb concentration was determined by monitoring the absorption coefficients at 510nm ($\epsilon_{510}=1.2 \times 10^4 \text{ M}^{-1}\text{cm}^{-1}$) and 560nm ($\epsilon_{560}=4.3 \times 10^3 \text{ M}^{-1}\text{cm}^{-1}$).

The intramolecular kinetics were determined by monitoring the heme absorption at 555nm for $(\text{NH}_3)_5\text{RuMb}$ and at 630nm for $(\text{NH}_3)_4(\text{isn})\text{RuMb}$. The respective ruthenium complexes do not absorb significantly in either oxidation state at these wavelengths. A detailed description of the flash apparatus and data acquisition and analysis has already appeared (chapter 4 and references therein).

The X-band ESR spectrometer and cryostat have already been described (chapter 3). A three-fold BrCN excess was allowed to react with 3mM Mb for 5 minutes. The sample was then flash frozen in LN_2 , after which spectra were recorded at 4°K.

Results and Discussion

To clarify further the variables in the kinetics interpretations, we took ESR spectra of the BrCN-Mb to determine the spin state of the heme. It has been suggested that hydrated metMb, in which it is thought that the heme has no water molecule bound to it, has a low spin heme.¹⁶ In contrast, the heme of the native metMb is high spin. Thus, we tried to determine with ESR whether BrCN modification of metMb caused high \rightarrow low spin conversion. The absorption spectrum of BrCN-Mb is characteristic of high spin,¹⁰ but it has been shown that mixtures containing significant amounts of low spin heme can still have an absorption spectrum like high spin.¹⁷ However, the ESR spectrum (figure 1) of BrCN-Mb is only high spin ($g=5.9$ and $g=2$). The peak at $g=5.9$ is significantly broader than in native metMb indicating a greater standard deviation of rhombicity ($S_{E/D}$). This result can be best interpreted as a greater conformational flexibility around the heme and is consistent with previous data in which larger size ligands in the sixth coordination site give less conformational flexibility (smaller spectrum of conformations).¹⁰

In the kinetics experiments, Ru(III)—[Fe(III)Mb] gets reduced initially by Ru(bpy)²⁺. A transient increase in signal was observed at 555nm corresponding, for the most part, to reduction of Fe(III) heme by the pendent (NH₃)₅Ru(II)⁻ (figure 2). Similarly, a transient increase was observed for oxidation of Fe(II) heme by the pendent (NH₃)₄(isn)Ru(III)⁻ at 630nm (figure 6). Note that there is an isosbestic in the BrCN-Mb heme spectrum between 555 and 630nm.^{10,14}

<u>Redox Entity</u>	<u>E° vs. NHE (mV)</u>
(NH ₃) ₅ RuHis48	85
BrCN-(FeMb)	180
(NH ₃) ₄ (isn)RuHis48	440

Figure 1. ESR spectrum of BrCN treated sperm whale myoglobin. Scan range was 4 kgauss, field set 2 kgauss, time constant 0.128 seconds, scan time 4 minutes. Modulation amplitude 4 gauss with frequency 100 kHz, 8×10^2 receiver gain with 2mW microwave power. 4,1°K was the temperature of acquisition.

Magnetic Field / G

WILMAD GLASS CO. INC.
11 W. 20th Street
New York, N.Y. 10011

4000

2000

0

1

2

3

4

5

6

7

8

9

10

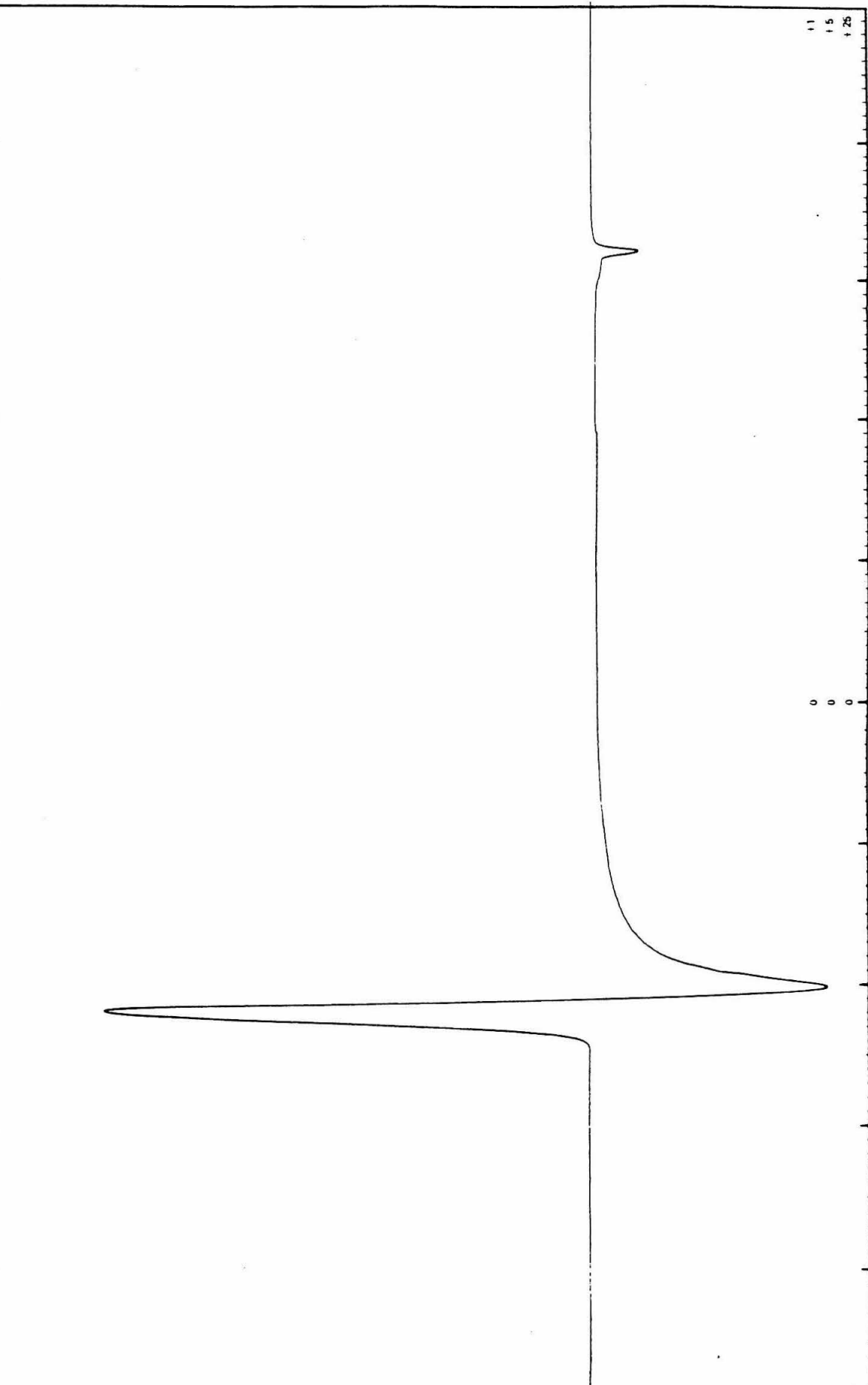
11

12

13

14

15



0

0

0

11

15

125

Spectrum No.

Figure 2. Transient absorption after flash photolysis of BrCN treated $(\text{NH}_3)_5\text{RuHis48}$ (SW myoglobin) at 4.5°C , $5\mu\text{M}$ protein.

tz430.001

6.900001E-02

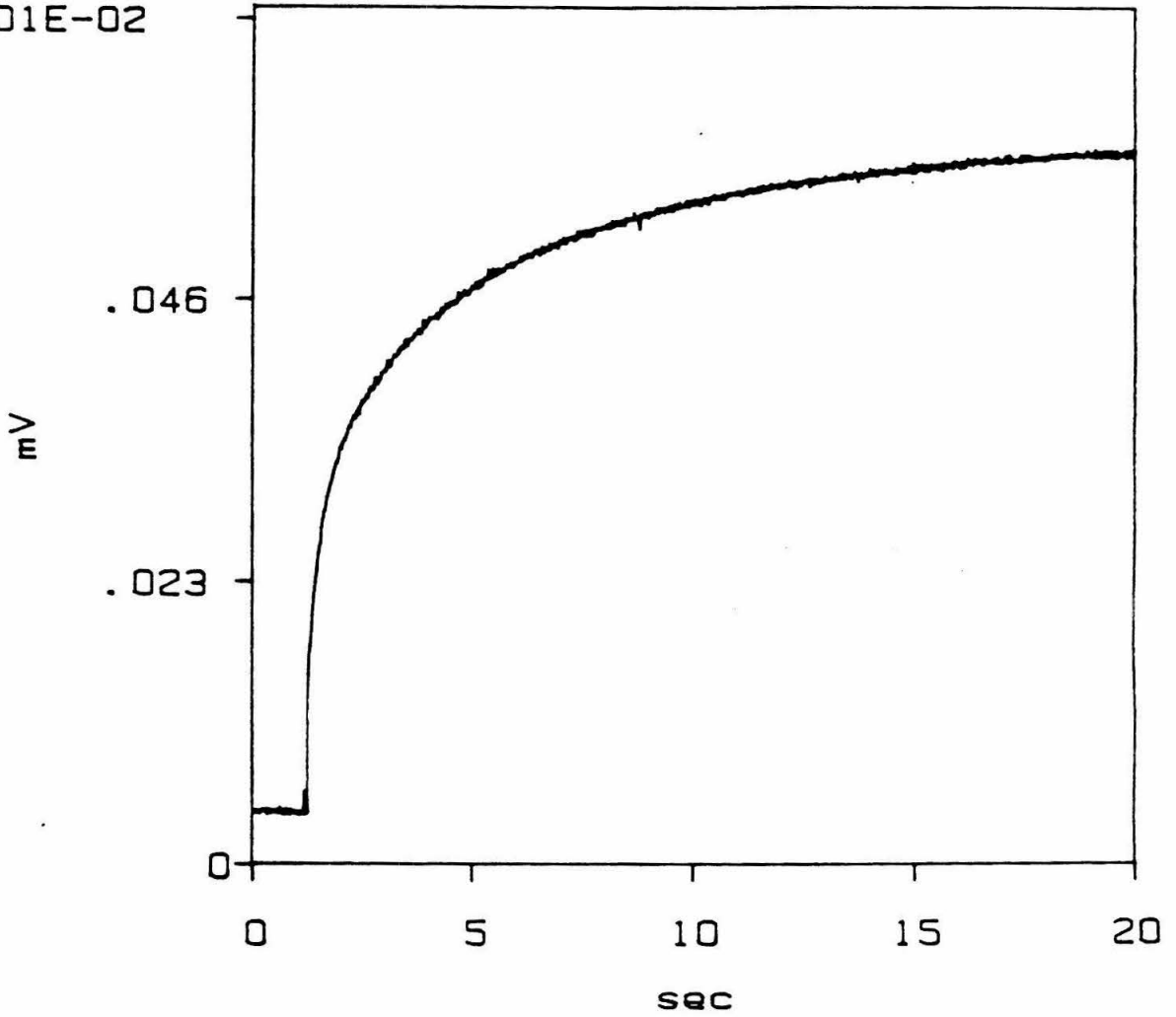


Figure 3. Three parameter monoexponential fit of first 2.5 seconds of data for
Figure 2. $k_{\text{obs}}=2.0 \text{ s}^{-1}$, $\chi^2=3.0 \times 10^{-4}$, 7.9 half-lives.

tz430.001 BrCN 4.5C

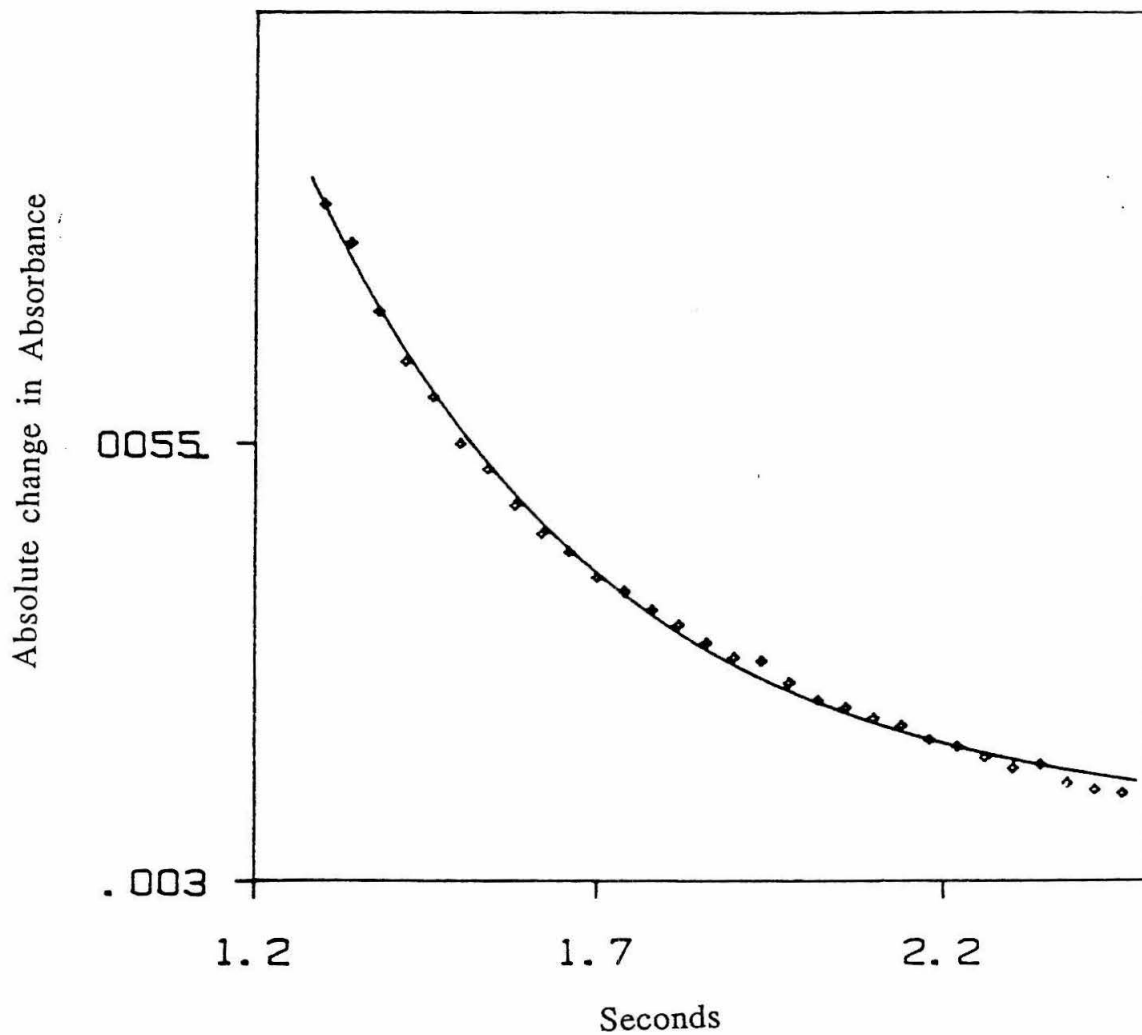
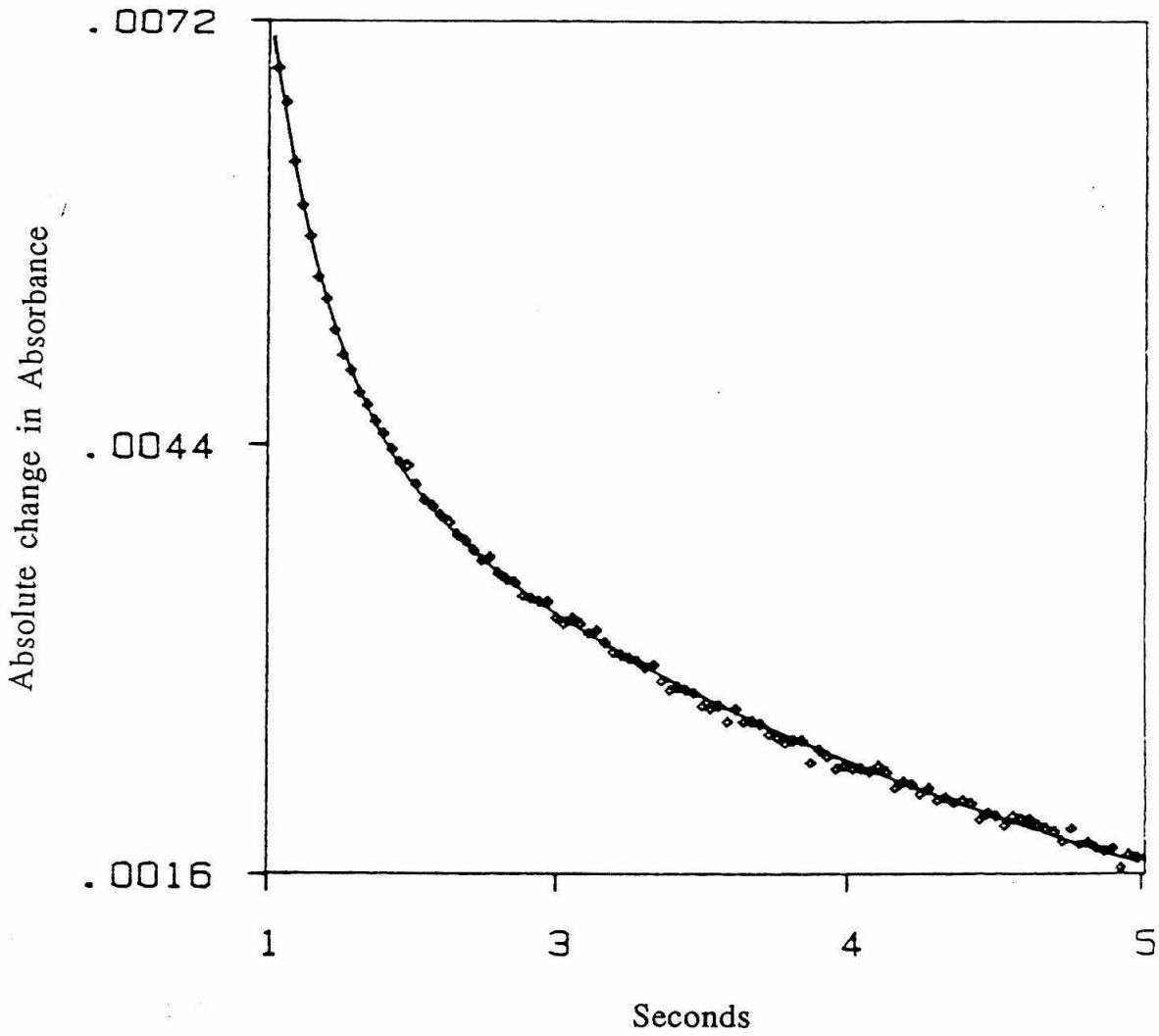


Figure 4. Four parameter monoexponential fit of data in Figure 2 for the first five seconds. $k_{obs}=2.5$ and 0.2 s^{-1} with $\chi^2=1.5 \times 10^{-9}$ for over 30 and 3 half-lives, respectively.

tz430.001 BrCN 4.5C 4p



The BrCN-(FeMb) potential had been measured previously⁴ (*vide supra*); it was assumed that ruthenium modification at His48 did not significantly affect this potential by extrapolating the perturbation of heme potential of native Mb ($\Delta E^{\circ} < 10\text{mV}$) when ruthenium complexes were attached to His48.¹⁵

The kinetic traces of the BrCN-(NH₃)₅RuMb and BrCN-Mb are shown in Figures 2 and 5, respectively. The data for BrCN-(NH₃)₅RuMb is primarily ($\approx 90\%$) composed of a fast signal ($2.0 \pm 0.5 \text{ s}^{-1}$) which can be fit to a monoexponential. We believe this rate corresponds to (NH₃)₅Ru(II)His48 \rightleftharpoons Fe(III) heme electron transfer. There also exists a slow component(s) which can be approximately fit to an exponential giving a pseudo unimolecular rate constant of 0.2 s^{-1} . This rate is probably not from an intramolecular rate process since the control flash trace of BrCN-Mb shows a transient absorbance change on the same time scale and similar intensity of the slow component(s) (Figure 5). The most likely origin of the slow component(s) is a reaction of the EDTA radicals formed in the flash solution with the heme of BrCN-Mb and BrCNRuMb as the lifetime of Ru(bpy)₂²⁺ is too short to be responsible for this process. BrCN-Mb is relatively stable in the flash solution prior to the flash. This slow rate(s) was hardly detectable in the BrCN-(NH₃)₄(isn)RuMb kinetic data (Figure 6), so that the data could be fit very well ($k_{\text{et}} = 5.5 \pm 0.5 \text{ s}^{-1}$) by a three parameter monoexponential routine (Figure 7). In fact, the χ^2 of this data increased with a greater number of half-lives fit (up to 16) in contrast to the BrCN-(NH₃)₅RuMb data in which best monoexponential fit was reached before 8 half-lives.

A variable temperature study of BrCN(NH₃)₅RuMb gave a ΔH^\ddagger of 7.4 ± 2.5 kcal/mol. This value of the enthalpy of activation matched that for the bimolecular reaction of BrCN-Mb with Ru(NH₃)₆²⁺ (5.6 ± 1.0 kcal/mole) confirming that the reorganization energy of the BrCN-Mb is less than that of Mb ($\Delta H^\ddagger = 20$ kcal/mole).¹⁹

Figure 5. Transient absorption after flash photolysis of BrCN treated SW myoglobin, 5 μ M protein.

tz511.001 sw BrCN 1st

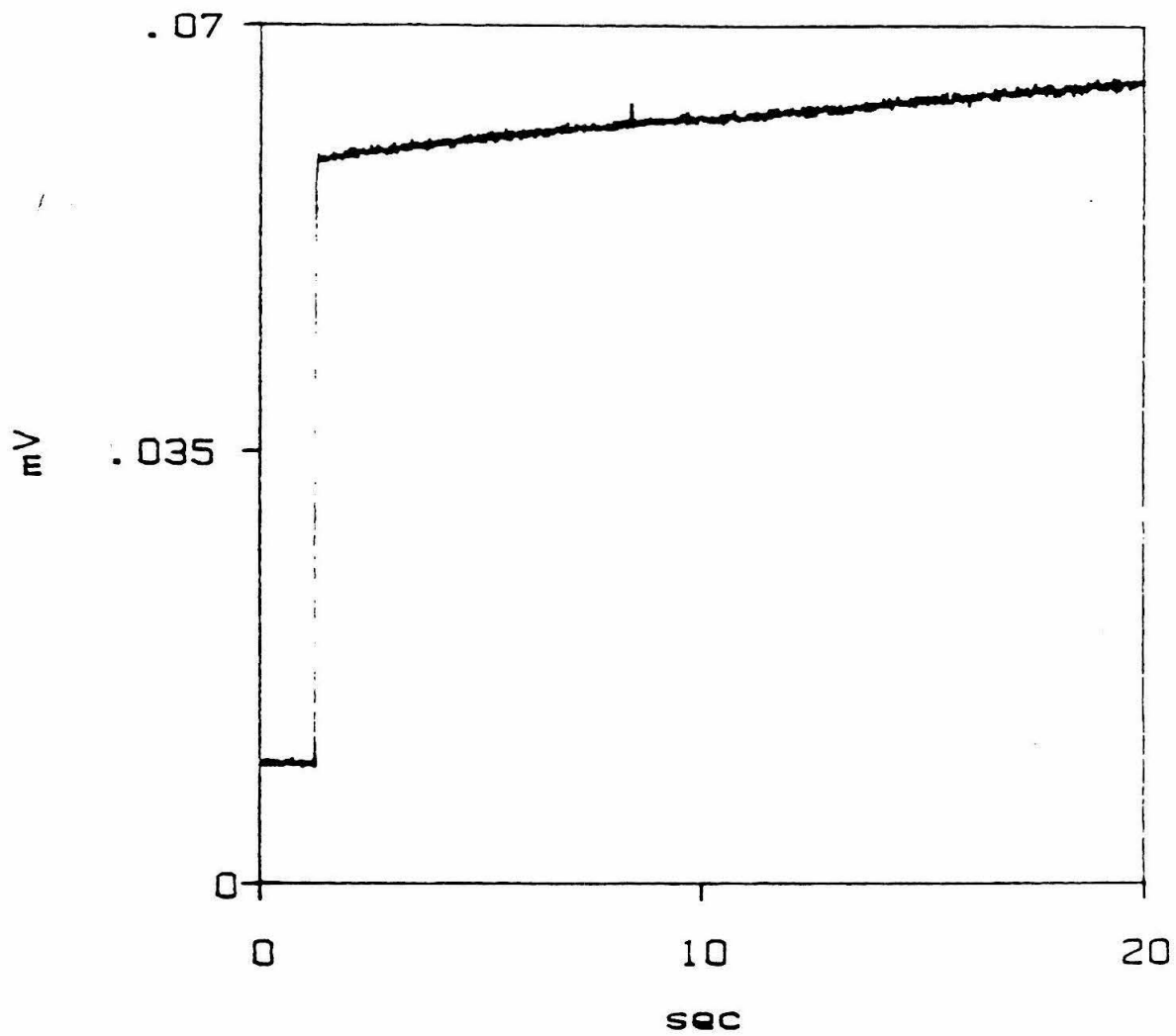


Figure 6. Transient absorption after flash photolysis of BrCN treated $(\text{NH}_3)_4(\text{isn})\text{RuHis48}$ SW myoglobin, $5\mu\text{M}$ protein.

BrCN-Mb His48Ru(isn)

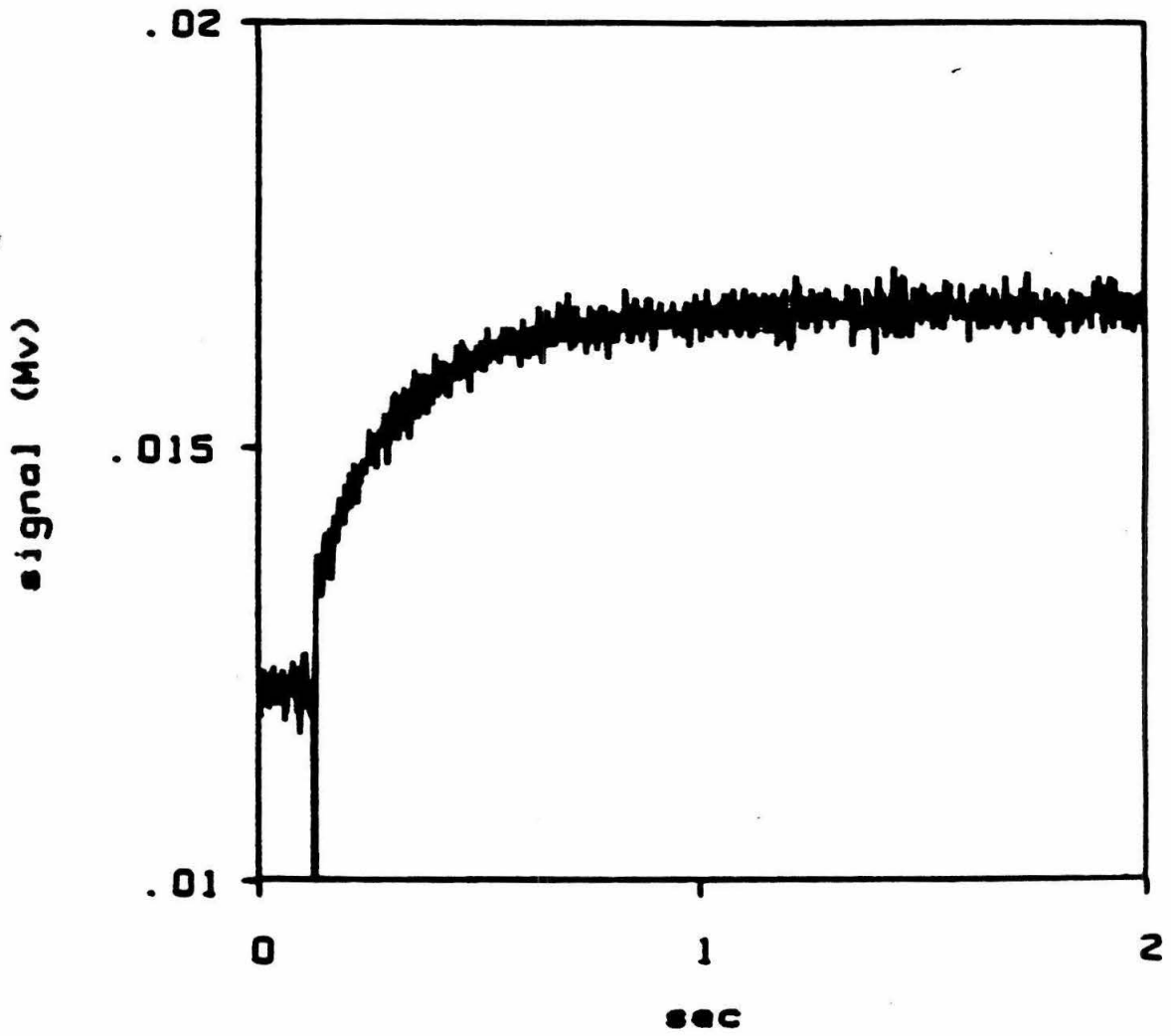


Figure 7. Three parameter monoexponential fit of data in Figure 6. $k_{\text{obs}}=5.4 \text{ s}^{-1}$, $\chi^2=4.6 \times 10^{-10}$, 15.8 half-lives was the best fit of the data.

BrCN-Mb His48Ru(isn) fit

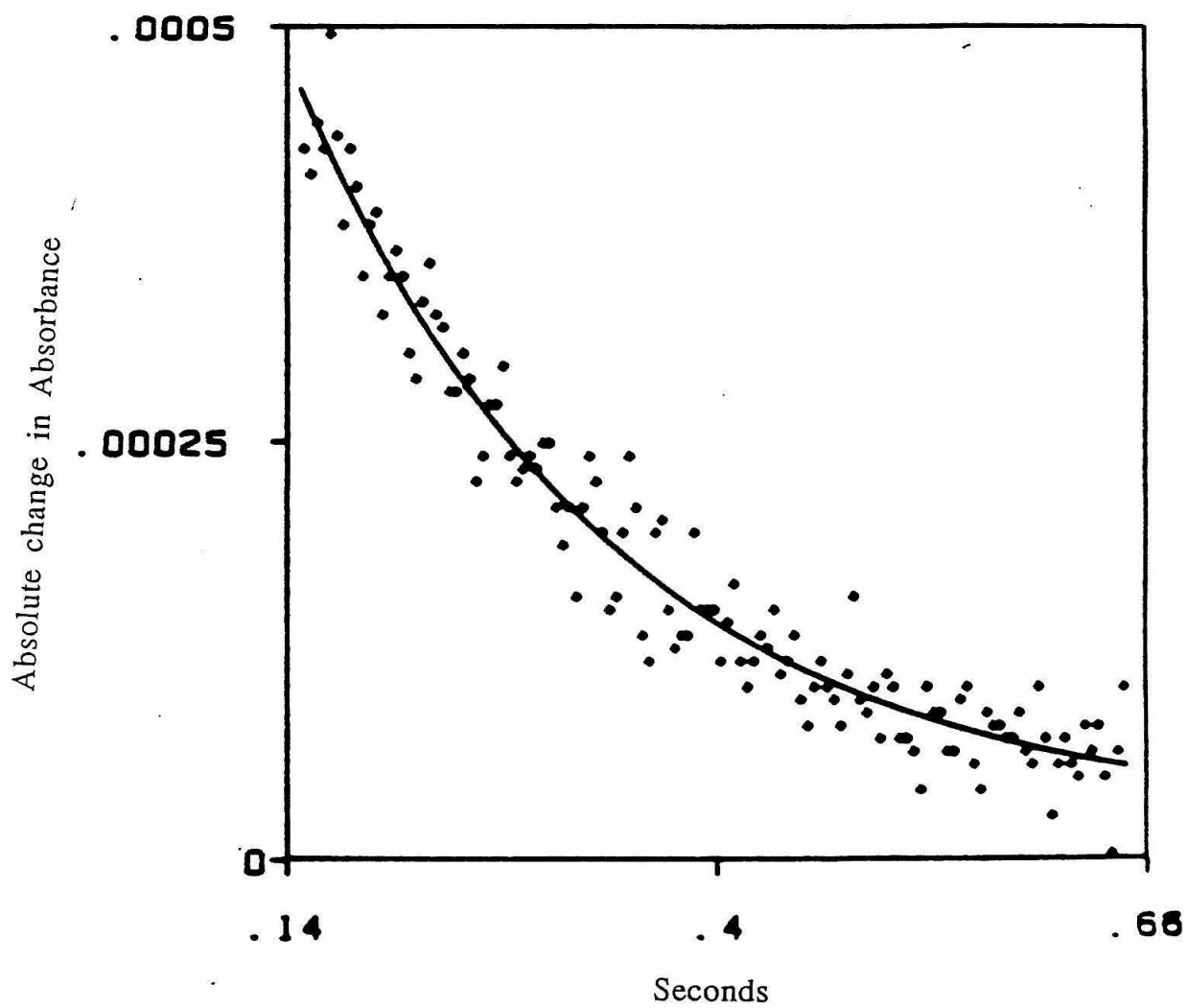
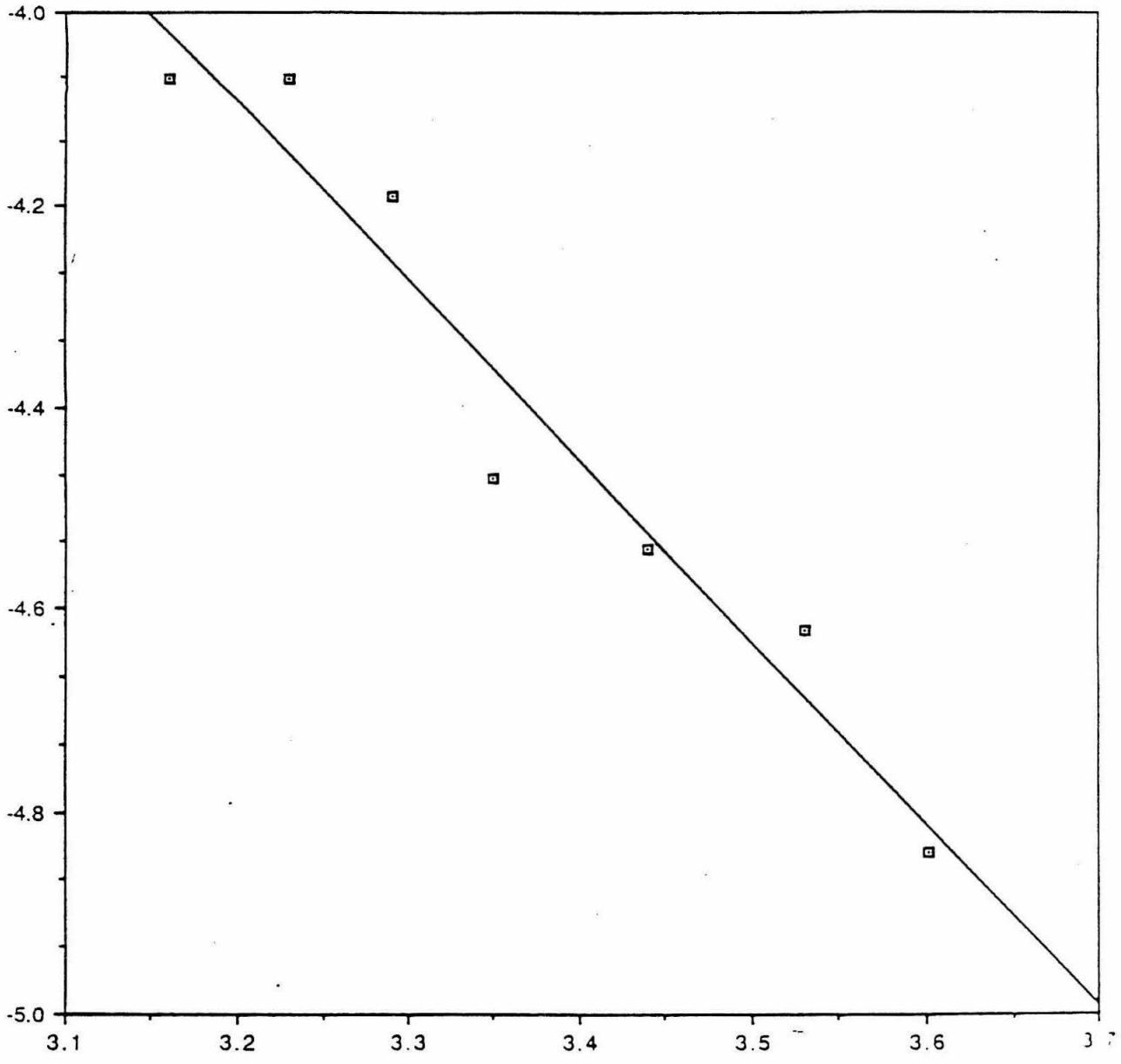


Figure 8. Arrhenius plot of k_{obs} data of BrCN modified $(\text{NH}_3)_5\text{RuHis48}$ (SW Mb). ΔH^\ddagger was calculated to be 7.3 kcal/mol. Averages of two to three traces are represented by each data point.

CNBr Mb

$$y = 1.6627 - 1.7982x \quad R^2 = 0.944$$



$1/T \times 10^3 \text{ (K}^{-1}\text{)}$

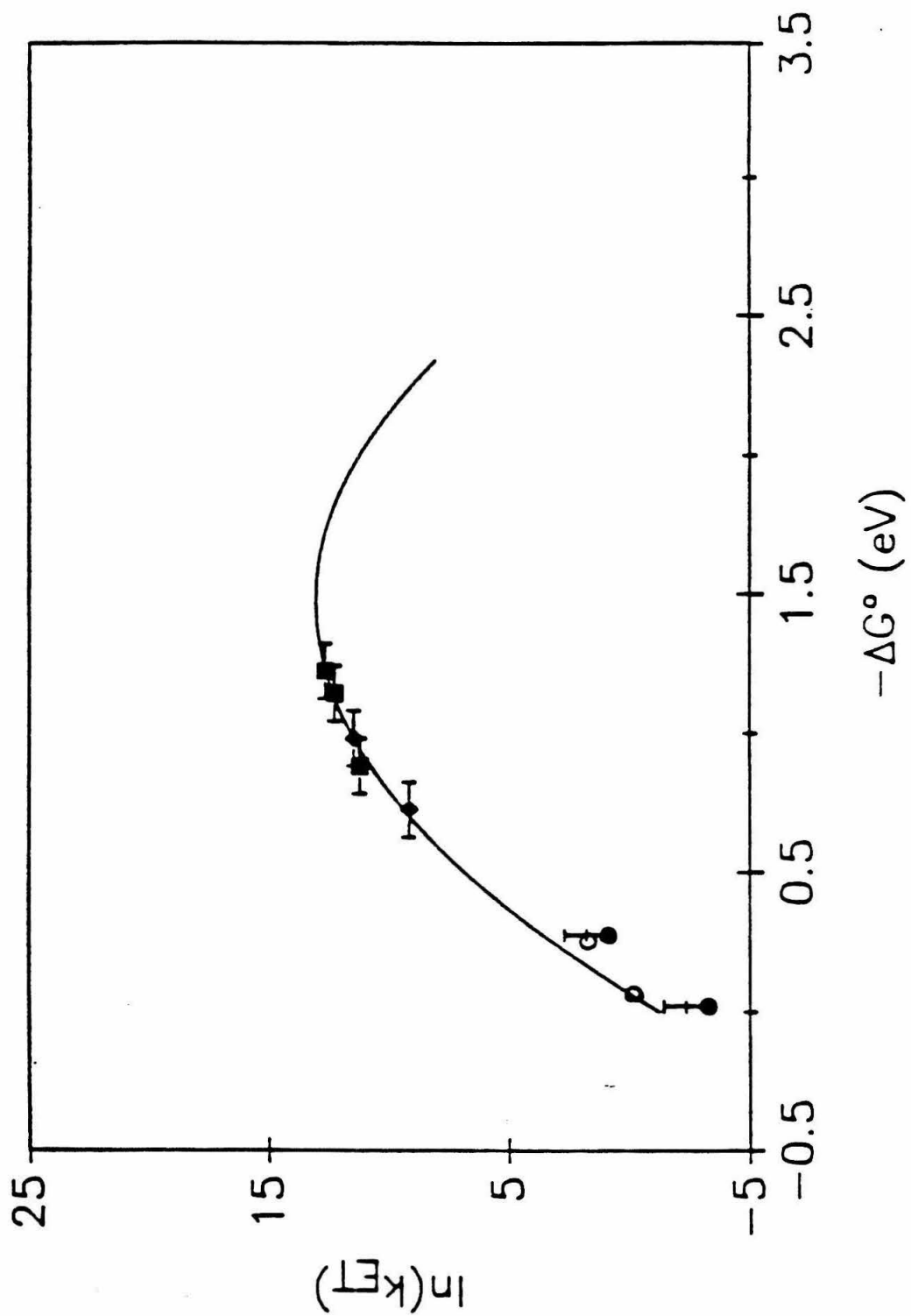
Using 1.45eV as the total reorganization energy of the ruthenium/myoglobin electron transfer system¹⁵ and scaling for driving force differences with the semi-classical Marcus expression,¹ we determine that the BrCN-(NH₃)₅RuMb rate is inherently 20 times faster than the (NH₃)₅RuMb rate. Similarly, the BrCN-(NH₃)₄(isn)RuMb rate is 10 times faster than its BrCN-unmodified counterpart. This effect is substantial, although not as great as that predicted from the disparities of BrCN-Mb and Mb self-exchange rates [(1x10⁴)^{1/2}=100-fold expected difference in intramolecular ET].

Applying these rate results to other results for ruthenium modified Mb derivatives¹⁵ (Figure 9), we see that the BrCN-Mb rates are much closer than the native RuMb rates to the best Marcus fit of the photoinitiated rates of intramolecular ET. It was suggested that the reason why the native Mb rates are so much slower (scaled with driving force) than the photoactive porphyrin-substituted rates is that the heme of native Mb has comparatively greater reorganization energy and/or weaker electronic coupling with the pendent ruthenium.¹⁵ The BrCN-RuMb data only "correct" for the extra reorganization energy of the water molecule coming off of the heme during ET compared with photoactive porphyrins where this is not the case. An additional reorganization difference between heme in the photoactive porphyrins is the spin change (and consequent geometry change) myoglobin hemes undergo during ET that photoactive porphyrins do not. BrCN-Mb heme also undergoes the spin change so that we cannot correct for this effect in the present study. However, several studies on porphyrin model systems²⁰ and Mb²¹ have estimated this effect to be relatively small. The reorganization energy due to spin change may be enough, however, to place the BrCN-RuMb points close to the fit in Figure 9.

The non-directionality of the electron transfer rate increase with BrCN modification in addition to the similar equality of forward and reverse ET rates

for native Mb argue against the BrCN effect originating from a protein conformational mechanism. This effect of an Fe—OH₂ bond breaking upon ET has a significant effect on reorganization energy of Mb (approximately 0.2eV derived from Marcus theory). Further, it is now clear that this change of ligation upon ET is a major reason why electron transfer is slower in myoglobin than in cytochrome c^{22,23}--probably more so than the reorganization energy involved with spin change.

Figure 9. Plot of $\ln k_{\text{et}}$ vs. $-\Delta G^\circ$ for the Ru-Mb ET reactions. The line is the best fit to semiclassical Marcus theory using only the photoexcited porphyrin to Ru(III) ET rates, $\lambda=1.45$ and $\nu_{\text{h}}k_{\text{e}}^\circ=4 \times 10^9 \text{ s}^{-1}$. The diamonds are photoexcited Pd porphyrin to Ru(III) ET; the squares are photoexcited Zn porphyrin to Ru(III) ET; the filled-in circles are Fe(II) to Ru(III) ET; and the open circles are BrCN treated Ru(II) to Fe(III) ET.



References

1. Marcus, R. A. and Sutin, N. *Biochim. Biophys. Acta* 811, 265 (1985).
2. Meyer, T. E. and Kamen, M. D. *Adv. Protein Chem.* 35, 105 (1982).
3. Cave, R. J., Siders, P., Marcus, R. A. *J. Phys. Chem.* 90, 1436 (1986).
4. Mayo, S. L., *et al.* *Science* 233, 948 (1986).
5. Marcus, R. A. *J. Phys. Chem.* 43, 679 (1965).
6. Bechtold, R. *et al.* *Nature* 322, 286 (1986).
7. Dreyer, J. L. *Experientia* 40, 653 (1984).
8. Jajczay, F. L. *Ph. D. Thesis* University of Alberta, Edmonton (1970).
9. Monishima, J., Shino, Y., and Wakino, T. *J. Am. Chem. Soc.* 107, 1063 (1984).
10. Shino, Y. and Morishima, I. *Biochemistry* 23, 4879 (1984).
11. Tsukahara, K. *Chem. Lett.* 1291 (1987).
12. Brunori, M. *et al.* *Biochemistry* 10, 1604 (1971).
13. Takano, T. J. *J. Mol. Biol.* 110, 537 (1977).
14. Tsukahara, K. *J. Am. Chem. Soc.* 111, 2040 (1989).
15. Karas, J. L. *Ph. D. Thesis* California Institute of Technology, Pasadena (1989).
16. Caughey, W. S. *et al.* *Biochemistry* 5, 1255 (1966).
17. Maltempo, M. M. and Moss, T. H. *Quarterly Reviews of Biophysics* 9, 181 (1976).
- 18.
19. Bradic, Z. *et al.* in *Frontiers in Bioinorganic Chemistry* Xavier, Wernheim, FRG, p.336 (1986).
20. Kadish, K. M. and Su, C. H. *J. Am. Chem. Soc.* 105, 177 (1983).
21. Tsukahara, K., Yamamoto, Y. *Biochemistry* 93, 15 (1983).

22. Ellis, W. R. *Ph. D. Thesis* California Institute of Technology, Pasadena (1986).

23. Crutchley, R. J., Ellis, W. R., Gray, H. B. *J. Am. Chem. Soc.* 107, 5002 (1985).

CHAPTER 6**LONG-RANGE ELECTRON TRANSFER IN
(NH₃)₄(isn)RU-MODIFIED SPERM WHALE MYOGLOBIN**

One approach to investigate how factors such as donor-acceptor distance, the reorganization energy, and driving force affect long-range biological protein electron transfer involves the modification of a single surface histidine site in metalloproteins with redox-active ruthenium-ammine complexes (a_4LRu , $a = NH_3$).¹⁻⁴ The resulting systems allow the effect of varying donor-acceptor separation and driving force on protein long-range ET to be studied systematically. The ET driving force can be varied by changing the ligand L *trans* to the histidyl imidazole in the modified protein ($L = NH_3$, Py, isonicotinamide),² and by replacing the heme with photoactive porphyrins MP ($M = Zn, Pd, Mg$; $P = \text{mesoporphyrin IX}$) in myoglobin (Mb)³ and substituting Fe with Zn in cytochrome c.⁴ Based on semi-classical Marcus theory,⁵ semi-logarithmic plots of the ET rate constant vs driving force have allowed the reorganization energy for ET in Mb modified at His-48 to be estimated at 1.4 eV.⁶ There are several data points at high driving forces ($\sim 1 \text{ eV}$) from studies of the photoactive MP-substituted proteins; there are also data points for relatively low driving forces ($[a_5Ru(\text{His-48})\text{-Mb(Fe)}]$, $-DG^\circ = 0.02 \text{ V}$; $[a_4(\text{Py})Ru(\text{His-48})\text{-Mb(Fe)}]$, $-DG^\circ = 0.275 \text{ V}$). However, there is no data for the region in between. In order to obtain data in this region we set out to measure the rate constant for the ET process $Fe(II)P + Ru(III) \rightarrow Fe(III)P + Ru(II)$ which in the modified protein $[a_4(\text{isn})Ru(\text{His-48})\text{Mb(Fe)}]$ has an ET driving force $-DG^\circ = 0.355 \text{ V}$.^{4b,6}

The modified protein was prepared as described,⁷ and purified by FPLC before use in flash photolysis experiments. The transient species $a_4(\text{isn})Ru^{3+}(\text{His-48})\text{Mb(Fe}^{2+})$ was generated by flash photolysis^{1d,8} of a solution of the fully oxidized protein complex, $[Ru(\text{bpy})_3]^{2+}$, and $EDTA^{2-}$. Flash photolysis generates the highly reactive species $[Ru(\text{bpy})_3]^{2+*}$, which is oxidatively quenched by the Ru^{3+} and/or Fe^{3+} centers in the protein complex. The $[Ru(\text{bpy})_3]^{3+}$ formed is scavenged by $EDTA^{2-}$. After the initial rapid

increase arising from protein reduction by $[\text{Ru}(\text{bpy})_3]^{2+*}$, the absorbance of the protein complex monitored at 550 nm in the concentration range 2 - 5.5 μM was time-invariant. Similar behavior in a pulse radiolysis study of ET from the heme iron to a surface Ru unit has been reported for $[\text{a}_4(\text{isn})\text{Ru}(\text{His-33})\text{-cyt c}]$.^{2c} This apparent absence of ET from the heme to the pendent surface ruthenium label despite a driving force of 0.14 V was interpreted as evidence for directional ET arising from protein conformation changes. Further experiments with $[\text{a}_4(\text{py})\text{Ru}(\text{His-33})\text{-cyt c}]$ contradicted this hypothesis in that ET from the heme to the ruthenium group was essentially on the timescale predicted by classical Marcus theory.⁹

Close examination of the absorption spectra (Figure 1) of metMb and deoxyMb, and the fully oxidized and reduced ruthenated counterparts reveals two important factors in the failure to observe ET at 550 nm. First, upon heme oxidation (or ET from Fe^{2+} to the surface Ru^{3+}), the heme absorbance at 550 nm drops; this absorbance reduction has been used to monitor ET in other systems such as $[\text{a}_4(\text{py})\text{Ru}(\text{His-48})\text{-Mb}]$.^{2b} For the $[\text{a}_4(\text{isn})\text{Ru}(\text{His-48})\text{-Mb}]$ complex, however, there is an intense Ru-to-isn MLCT absorption band centered at ca. 500 nm¹⁰ with a substantial absorbance at 550 nm when the ruthenium complex is reduced (Figure 1). Hence, upon ET from Fe^{2+} to Ru^{3+} after flash photolysis, the heme absorption decreases while the MLCT band of the Ru label grows in intensity. In turn, the two absorption bands cancel each other reducing the effective De value at 550 nm. Secondly, the *initial* rise in absorbance generated by protein reduction is much higher in the $\text{a}_4(\text{isn})\text{Ru}$ - compared to the a_5Ru - and $\text{a}_4(\text{py})\text{Ru}$ -modified proteins because of the Ru(II)-to-isn MLCT band. Thus, a background signal was created which was so large compared to the small De for the ET process that the data did not have sufficient signal-to-noise ratios for a rate constant to be determined. Since the heme

absorption at 550 nm for cyt c also drops upon oxidation, the mutually cancelling heme and ruthenium absorbances in combination with the enormous background signal give a plausible explanation of the earlier failure to observe ET in the $[a_4(\text{isn})\text{Ru}(\text{His-33})\text{-cyt c}]$ complex.^{2c}

The increase in Mb heme absorption at 630 nm upon oxidation is much less affected by the MLCT absorption band in the ruthenium label (Figure 1). We therefore monitored the ET reaction at this wavelength (Figure 2). The absorbance changes were satisfactorily fit to a three parameter monoexponential decay function ($\tau = 4 - 9 \times 10^{-10}$, 6 - 10 half-lives). Four parameter biexponential fits gave slightly worse results. The ET rate constant of $3.0 \pm 0.4 \text{ s}^{-1}$ thus obtained was independent of concentration in the range 2.5 - 11 mM, further confirming the intramolecular nature of the ET reaction. The methodology was also validated by the satisfactory agreement of the k_{obs} measured at 630 nm for the ET processes in $[a_5\text{Ru}(\text{His-48})\text{-Mb}]$ with published values.^{2a,2b}

The Fe(II) to Ru(III) ET rate constant ($3.0 \pm 0.4 \text{ s}^{-1}$) in $[a_4(\text{isn})\text{Ru}(\text{His-48})\text{-Mb}]$ is surprisingly similar to that in the pyridine derivative ($2.5 \pm 0.5 \text{ s}^{-1}$)^{2b} despite the higher driving force (0.355 V vs 0.275 V) in the former. Using classical Marcus theory, and assuming identical donor-acceptor coupling and reorganization energy (1.4 eV) for both modified proteins, an ET rate constant of 8.36 s^{-1} is calculated for the isonicotinamide derivative. Since the redox potentials of the ET sites have been determined experimentally by differential pulse polarography,^{4b,6} this unexpected result must arise from other factors. Thus, the donor-acceptor coupling in the $a_4(\text{isn})\text{Ru(III)}\text{-MbFe(II)}$ species may be reduced compared to the py analogue due to the stronger s-withdrawing effect of isn compared to py. Such effects are, however, expected to be too small to counterbalance the increased ET driving force.

A second possibility is that strong p back-donation in the Ru(II)-isn label results in higher than expected values of both the inner sphere (because of a stronger Ru-N(isn) bond) and outer sphere (because the amide oxygen has higher electron density) reorganization energy of the $a_4(\text{isn})\text{Ru}$ label, leading to slower ET compared to $[a_4(\text{py})\text{RuMb}]$. Alternatively, it may be argued that the $[a_4(\text{py})\text{RuMb}]$ ET rate constant is faster than expected because replacement of a hydrophilic ammine ligand by the hydrophobic pyridine may reduce the outer sphere reorganization energy of $[a_4(\text{py})\text{RuMb}]$ label below 1.4 eV. On the other hand, increased solvation because of the amide group on the py ring for isn could raise the reorganization energy of a $a_4(\text{isn})\text{Ru}$ label to a value comparable to that of a $a_5\text{Ru}$ label. The outer sphere self-exchange rate constants of the couples $[a_5\text{RuL}]^{3+/2+}$ are of interest here (Table 1). From semi-classical theory,⁵ $k_{\text{ex}} = (2p/h)|H_{\text{ab}}|^2\exp(-I/4)$ where H_{ab} is the intermolecular donor-acceptor coupling and I is the reorganization energy. The increase in rate from $L = \text{NH}_3$ to py and isn is mainly due to increased metal-to-ligand electron delocalization leading to higher intermolecular coupling. Since there is stronger p back-donation from ruthenium to isn than to py, the electronic coupling in the py couple is expected to be lower. The equal self-exchange rates therefore suggest that I in the py couple is lower, presumably due to the hydrophobic nature of the py ligand which excludes high-dielectric solvent molecules from the metal center. Assuming $I = 1.4$ eV for ET in $[a_4(\text{isn})\text{Ru}(\text{His-48})\text{Mb}]$, I for $[a_4(\text{py})\text{Ru}(\text{His-48})\text{-Mb}]$ is calculated to be 1.29 eV. This enhancement of ET rate constants caused by a reduction of outer sphere reorganization energy by the presence of hydrophobic groups parallels the faster relative ET rates of cytochrome c (4% solvent-exposed heme) vs myoglobin (18% solvent-exposed heme).¹¹

Table 1: Formal potentials, MLCT bands, and rate constants of electron-exchange for $[\text{Ru}(\text{NH}_3)_5\text{L}]^{3+/2+}$ couples.

L	E° (V vs NHE) ^a	λ_{max} (nm)	ϵ_{max} ($\text{M}^{-1}\text{cm}^{-1}$)	k_{ex} ($\text{M}^{-1}\text{s}^{-1}$)
NH_3	0.067	-	-	4.3×10^3 ^b
Py	0.299	407 ^c	7.80×10^3 ^c	4.7×10^5 ^a
Isn	0.384	478 ^d	1.19×10^4 ^e	4.7×10^5 ^a

a. Taken from Brown, G. M., Krentzien, H.J., Abe, M., Taube, H. *Inorg. Chem.* **1979**, *18*, 3374.

b. Meyer, T. J., Taube, H. *Inorg. Chem.* **1968**, *7*, 2369.

c. Ford, P., Gaunder, R., Rudd, Def. P., Taube, H. *J. Am. Chem. Soc.* **1968**, *90*, 1187.

d. Reference 10.

e. Shepherd, R., Taube, H. *Inorg. Chem.* **1973**, *12*, 1392.

Figure 1. (a) The absorption spectra of metMb (i) and deoxyMb (ii) in 50 mM Tris buffer. (b) The absorption spectra of the fully oxidized [Fe(III);Ru(III)] (i) and fully reduced [Fe(II);Ru(II)] (ii) modified protein [$a_4(\text{isn})\text{Ru}(\text{His-48})\text{-Mb}$].

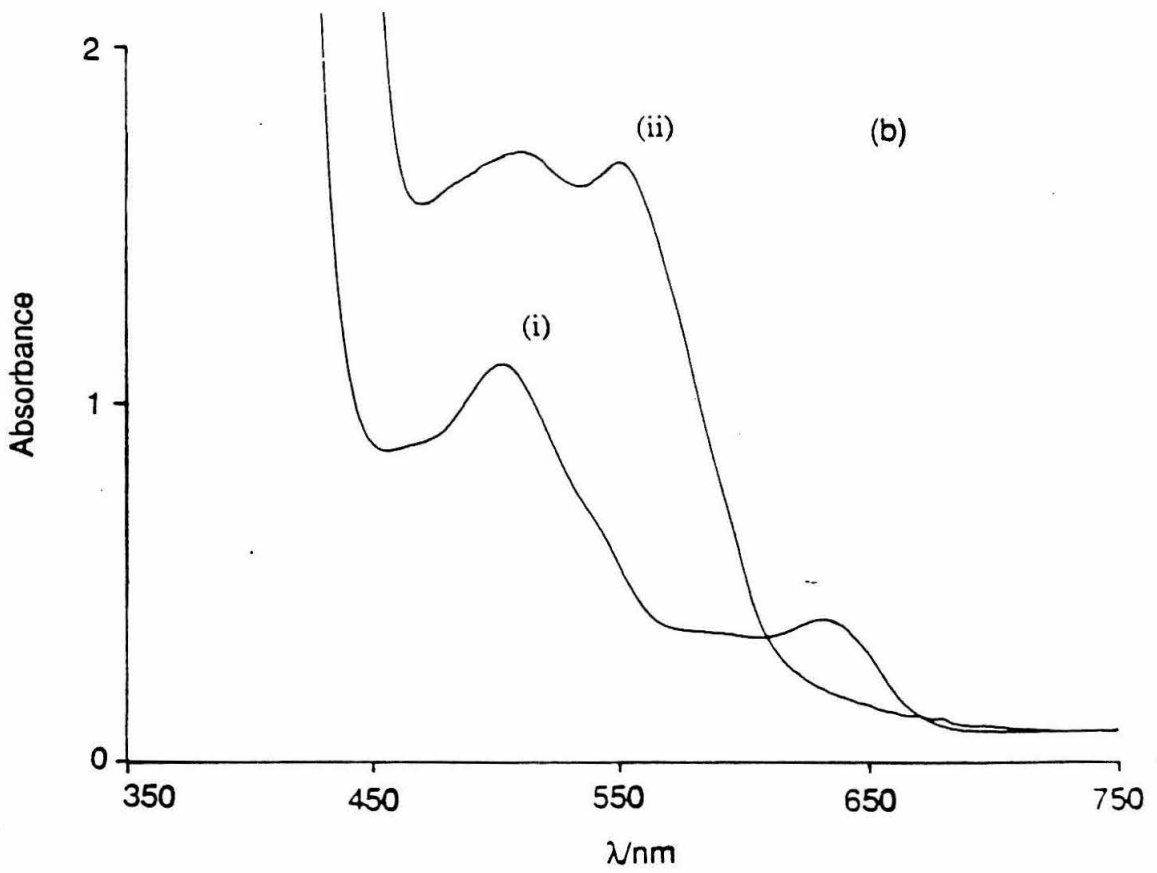
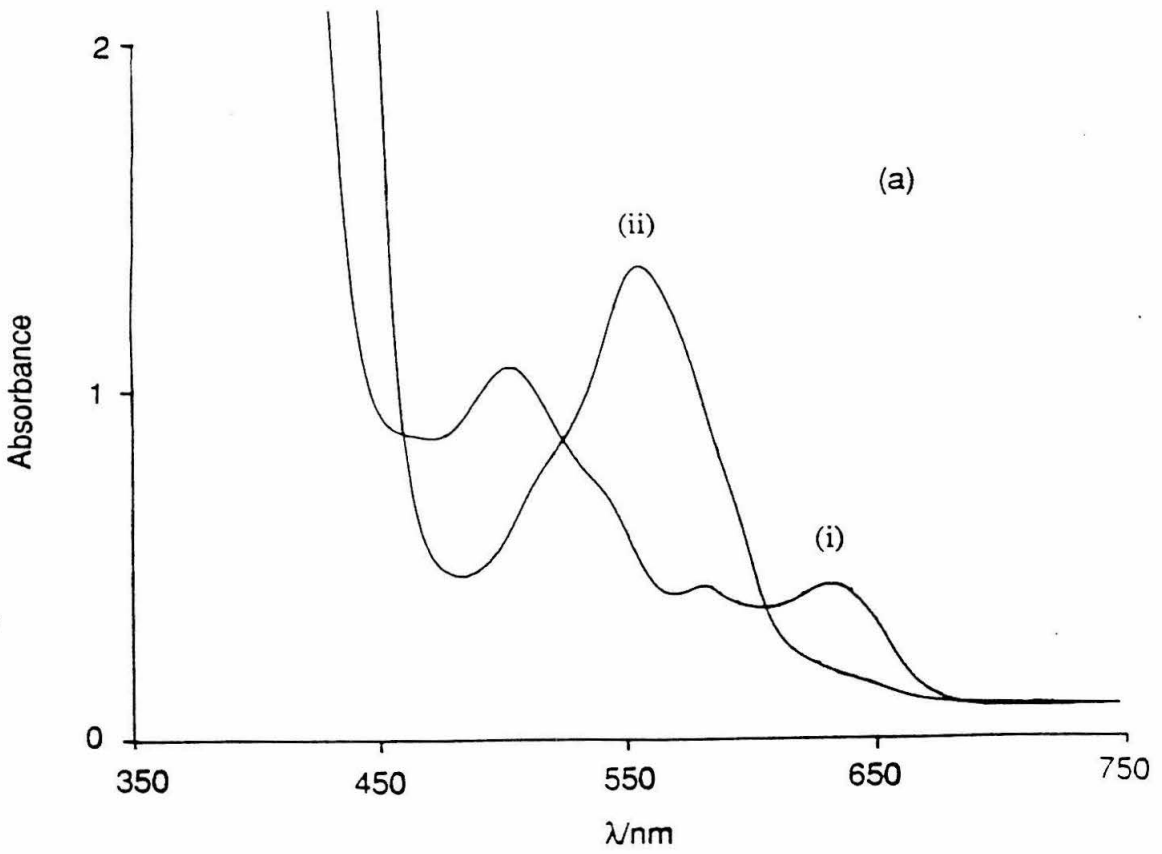
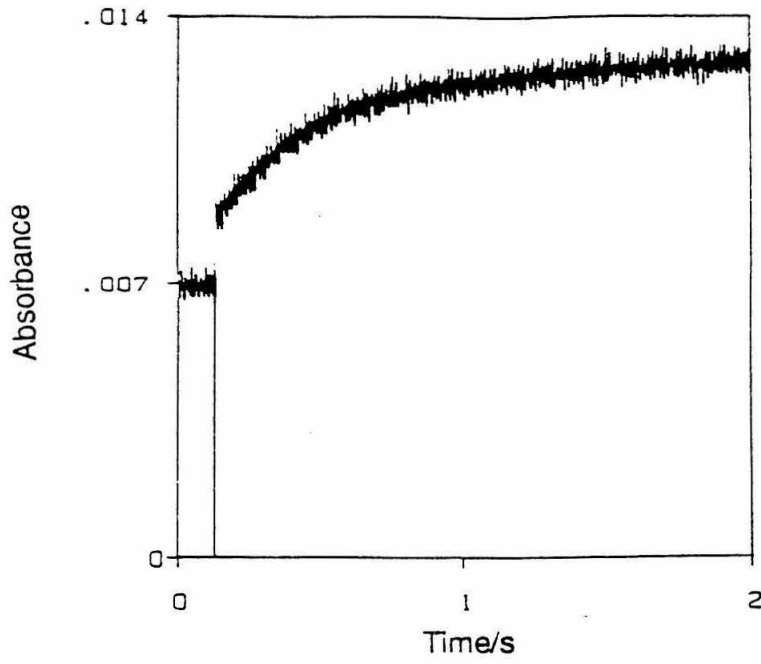
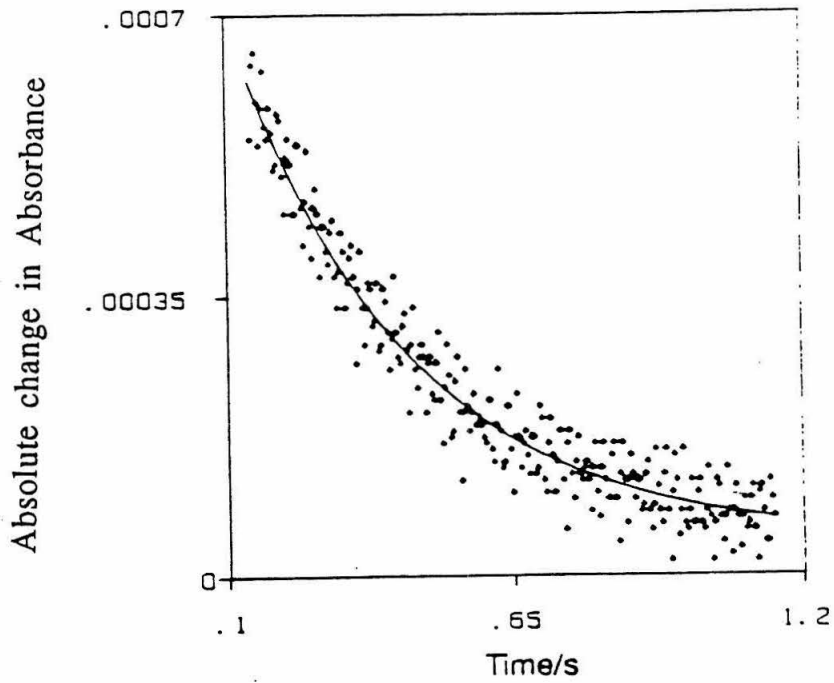


Figure 2. (a) Absorbance change at 630 nm following flash photolysis of a 0.1 M, pH 7 phosphate solution containing $[\alpha_4(\text{isn})\text{Ru}(\text{His-48})\text{-Mb}]$ (5.5 mM), $[\text{Ru}(\text{bpy})_3]^{2+}$ (50mM), and EDTA^{2-} (50mM) at 298°K. (b) Three parameter monoexponential fit to the experimental data. The first order rate constant was $3.0 \pm 0.4 \text{ s}^{-1}$ at 298°K.



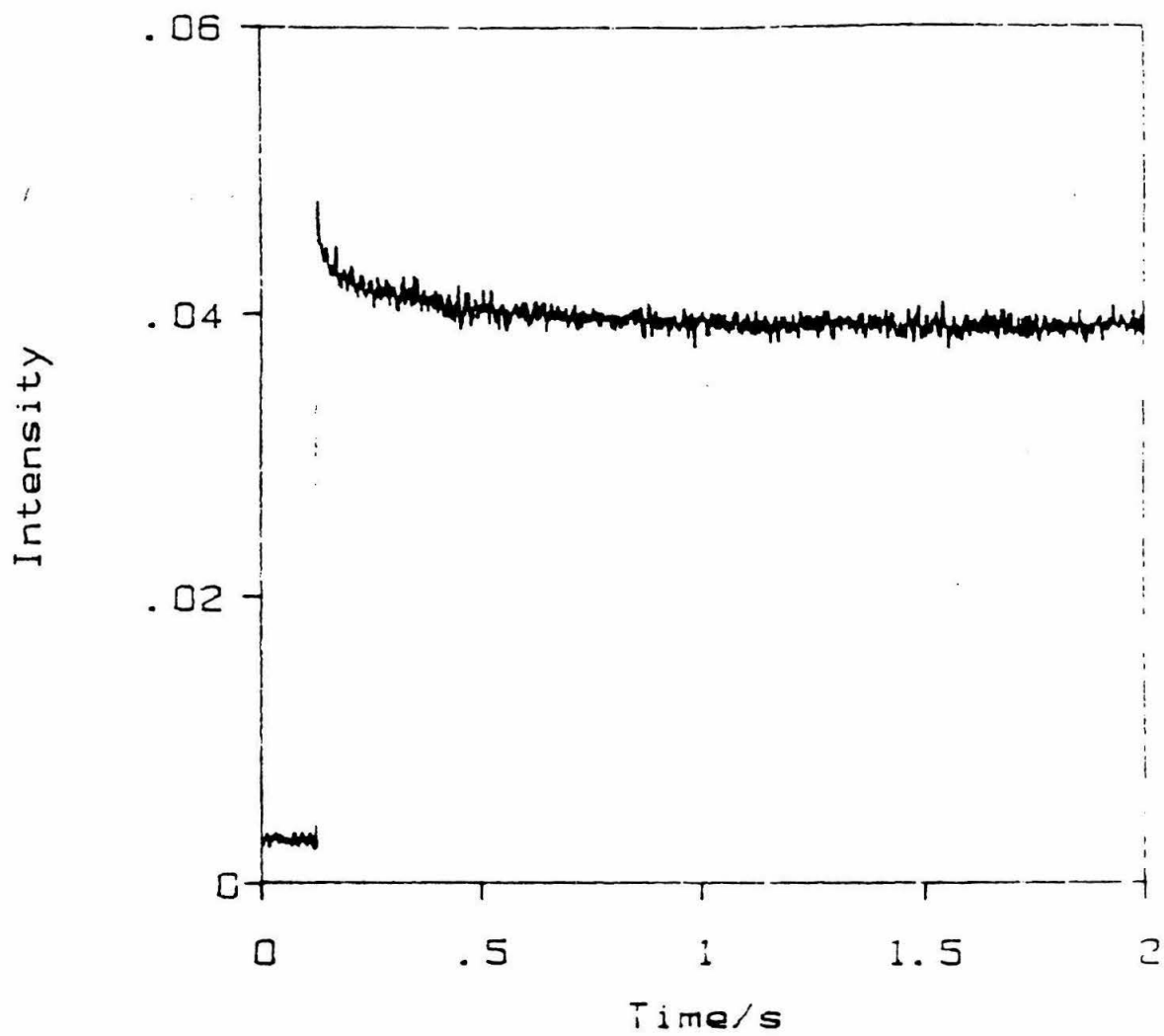
(a)



(b)

Figure 3. Absorbance change at 585nm following flash photolysis of same sample, conditions as in figure 2 except 0.012mM modified protein.

Ru(isn)Mb 298K 585nm 12uM 5V G100.



References

1. (a) Yocum, K. R., Shelton, J. B., Shelton, J. R., Schelton, J. R., Schroeder, W. A., Worosila, G., Isied, S. S., Bordignon, E., Gray, H. B. *Proc. Natl. Acad. Sci. U. S. A.* 79, 7052 (1982).
(b) Isied, S. S. *et al.*, *J. Am. Chem. Soc.* 104, 7659 (1982).
(c) Winkler, J. R. *et al.*, *J. Am. Chem. Soc.* 104, 5798 (1982).
(d) Nocera, D. G. *J. Am. Chem. Soc.* 106, 5145 (1984).
(e) Kostic, N. M. *et al.*, *J. Am. Chem. Soc.* 105, 7765 (1983).
Isied, S. S. *et al.*, *J. Am. Chem. Soc.* 106, 1722 (1984).
(f) Margalit, R. *et al.*, *Proc. Natl. Acad. Sci. U. S. A.* 84, 6554 (1984).
(g) Mayo, S. L. *et al.*, *Science (Washington, D. C.)* 233, 948 (1986).
(h) Osvath, P. *et al.*, *J. Am. Chem. Soc.* 110, 7114 (1988).
2. (a) Crutchley, R. J. *et al.*, *J. Am. Chem. Soc.* 107, 5002 (1985).
(b) Lieber, C. M. *et al.*, *J. Am. Chem. Soc.* 109, 3778 (1987).
(c) Bechtold, R. *et al.*, *Nature (London)* 322, 286 (1986).
3. (a) Axup, A. W. *et al.*, *J. Am. Chem. Soc.* 110, 435 (1988).
(b) Karas, J. L. *et al.*, *J. Am. Chem. Soc.* 110, 599 (1988).
(c) Cowan, J. A. *et al.* *Ann. N. Y. Acad. Sci.* 550, 68 (1988).
4. (a) Elias, H. *et al.*, *J. Am. Chem. Soc.* 110, 429 (1988).
(b) Meade, T. J. *et al.*, *J. Am. Chem. Soc.* 111, 4353 (1989).
5. Marcus, R. A. and Sutin, N. *Biophys. Biochim. Acta* 811, 265 (1985).
6. Karas, J. L. *Ph. D. Thesis*, California Institute of Technology, 1989.
7. The only modification to the procedure described in Ref. 6 was the use of $[\text{Co}(\text{5-NO}_2\text{-Phen})_3]^{3+}$ as the oxidant in the preparation.
8. Milder, J. J. *et al.*, *J. Am. Chem. Soc.* 102, 6767 (1980).
9. Meade T. J.; and Gray, H. B., to be published.
10. Stanbury, D. M., Haas, O., Taube, H. *Inorg. Chem.* 19, 518 (1980).
11. Stellwagen, E. *Nature (London)* 275, 73 (1978).